Title

NATURAL DECAYS OF THE y/ MESON.

Author
Risser, Thomas Bard.

Publication Date
1970-08-01

Thesis/dissertation

UCRL-20039

c.2

NEUTRAL DECAYS OF THE η^0 MESON

Thomas Bard Risser
(Ph. D. Thesis)

August 1, 1970

AEC Contract No. W-7405-eng-48

UCRL-20039 c.2

LAWRENCE RADIATION LABORATORY
UNIVERSITY of CALIFORNIA BERKELEY

DISCLAIMER

Contents

NEUTRAL DECAYS OF THE η^o MESON

Thomas Bard Risser

Lawrence Radiation Laboratory
University of California
Berkeley, California

ABSTRACT

Eta mesons have been produced by the reaction $\pi^- p \rightarrow \eta^o n$. Veto counters surrounding the hydrogen target in which this interaction takes place eliminate all reactions involving charged particles. The neutral decays of the eta meson are studied with a cubical array of lead plate spark chambers for the conversion of gamma rays. The eta producing reaction is identified by the time of flight of the neutron from the hydrogen target. The neutron is detected by one of twenty large scintillation counters.

We find that our data are consistent with zero decays of the type $\eta^o \rightarrow \pi^o\gamma\gamma$. With the assumption that only the neutral decays $\eta^o \rightarrow \gamma\gamma$ and $\eta^o \rightarrow 3\pi^o$ are present, we find

$$R\left(\frac{\eta^o \rightarrow \gamma\gamma}{\eta^o \rightarrow \text{all neutrals}}\right) = 0.580 \pm 0.013$$

$$R\left(\frac{\eta^o \rightarrow 3\pi^o}{\eta^o \rightarrow \text{all neutrals}}\right) = 0.420 \pm 0.015\ .$$

Furthermore, we find that, with 95% confidence

$$R\left(\frac{\eta^o \rightarrow \pi^o\gamma\gamma}{\eta^o \rightarrow \text{all neutrals}}\right) < 0.061.$$

I. INTRODUCTION

A. Discovery of the η^o and its Quantum Numbers

In the fall of 1961 Pevsner et al.[1] discovered the η meson in film from a deuterium bubble chamber exposure. It appeared as an enhancement in the three pion mass spectrum from the reaction

$$\pi^+ + n \rightarrow p + \pi^+ + \pi^- + \pi^o.$$

They could make no positive statement about its quantum numbers because of limited statistics. Soon thereafter Carmony et al.[2] demonstrated that the η was an isotopic singlet. They failed to observe the reactions

$$\pi^{\pm} + p \rightarrow p + \eta^{\pm}$$
$$\eta^{\pm} \rightarrow \pi^{\pm} + \pi^o + \pi^o.$$

Simultaneously, Bastien et al.[3] reported observing the η^o in the reaction

$$K^- + p \rightarrow \Lambda^o + \eta^o$$
$$\eta^o \rightarrow \pi^+ + \pi^- + \pi^o$$

and in the reaction

$$K^- + p \rightarrow \Lambda^o + \eta^o$$
$$\eta^o \rightarrow \text{neutral particles}$$

with the branching ratio

$$\frac{\pi^o \rightarrow \pi^+\pi^-\pi^o}{\eta^o \rightarrow \text{neutrals}} = 0.31 \pm .11.$$

The large number of neutral decays and a limited statistics Dalitz plot led Bastien et al. by means of intricate and elegant arguments to suggest that the η had quantum numbers $I^G(J^P) = 0^+(0^-)$ and decayed electromagnetically. The extremely short lifetime argued against weak decays. A strong decay scheme would imply $G(\eta^o) = -1$ because $G(3\pi) = -1$. Then, $\eta^o \rightarrow \pi^o\pi^o$ would be forbidden by G-parity conservation. If $I(\eta^o) = 0$, as the evidence had suggested, $\eta \rightarrow 3\pi^o$ would not occur either in an

I-conserving strong decay. Symmetry forbids the existence of an $I = 0$ state to $3\pi^o$. Consequently the η^o should have no neutral strong decays. However, approximately 76% of the η^o decays were observed to be neutral.

The Dalitz plot distribution for the decay $\eta^o \to \pi^+\pi^-\pi^o$ also suggested electromagnetic decays. The reasoning is as follows: The symmetry requirement on an $I = 0$ system of three pions is such that the Dalitz plot density must have sextant symmetry and must vanish either at the boundary $(J^P = 1^-, 2^+)$ or at the center $(J^P = 0^-, 1^+, 2^-)$[4]. The observed density, with only 23 data points, did not vanish at the center or periphery and did not appear to have sextant symmetry. Therefore, one must examine $I > 0$ states. Considering only $J \leqslant 2$, a Dalitz plot with the observed density is consistent with $I = 1$ and $J^P = 0^-, 2^-$. (See, for example, Zemach, Ref. 4.) If $I(3\pi) = 1$ and $I(\eta) = 0$ the transition must involve a change in isotopic spin. This implies an electromagnetic transition involving a virtual photon which is emitted and reabsorbed. It changes the isotopic spin by one unit at one vertex and does not change I at the other vertex. For example

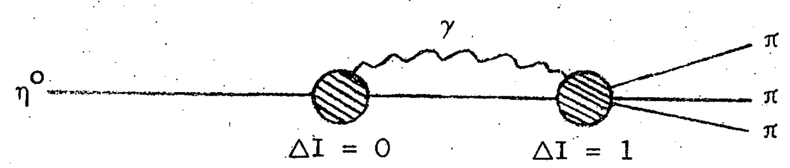

Since $G = C(-1)^I$ for a neutral non-strange system of mesons, and since C is conserved in electromagnetic interactions, such an I-changing transition also changes G. Note that in such a model the $\eta^o \to 3\pi$ transition rate is proportional to α^2 where $\alpha = 1/137$ is the fine structure constant. The authors pointed out that an electromagnetic decay scheme for η^o with $I^G(J^P) = 0^+(0^-)$ might include the following allowed decays:

$$\eta_o \rightarrow \gamma\gamma, \quad \eta_o \rightarrow \pi^+\pi^-\gamma, \quad \eta^o \rightarrow 3\pi^o.$$

None of these decays was actually observed due to the tiny probability of gamma ray materialization in a hydrogen bubble chamber. However, if the $\pi^+\pi^-\gamma$ decay occurred with a frequency comparable to that of the $\pi^+\pi^-\pi^o$ mode it should have been seen.

While the data of Bastien et al. favored $0^+(0^-)$ they could not definitely rule out $0^-(1^-)$. However, supporting arguments and evidence for the $0^+(0^-)$ assignment began to materialize: (1) Brown and Singer[5] pointed out that the high yield of neutrals favored $0^+(0^-)$. If the η^o were $0^-(1^-)$ the expected neutral decay modes would be $\pi^o\gamma$ and $\pi^o\pi^o\gamma$ (exactly as for the ω^o meson which has a low yield of neutrals) and they showed a reasonable estimate of $R = \dfrac{\eta^o \rightarrow \text{neutrals}}{\eta^o \rightarrow \text{charged}}$ would be $R \lesssim 0.6$. This is in gross disagreement with the observed value $R \cong 3.3$. (2) Gell-Mann, Sharp, and Wagner[6] produced a model which explained why $\eta^o \rightarrow \pi^+\pi^-\gamma$ might be rare and hitherto unobserved. Without some such model there would be difficulty in explaining why the decay $\eta^o \rightarrow \pi^+\pi^-\gamma$, with more phase space and with a matrix element one order lower in α, should not be vastly greater than $\eta^o \rightarrow \pi^+\pi^-\pi^o$. (3) Rosenfeld et al.[7] failed to find $\rho^o \rightarrow \eta^o + \pi^o$ which Feinberg[8] had predicted to be large if the η^o were $0^-(1^-)$. Although no further direct experimental evidence had been announced, Puppi, reviewing 3π resonances at the 1962 CERN conference, could say that the quantum numbers $I^G(J^P) = 0^+(0^-)$ were "generally accepted."[9]

The first definite proof of the $0^+(0^-)$ assignment came when Chretien et al.[10] observed unambiguously the decay $\eta \rightarrow \gamma\gamma$ in a heavy liquid bubble chamber. This proves that $G(\eta) = C(\eta) = +1$ because $C(\gamma\gamma) = +1$ and C is conserved. Furthermore $\eta^o \rightarrow \gamma\gamma$ is forbidden by angular momentum conservation if J = 1. A Dalitz plot for 287 $\eta \to \pi^+\pi^-\pi^o$ decays, compiled from various experiments by Alff et al.,[11] bears out the original conclusions of Bastien et al. Fowler et al.[12] found the $\pi^+\pi^-\gamma$ mode and measured the branching ratio $\frac{\eta^o \to \pi^+\pi^-\gamma}{\eta^o \to \pi^+\pi^-\pi^o} = .26 \pm .08$. Crawford et al.[13] definitely observed $\eta^o \to 3\pi^o$. Their branching ratio measurements, based on very limited statistics, were inconsistent with later experimental results, however.

There are two other permitted decay modes for an η^o with $I^G(J^P) = 0^+(0^-)$ which are not included in the list above from Bastien et al. $\eta^o \to \pi^o\gamma\gamma$ is allowed to proceed electromagnetically and is discussed below. In addition, the decay $\eta^o \to 4\pi^o$ is allowed to proceed by the strong interaction. Despite the stronger coupling, the rate for this decay is expected to be infinitesimal because of a large angular momentum barrier and extremely limited four body phase space (Q = 9 MeV). No hint of this decay mode has ever been reported.

B. η^{o} Branching Ratios before April, 1966

1. The General Decay Scheme

By June of 1963 all the decay modes predicted by Bastien et al. had been observed. The charged branching ratios were well established as was the ratio of charged to neutral modes:

$$\frac{\eta \to \pi^{+}\pi^{-}\pi^{o}}{\eta \to \text{all modes}} = .23 \qquad (1)$$

$$\frac{\eta \to \pi^{+}\pi^{-}\gamma}{\eta \to \text{all modes}} = .06 \qquad (2)$$

$$\frac{\eta \to \text{neutrals}}{\eta \to \text{all modes}} = .71. \qquad (3)$$

These values have not changed appreciably to the present day. (See, for example, Rosenfeld et al.[14])

The measurements of the above ratios were done using bubble chambers and are quite reliable. The bubble chamber is not, however, a good instrument for unravelling the neutral decay scheme. The enormous amount of published literature about the composition of the neutral decays is evidence for the experimental difficulties involved. The history of the investigations into the neutral decay branching ratios can be conveniently divided into two periods. The first era, lasting from the discovering of the η^{o} until April of 1966, is dominated by speculation and the bubble chamber. During this period much attention was focussed on what the neutral branching ratios ought to be from general considerations and indirect evidence. The direct experiments were not in good agreement with the speculations. However, this was not particularly alarming due to the inadequacy of the bubble chamber for such measurements. The second era, that of counter and spark chamber experiments, began in April of 1966 with the work of DiGiugno et al.[15] This first experiment of the second period indicated that the previous speculations, largely untested experimentally, had been completely inadequate. A flurry of excitement ensued. New speculations were introduced and discarded as the experimental situation changed again. A large number of spark chamber experiments, the most recent of which is the present work, have indicated that the speculations of the first era were essentially correct.

In June of 1963 the neutral decay modes were assumed to be entirely $\gamma\gamma$ or $3\pi^{o}$, both of which had been observed. The precise amount of each was unknown because all the experiments had been bubble chamber experiments with a low probability of observing gamma rays. However, theoretical estimates of $\frac{\eta^{o} \to \pi^{o}\pi^{o}\pi^{o}}{\eta^{o} \to \pi^{+}\pi^{-}\pi^{o}}$ (see, for example, Wali[16]) suggested that

$$\frac{\eta^{o} \to \pi^{o}\pi^{o}\pi^{o}}{\eta^{o} \to \text{all modes}} \lesssim .39. \tag{4}$$

Then, by process of elimination we have

$$\frac{\eta^{o} \to \gamma\gamma}{\eta^{o} \to \text{all modes}} \gtrsim .32. \tag{5}$$

Another decay mode, $\eta^{o} \to \pi^{o}\gamma\gamma$ is permitted but was largely ignored. Its possible existence was noted by Bacci et al.[17] in July, 1963 but it was not taken seriously until the work of DiGiugno et al.[15] in April of 1966. Few theoretical papers before that time discuss this mode. They approach the η^{o} decay problem with the assumption that the neutral modes are composed entirely of $\gamma\gamma$ or $3\pi^{o}$.

The decay mode $\eta^{o} \to \pi^{o}\gamma\gamma$ is difficult to observe, particularly in bubble chambers. Any event involving a number of observed gamma rays less than six can be interpreted as an $\eta^{o} \to 3\pi^{o} \to 6\gamma$ event where a number of gamma rays escaped detection. The $\eta^{o} \to \gamma\gamma$ mode has well defined kinematics and can be truly identified; analysis of events involving more than two gamma rays is difficult. On the theoretical side, the modes $\eta^o \to \pi^o\gamma\gamma$ and $\eta^o \to \pi^+\pi^-\gamma$ can be realistically compared. The phase space available to each of these three body decays is comparable. The $\eta^o \to \pi^o\gamma\gamma$ mode has a coupling which is weaker by a factor of $\alpha(= 1/137)$. One would therefore expect the $\eta^o \to \pi^o\gamma\gamma$ decay to be two orders of magnitude smaller than the already small (~ 6%) $\eta^o \to \pi^+\pi^-\gamma$ mode.

It is interesting to attempt to understand the above η^o branching ratios [i.e. equations (1) to (5)] by considering simple estimates of couplings, matrix element angular momentum properties, and phase spaces. The partial width for an arbitrary decay mode of the η^o is

$$\Gamma_i \sim \int_{\substack{\text{phase}\\\text{space}}} |M_i|^2 \, d\rho_i$$

where M_i is the transition amplitude to that final state and $d\rho_i$ is the differential element of phase space. For electromagnetic processes we may approximate

$$M_i \sim \alpha^{n/2} \, F(k_1, k_2, \ldots).$$

Here α is the fine structure constant (= 1/137), n is the number of electromagnetic vertices, and $F(k_1, k_2, \ldots)$ is a function of the final state momenta. The function $F(k_1, k_2, \ldots)$ expresses the momentum dependence of the simplest matrix element with the correct angular momentum properties. Table I shows the relative widths for the allowed decay modes using the simple approximation

$$\Gamma_i \sim \alpha^n \, \langle F(k_1, k_2, \ldots)^2 \rangle_{av} \int_{\substack{\text{phase}\\\text{space}}} d\rho_i .$$

Table I. Branching ratio estimates, June, 1963

Decay mode	α^n	Simplest matrix element squared $\lvert F(k_1,k_2,\ldots)\rvert^2$	Momentum barrier $\langle F^2\rangle$	Relative phase space	Relative width Predicted	Observed
$\gamma\gamma$	α^2	$2\lvert f\rvert^2 k^4$	.12	14.6	1.75	1.4
$\pi^+\pi^-\gamma$	α	$\lvert f\rvert^2 q^2k^2 \sin^2\theta$	.0008	2.4	.275	.26
$\pi^o\gamma\gamma$	α^2	$k_1^{\,2}\, k_2^{\,2}\, f(\theta)$	.004	4.2	.017	0(?)
$\pi^+\pi^-\pi^o$	α^2	1	1	1	1	1
$\pi^o\pi^o\pi^o$	α^2	1.5	1	1.15	1.7	1.7

The matrix elements are derived in Appendix A and Sec. B. 2. below where the notation is explained. The treament of momentum barriers and phase spaces is included in Appendix B. The unknown form factors, $|f|^2$, are taken to be unity.

The predictions based on these simple considerations agree reasonably well with the branching ratios as they were understood to be in the summer of 1963. It must be pointed out, however, that such calculations involve a liberal dash of black magic: (1) The normalization of three body phase space depends on an unknown interaction radius r_0. In strong interaction calculations r_0 is usally taken to be $\lambda\!\!\!^-_\pi$, the pion Compton wavelength. In the calculations presented in Table I an interaction radius of $3\lambda\!\!\!^-_\pi$ was required to make the predictions agree with the observed branching ratios. As we are dealing with electromagnetic decays a longer radius may be called for, but we are not on very firm ground. (2) The momentum barriers used in the above calculations are very severe ($\sim k/m_\eta$). Usually momentum barriers are estimated to be much lower. The rationale for the above approach is presented in Appendix B. (3) The form factors are not known and are simply ignored.

Let us consider some other possible choices for interaction radius and momentum barriers: (1) $r_o = \lambda\!\!\!^{-}_{\pi}$, severe momentum barriers ($\sim k/m_\eta$). All the modes will agree among themselves except for $\eta^o \rightarrow \gamma\gamma$ which is then predicted to be roughly nine times larger than observed. (2) $r_o = \lambda\!\!\!^{-}_{\pi}$, no angular momentum barriers (take $k^n \sim 1$). All three modes involving real photons are then predicted to be much larger relative to the three pion modes than they are observed to be. The $\eta^o \rightarrow \pi^+\pi^-\gamma$ decay should also be somewhat larger relative to the $\eta^o \rightarrow \gamma\gamma$ mode. (3) $r_o = 3\lambda\!\!\!^{-}_{\pi}$, no angular momentum barriers. Again, all the modes involving real photons should be much larger than the three pion modes. The $\eta^o \rightarrow \pi^+\pi^-\gamma$ mode should be bigger than the $\eta^o \rightarrow \gamma\gamma$ mode.

It is only possible to account for the observed branching ratios in the manner above by treating phase space and momentum barriers in a rather extreme way. The general feeling among physicists is that, without examining specific models, the $\gamma\gamma$ and $\pi^+\pi^-\gamma$ modes should be much larger relative to the three pion modes than they are observed to be and that the $\pi^+\pi^-\gamma$ decay should compete more favorably with the $\gamma\gamma$ mode. The $\pi^o\gamma\gamma$ mode should not compete favorably with either $\gamma\gamma$ or $\pi^+\pi^-\gamma$ although it might compete with the three pion mode. The major problem with with the decays into three pions. They are just too large relative to the others. In attempting to resolve the apparent discrepancies a number of models have been considered.

Brown and Singer[18] advanced the attractive hypothesis that the η^o decayed via a G-parity violating electromagnetic process into a π^o and a dipion resonance $\sigma^o[I^G(J^P) = 0^+(0^+)]$. The σ^o, with a mass ~ 400 MeV and width ~ 85 MeV, then decayed strongly into $\pi^+\pi^-$ or $\pi^o\pi^o$. Such a model eliminates the principal problem in the η^o decay scheme in that the three pion decays are really two body processes and are not suppressed due to the more limited three-body phase space. Furthermore, $\eta^o \rightarrow \sigma^o + \gamma$ is forbidden by C conservation so that the $\pi^+\pi^-\gamma$ and $\pi^o\gamma\gamma$ modes remain limited phase space three body decays. Unfortunately there is no direct experimental evidence for the existence of a σ meson.

Bronzan and Low[19] proposed a selection rule for bosons which would explain why the $\gamma\gamma$ and $\pi^+\pi^-\gamma$ modes were suppressed relative to the three pion decays. In this scheme each boson has a quantum number $A = \pm 1$ which is approximately conserved. For example, $A(\gamma) = A(\rho) = A(\phi) = +1$ and $A(\pi) = A(K) = A(\eta) = A(\omega) = -1$. Decays do occur which violate A invariance by several percent, such as $\pi^o \rightarrow \gamma\gamma$, $\eta^o \rightarrow \gamma\gamma$, and $\eta^o \rightarrow \pi^+\pi^-\gamma$. The decays $\eta^o \rightarrow \pi^o\gamma\gamma$ and $\eta^o \rightarrow 3\pi$ are allowed transitions. It is difficult to understand how the ω and ϕ mesons can mix in a unitary symmetry scheme if they have opposite quantum numbers such as A. Also, the A invariance scheme permits a $\pi^o\gamma\gamma$ decay mode which should then compete favorably with $\eta \rightarrow 3\pi$.

Gell-Mann, Sharp, and Wagner[6] proposed a "rho dominance" model which attempted to relate the several decay modes of the ω meson and the decay $\pi^o \rightarrow \gamma\gamma$. It incidentally made the prediction that the branching ratio

$$\frac{\eta^o \rightarrow \pi^+\pi^-\gamma}{\eta^o \rightarrow \gamma\gamma} \sim 0.2$$

on the basis of coupling constants alone. This would explain the apparent difficulty with the relative rates for these two decay modes. In this model (which is based on the equivalent quantum numbers of the ρ and the photon) the η^o decays virtually into two ρ^o mesons which then decay into a single photon or into $\pi^+\pi^-$. The model makes no attempt to discuss the anomalously large three pion decay modes.

2. The Three Pion Decays

The peculiarities of the overall η^o decay scheme have not yet been satisfactorily explained. Because physicists do not really know how to predict absolute decay rates from first principles this is not particularly surprising. However, in discussing the three pion modes one should be on firm ground. No matter what difficulties arise in comparing decays involving real photons to those involving three pions, the $\eta^o \to \pi^o\pi^o\pi^o$ decay mode should be related exactly to the $\eta^o \to \pi^+\pi^-\pi^o$ mode. The difference between these two modes should depend only on calculable isotopic spin and symmetry effects.

Following Zemach[4] we describe the most general amplitude for decay into a $J^P = 0^-$ and $I = 1$ system of three pions as

$$M = A\ \underline{a}\ (\underline{b} \cdot \underline{c}) + B\ \underline{b}\ (\underline{a} \cdot \underline{c}) + C\ \underline{c}\ (\underline{a} \cdot \underline{b}).$$

Here $\underline{a}$, $\underline{b}$, $\underline{c}$ are vectors representing the isotopic spins of π_1, π_2, π_3 respectively and A, B, C are form factors describing the structure of the final state interactions among the pions. In order that the total amplitude M be symmetric under the interchange of any two pions we must have

$$A(\pi_1;\ \pi_2,\ \pi_3) = A(\pi_1;\ \pi_3,\ \pi_2)$$

and

$$A(\pi_1;\ \pi_2,\ \pi_3) = B(\pi_2;\ \pi_3,\ \pi_1) = C(\pi_3;\ \pi_1,\ \pi_2).$$

In terms of the charged states of the pions we have, for a transition to a final state with $|I, I_z> = |1, 0>$

$$M = A(a_o b_o c_o + a_o b_+ c_- + a_o b_- c_+) + B(b_o c_o a_o + b_o c_+ a_- + b_o c_- a_+)$$
$$+ C(c_o a_o b_o + c_o a_+ b_- + c_o a_- b_+).$$

In placing the experimental points for $\eta^o \to \pi^+\pi^-\pi^o$ on a triangular Dalitz plot we adopt the convention that π_1, π_2, π_3 (represented by isotopic spin vectors a, b, c) are π^+, π^-, π^o respectively. That is, we relabel the pions by their charge. Then $M(\eta^o \to \pi^+\pi^-\pi^o) = C$. We cannot distinguish among the three π^o so we plot the experimental points for $\eta^o \to \pi^o\pi^o\pi^o$ in a single sextant region of the Dalitz plot. The amplitude for this process is then $M(\eta^o \to \pi^o\pi^o\pi^o) = A + B + C$. With the pions in $\eta^o \to \pi^+\pi^-\pi^o$ labelled by their charge the distribution of density on the Dalitz plot is determined by the amplitude $C(\pi^o;\pi^+,\pi^-) = C(\pi^o;\pi^-,\pi^+)$. A labelling system based on charge is inconvenient when comparing the $\pi^+\pi^-\pi^o$ and $\pi^o\pi^o\pi^o$ decay modes. For the purpose of computing the branching ratio we place all the points for each mode in one sextant region of the Dalitz plot. Zemach shows that the branching ratio is then

$$R\left[\frac{\pi^o\pi^o\pi^o}{\pi^+\pi^-\pi^o}\right] = \frac{\int\limits_{\substack{\text{phase}\\ \text{space}}} |A + B + C|^2 \, d\rho}{2\int\limits_{\substack{\text{phase}\\ \text{space}}} \left(|A|^2 + |B|^2 + |C|^2\right) d\rho}$$

where the integral is computed over the single sextant region. $R\left(\frac{\pi^o\pi^o\pi^o}{\pi^+\pi^-\pi^o}\right)$ is a maximum for the "completely symmetric" situation where $A = B = C =$ constant. Then,

$$R\left(\frac{\pi^o\pi^o\pi^o}{\pi^+\pi^-\pi^o}\right) = \frac{9|A|^2 \int d\rho_{ooo}}{6|A|^2 \int d\rho_{+-o}} = 1.5\,\frac{\rho(\pi^o\pi^o\pi^o)}{\rho(\pi^+\pi^-\pi^o)} = 1.73.$$

If there are final state interactions and the form factors are not constant then

$$R\left(\frac{\pi^o\pi^o\pi^o}{\pi^+\pi^-\pi^o}\right) < 1.73.$$

Consider the behavior of the form factors by expanding them in a power series in energy:

$$A = A_o\left(1 + \alpha S_+ + \beta S_+^{\,2} + \gamma\, S_- S_o + \ldots\right)$$

$$B = A_o\left(1 + \alpha S_- + \beta S_-^{\,2} + \gamma\, S_o S_+ + \ldots\right)$$

$$C = A_o\left(1 + \alpha S_o + \beta S_o^{\,2} + \gamma\, S_+ S_- + \ldots\right)$$

where A_o, α, β, γ are complex coefficients and the S_i are energy variables $S_i = W_i - 1/3\, M_\eta$. (Note that $S_+ + S_- + S_o = 0$.) If $A = B = C = A_o$ we have: (1) a uniform Dalitz plot density for $\eta^o \to \pi^+\pi^-\pi^o$, (2) a uniform Dalitz plot density for $\eta^o \to \pi^o\pi^o\pi^o$, and (3) the maximum branching ratio

$$R\left(\frac{\pi^o\pi^o\pi^o}{\pi^+\pi^-\pi^o}\right) = 1.73.$$

The next simplest situation is $A = A_o(1 + \alpha S_+)$, etc. and the amplitude for $\eta^o \to \pi^+\pi^-\pi^o$, $C = A_o(1 + \alpha S_o)$, does not yield a constant Dalitz plot density. For this situation we have: (1) a Dalitz plot density $\eta^o \to \pi^+\pi^-\pi^o$ which depends on S_o, the energy of the neutral pion, (2) a uniform Dalitz plot density for $\eta^o \to \pi^o\pi^o\pi^o$ $\left(M[\pi^o\pi^o\pi^o] = A + B + C = A_o[3 + \alpha(S_+ + S_- + S_o)] = 3A_o \text{ because } S_+ + S_- + S_o = 0\right)$, and (3) a branching ratio less than the maximum $R\left(\frac{\pi^o\pi^o\pi^o}{\pi^+\pi^-\pi^o}\right) = 1.73$. It should be pointed out that the absence of a linear term in the completely symmetric amplitude for $\eta^o \to \pi^o\pi^o\pi^o$ makes the Dalitz plot for this process an excellent place to look for the presence of quadratic terms in the form factor.

Within a year after the discovery of the η^o attention began to focus on the S_o energy dependence of the Dalitz plot density for $\eta^o \to \pi^+\pi^-\pi^o$ and its relation to the branching ratio $R\left(\frac{\pi^o\pi^o\pi^o}{\pi^+\pi^-\pi^o}\right)$. The decay of the η^o into three pions has features which are very similar to the decays of K mesons into three pions. In each situation the pions are presumed to be in a pure $I = 1$ state although the mechanisms leading to this state are quite different. In addition, the total energy, Q, available for pionic motion is comparable (and low) in each case. If any structure is due to final state interactions among the pions, then the two situations ought to exhibit a behavior which is similar, perhaps identical. It had been demonstrated by Ferro-Luzzi et al.[20] that τ decay ($K^+ \to \pi^+\pi^+\pi^-$) fits a linear matrix element (analagous to $C = A_o(1 + \alpha S_o)$ for $\eta^o \to \pi^+\pi^-\pi^o$). Further, it had been noted from the earliest Dalitz plot[3] for $\eta^o \to \pi^+\pi^-\pi^o$ that the density had a marked dependence on S_o.

A number of authors[16,21-24] pointed out the similarities between the η and K decays. Of particular interest are the papers by Wali[16] and Berley, Colley, and Schultz.[23] Wali worked out the relationship between the π^o energy spectrum and the branching ratio $R\left(\frac{\pi^o\pi^o\pi^o}{\pi^+\pi^-\pi^o}\right)$. Recasting his formulas in terms of T_o in order to conform to later usage,[25,26] we have $M(\eta^o \to \pi^+\pi^-\pi^o) \sim 1 + \alpha\left(\frac{2T_o}{T_{max}} - 1\right)$ and $R\left(\frac{\pi^o\pi^o\pi^o}{\pi^+\pi^-\pi^o}\right) = \frac{1.73}{1 + \frac{1}{4}|\alpha|^2}$. Wali calculated the shape of the π^o energy spectrum and the corresponding prediction for $R\left(\frac{\pi^o\pi^o\pi^o}{\pi^+\pi^-\pi^o}\right)$ for various values of α. Although the data were insufficient for exact determination of α, he found that the slope of the energy dependence seemed to agree with the prediction from τ decay and that $R\left(\frac{\pi^o\pi^o\pi^o}{\pi^+\pi^-\pi^o}\right)$ probably lay between 1.6 and 1.7. Berley, Colley, and Schultz[23] examined the available τ, τ' and η decays and demonstrated that the slopes of the energy dependence (i.e., α) agreed very well indeed.

A linear dependence on the π^o energy is not the only simple possibility for the form factor. An s-wave $\pi\pi$ resonance will also lead to a non-uniform Dalitz plot density. Brown and Singer have attempted to describe the Dalitz plot and branching ratio $R\left(\frac{\pi^o\pi^o\pi^o}{\pi^+\pi^-\pi^o}\right)$ using their σ resonance model.[27,28] In this model the matrix element form factor has a resonance behavior rather than a linear energy dependence. In the limit $\Gamma_\sigma = 0$ the branching ratio $R\left(\frac{\eta^o \to \pi^o\pi^o\pi^o}{\eta^o \to \pi^+\pi^-\pi^o}\right)$ is simply the branching ratio $R_\sigma\left(\frac{\sigma^o \to \pi^o\pi^o}{\sigma^o \to \pi^+\pi^-}\right) = 0.5$ (or 0.55 if the $\pi^\pm - \pi^o$ mass difference is accounted for). A non-zero resonance width increases the ratio R. For the range of values of M_σ and Γ_σ which might fit the data, Brown and Singer showed that the ratio $R\left(\frac{\pi^o\pi^o\pi^o}{\pi^+\pi^-\pi^o}\right)$ might take on any value between 1.2 and 1.5.

Crawford et al.,[25] with a highly purified sample of 109 events, studied the $\eta^o \to \pi^+\pi^-\pi^o$ Dalitz plot. They were able to find acceptable fits to the π^o energy dependence with either model. The fit to a linear matrix element gave $\alpha = 0.45 \pm 0.07$ which implies $R\left(\frac{\pi^o\pi^o\pi^o}{\pi^+\pi^-\pi^o}\right) = 1.63 \pm 0.03$. The slightly better fit to the σ model gave $M_\sigma = 392 \pm 9$ MeV and $\Gamma_\sigma = 88 \pm 15$ MeV which implies $R\left(\frac{\pi^o\pi^o\pi^o}{\pi^+\pi^-\pi^o}\right) = 1.28 \pm .07$. Foster et al.[26] analyzed 274 background-free decays $\eta^o \to \pi^+\pi^-\pi^o$. They found a good fit to a linear matrix element with $\alpha = 0.41 \pm 0.06$ (which implies $R\left(\frac{\pi^o\pi^o\pi^o}{\pi^+\pi^-\pi^o}\right) = 1.63 \pm 0.02$ in good agreement with Crawford et al.) They were also able to fit the σ model with resonance parameters $M_\sigma = 407^{+25}_{-12}$ MeV and $\Gamma_\sigma = 117 \pm 15$ MeV. This implies $R\left(\frac{\pi^o\pi^o\pi^o}{\pi^+\pi^-\pi^o}\right) = 1.49 \pm 0.07$ and is not in particularly good agreement with Crawford et al.

It appeared that both models could explain the experimental data on the π^o energy dependence. The chief difference was that the linear matrix element model predicted higher values of $R\left(\frac{\pi^o\pi^o\pi^o}{\pi^+\pi^-\pi^o}\right)$, close to the allowed maximum. However, the Brown and Singer model was not as successful when applied to K decays.[29,30] The resonance parameters needed to fit the K decay spectra were not in agreement with those for the η decay. This is perhaps not a severe criticism of the σ model because there is not enough energy, Q, available in K decays to produce the σ on the mass shell. Taylor et al.,[31] in a very interesting paper, pointed out that one could get a fit to the σ model and determine the resonance parameters by expanding the resonance form in a power series about $T_o = 0$ and dropping quadratic and higher terms. In this approximation the σ model is mathematically equivalent to the linear matrix element model and the data cannot distinguish between them; only in a situation where the π^o energy spectrum cannot be described by a linear approximation can a definitive test be made.

In early 1966 the experimental situation on the parameter α was relatively clear. The π^o energy spectrum is well fit by a linear matrix element. The linear matrix element model then makes a unique prediction for $R\left(\frac{\pi^o\pi^o\pi^o}{\pi^+\pi^-\pi^o}\right) \cong 1.63$. If the σ resonance model is considered, lower values of $R\left(\frac{\pi^o\pi^o\pi^o}{\pi^+\pi^-\pi^o}\right)$ can be obtained. However, this model does not give a consistent picture for K and η decays (the linear matrix element model does) and, as we have noted above, there is little direct evidence for the existence of a σ meson.

If the experimental measurements of the parameter α are in agreement and unambiguously imply $R\left(\frac{\pi^o\pi^o\pi^o}{\pi^+\pi^-\pi^o}\right) \simeq 1.63$, the experimental measurements of R are less certain. All but one of the experiments measuring R were done in bubble chambers which are inadequate for such a measurement. If the probability of observing a single gamma ray from a decay is P_γ, then the probability of observing six gamma rays from the same decay is proportional to $(P_\gamma)^6$. If P_γ is small, as it is in a bubble chamber, a slight mis-estimate of P_γ is disastrous. For instance, Crawford et al.[13] found $\frac{\eta^o \to \gamma\gamma}{\eta^o \to \text{charged}} = .99 \pm .48$ and $\frac{\eta^o \to \pi^o\pi^o\pi^o}{\eta^o \to \text{charged}} = .66 \pm .25$. This implies that $\frac{\eta^o \to \text{neutrals}}{\eta^o \to \text{charged}} = 1.65 \pm .53$ and is in gross disagreement with the more reliable experiments which measure this rate by counting missing neutrals (see, for example Ref. 3). Perhaps the best experiment on the neutral branching ratios up to this time (April, 1966) was that of Bacci et al.[17] In this experiment lead glass counters were used to detect the gamma rays. Although such a technique is fraught with difficulties it should yield better results than bubble chamber experiments. They found

$$\frac{\eta^o \to \gamma\gamma}{\eta^o \to \text{other neutral modes}} = 0.8 \pm .2$$

but made no attempt to resolve the "other neutral modes" into contributions from $\pi^o\gamma\gamma$ and $3\pi^o$. If the "other neutral modes" were entirely $\eta^o \to \pi^o\pi^o\pi^o$, this measurement, along with $\frac{\eta^o \to \text{neutrals}}{\eta^o \to \text{all modes}} \simeq .7$ and $\frac{\eta^o \to \pi^+\pi^-\pi^o}{\eta^o \to \text{all modes}} \simeq .23$ (both reasonably reliable numbers), gives $R\left(\frac{\pi^o\pi^o\pi^o}{\pi^+\pi^-\pi^o}\right) = 1.71^{+.30}_{-.21}$.

As of early April, 1966 there was no compelling reason to believe that $R\left(\frac{\pi^o\pi^o\pi^o}{\pi^+\pi^-\pi^o}\right)$ was not consistent with the predictions of the linear matrix element model which, based on reliable data, explained the π^o energy spectrum in $\eta^o \to \pi^+\pi^-\pi^o$.

C. η^o Branching Ratios after April, 1966

On April 25, 1966 a paper published by DiGiugno et al.[15] announced experimental evidence for the large branching ratio

$$\frac{\eta^o \to \pi^o\gamma\gamma}{\eta^o \to \text{neutrals}} = .375 \pm .036.$$

Their measurement of $\dfrac{\eta^o \to \gamma\gamma}{\eta^o \to \text{"other neutrals"}} = 0.7$ agrees rather well with the earlier results of Bacci et al.[17] Therefore, the change in the experimental situation is simply that the "other neutral modes" (other than $\eta^o \to \gamma\gamma$) are not entirely $\eta^o \to 3\pi^o$ as had been previously supposed. The introduction of a large $\eta^o \to \pi^o\gamma\gamma$ decay mode does not alter any of the previous branching ratio results except to decrease the amount of $\eta^o \to 3\pi^o$ and the ratio $R\left(\dfrac{\pi^o\pi^o\pi^o}{\pi^+\pi^-\pi^o}\right)$. With the DiGiugno et al. measurement of $\dfrac{\eta^o \to 3\pi^o}{\eta^o \to \text{neutrals}} = .209 \pm .027$ and the previously established ratios $\left(\dfrac{\eta^o \to \pi^+\pi^-\pi^o}{\eta^o \to \text{all modes}} = .23 \text{ and } \dfrac{\eta^o \to \text{neutrals}}{\eta^o \to \text{all modes}} = .71\right)$ we have $R\left(\dfrac{\pi^o\pi^o\pi^o}{\pi^+\pi^-\pi^o}\right) \simeq 0.65$. This is well below the predictions of any existing models including the σ model of Brown and Singer and indicates something really amiss.

Several months ago after DiGiugno et al. announced their findings, Wahlig et al.[32] published the results of a spark chamber experiment which yielded $\dfrac{\eta^o \to \pi^o\gamma\gamma}{\eta^o \to \gamma\gamma} \leq .32 \pm .09$, more consistent with the earlier picture η decays. (The DiGiugno results imply $\dfrac{\eta^o \to \pi^o\gamma\gamma}{\eta^o \to \gamma\gamma} = .90 \pm .10$.) The ratio of Wahlig et al. is an upper limit. They examined only events with 2γ or 4γ in their spark chambers. They pointed out that all their observed 4γ events in the η^o region could be explained by feed-down from $\eta^o \to 3\pi^o \to 6\gamma$ events where two gamma rays are lost. Thus, their results could be interpreted as a complete absence of $\eta^o \to \pi^o\gamma\gamma$ with an experimental uncertainty expressed as an upper limit on the ratio $\dfrac{\eta^{o} \to \pi^{o}\gamma\gamma}{\eta^{o} \to \gamma\gamma}$.

While the two preceeding experiments are in rather gross disagreement, the question of the existence of a large amount of $\eta^{o} \to \pi^{o}\gamma\gamma$, and consequently a small $R\left(\dfrac{\pi^{o}\pi^{o}\pi^{o}}{\pi^{+}\pi^{-}\pi^{o}}\right)$, has been raised. A number of theoretical papers on the subject followed as well as a large number of experiments (see Table II below). If the results of DiGiugno et al. are incorrect and there is essentially no $\eta^{o} \to \pi^{o}\gamma\gamma$ decay mode (the results of Wahlig et al. could be interpreted this way) then the theoretical speculations of Sec. I. B. 2. do not need to be revised. In that case the $\eta \to 3\pi$ modes are consistent with a linear matrix element. If DiGiugno et al. are correct a radical revision of the theoretical explanation of the $\eta \to 3\pi$ decays is in order.

Veltman and Yellin[33] suggested that (in the presumed absence of resonance behavior in the $\pi\pi$ system) a value of $R\left(\dfrac{\pi^{o}\pi^{o}\pi^{o}}{\pi^{+}\pi^{-}\pi^{o}}\right)$ more than 15 to 20% below the allowed maximum of $R = 1.73$ would imply the presence of a $\Delta I = 3$ transition. If C is conserved the 3π system can only be in $I = 1$ or $I = 3$ states $[G(3\pi) = -1,\ C(3\pi) = C(\eta^{o}) = +1,$ and $G(3\pi) = C(-1)^{I}]$. Consequently, in the absence of C violation only $\Delta I = 1$ and $\Delta I = 3$ transitions can occur from the initial state of the η^{o} with $I = 0$. Feinberg and Pais[34] have shown that, if the final state of the three pions from $\eta \to 3\pi$ is a mixture of $I = 1$ and $I = 3$, then $R\left(\dfrac{\pi^{o}\pi^{o}\pi^{o}}{\pi^{+}\pi^{-}\pi^{o}}\right) = \left|\dfrac{\sqrt{2}\,\mu - \sqrt{3}}{\sqrt{3}\,\mu + \sqrt{2}}\right|^{2} \times 1.14$

where μ is the ratio of the amplitudes

where μ is the ratio of the amplitudes $\mu = \dfrac{M(\Delta I = 3)}{M(\Delta I = 1)}$ and the factor 1.14 is the ratio of the phase spaces $\dfrac{\rho_{ooo}}{\rho_{+-o}}$. If $\mu = 1/137$, that is, if the $\Delta I = 3$ transition is a second order electromagnetic transition (two virtual photons are emitted and reabsorbed and $\Delta I = 1$ at three of the four vertices) then we would have $R\left(\dfrac{\pi^{o}\pi^{o}\pi^{o}}{\pi^{+}\pi^{-}\pi^{o}}\right) = 1.67$, only slightly lower than the allowed maximum of 1.73. Veltman and Yellin noted that $R\left(\frac{\pi^0\pi^0\pi^0}{\pi^+\pi^-\pi^0}\right) \simeq 0.5$ implies $|\mu| \geq 0.31$ so that the data of DiGiugno et al. might well indicate a substantial $\Delta I = 3$ amplitude. They did not speculate as to what sort of $\Delta I = 3$ transition might exist in nature.

Woo[35] also addressed the problem of a small experimental value for $R\left(\frac{\pi^0\pi^0\pi^0}{\pi^+\pi^-\pi^0}\right)$. Woo noted that a $\Delta I = 3$ transition was a possibility but also considered a quadratic matrix element involving P-waves in the $\pi\pi$ system. If P-waves were only present in the $\eta^0 \to \pi^+\pi^-\pi^0$ decay and the S-waves were somehow suppressed, a small value of $R\left(\frac{\pi^0\pi^0\pi^0}{\pi^+\pi^-\pi^0}\right)$ might be obtained. However, by using S and P-waves which were consistent with what was known about the $\pi\pi$ interaction, Woo was unable to explain a value of $R\left(\frac{\pi^0\pi^0\pi^0}{\pi^+\pi^-\pi^0}\right)$ less than 1. As did Veltman and Yellin, Woo concluded that the DiGiugno et al. value of $R\left(\frac{\pi^0\pi^0\pi^0}{\pi^+\pi^-\pi^0}\right) \simeq .65$ would demand a $\Delta I = 3$ transition.

Adler,[36] in a very exciting paper, made a definite (and exotic) proposal on what sort of $\Delta I = 3$ transition might exist which would explain the $\eta \to 3\pi$ puzzle. The successes of current algebra calculations in explaining $K \to 3\pi$ decay parameters had led a number of authors (see the references in Adler's paper) to apply similar calculations to $\eta \to 3\pi$ decays. There was some reason to suspect that a first order electromagnetic transition $\eta \to 3\pi$ might be forbidden or suppressed in a current algebra scheme. Adler observed that a second order electromagnetic transition (which might include a $\Delta I = 3$ part without any revision of the present picture of the electromagnetic interaction) would also be forbidden. He therefore proposed a $C = +1$ iso-tensor addition to the electromagnetic current. He showed that such an interaction could explain the π^0 energy dependence of the $\eta^0 \to \pi^+\pi^-\pi^0$ decay within the framework of current algebra and would lead to an $I = 3$ admixture in the 3π final state. Adler also observed that such a C = + 1 electromagnetic iso-tensor interaction was not in conflict with any existing experimental data.

Several months later Adler published a short erratum.[36] It stated that his observation about the forbidden nature of a second order electromagnetic transition in the current algebra scheme was incorrect. An I = 3 admixture in the 3π final state might arise because the first order ($\sim \alpha^2$) electromagnetic transition $\eta \to 3\pi$ was forbidden while the second order ($\sim \alpha^4$) was not. Consequently it is not necessary to invent a C = +1 iso-tensor electromagnetic current to account for the experimental situation. As we have noted above, however, the $\eta \to 3\pi$ decays are already much "too large." A noticeable transition with a coupling $\sim \alpha^4$ is difficult to imagine since the $\eta \to 3\pi$ decay modes are inexplicably large even with α^2 coupling. If $\Delta I = 3$ transitions are needed to explain a low value of $R\left(\frac{\pi^o\pi^o\pi^o}{\pi^+\pi^-\pi^o}\right)$ Adler's model is still an attractive possibility. In this picture a virtual photon, emitted and reabsorbed, can cause a $\Delta I = 3$ transition by changing I by $\Delta I = 1$ at one vertex and $\Delta I = 2$ at the other.

The possible existence of a $\Delta I = 3$ transition for $\eta \to 3\pi$, whatever that implies, makes it very desirable to clear up the experimental situation on $R\left(\frac{\pi^o\pi^o\pi^o}{\pi^+\pi^-\pi^o}\right)$. A large number of experiments, discussed below, have followed the papers of Adler and DiGiugno et al.[15]

It is interesting to note that a number of more recent experiments[37-40] with more statistics on the $\eta^o \to \pi^+\pi^-\pi^o$ Dalitz plot bear out the conclusions of the earlier experiments.[25,26] The Dalitz plot density is consistent with a linear matrix element and the value of the parameter α has not changed appreciably. The linear matrix element model which accounts for the $\eta^o \to \pi^+\pi^-\pi^o$ Dalitz plot density variation in a simple way still predicts $R\left(\frac{\pi^o\pi^o\pi^o}{\pi^+\pi^-\pi^o}\right) \simeq 1.6$. Price and Crawford[37] were able to account for the $\eta^0 \to \pi^+\pi^-\pi^0$ Dalitz plot for 640 events with quadratic and cubic matrix elements as well as a linear matrix element. They were able to obtain an excellent fit to the data with a cubic matrix element which implied a value of $R\left(\frac{\pi^0\pi^0\pi^0}{\pi^+\pi^-\pi^0}\right)$ as low as 0.7. A large cubic term was necessary, however, to predict a value of $R < 1.1$. Price and Crawford did not constrain the coefficients for the cubic matrix element in any way. Such a matrix element implies the presence of D-waves and is not particularly attractive. However, they were able to demonstrate that a pure $I = 1$ transition might be able to account for a low experimental value of $R\left(\frac{\pi^0\pi^0\pi^0}{\pi^+\pi^-\pi^0}\right)$. Of course it is not pleasant to contemplate the presence of a D-wave momentum barrier in a transition which is anomalously large to begin with.

Table II lists the published experiments on the neutral branching ratios in chronological order beginning with the work of DiGiugno et al. in April of 1966. The results are in terms of the following ratios:

$$R_1 = \frac{\eta^0 \to \gamma\gamma}{\eta^0 \to \text{all neutrals}}$$

$$R_2 = \frac{\eta^0 \to \pi^0\pi^0\pi^0}{\eta^0 \to \text{all neutrals}}$$

$$R_3 = \frac{\eta^0 \to \pi^0\gamma\gamma}{\eta^0 \to \text{all neutrals}}$$

$$R_4 = \frac{\eta^0 \to \pi^0\gamma\gamma}{\eta^0 \to \gamma\gamma}$$

$$R_5 = \frac{\eta^0 \to \pi^0\pi^0\pi^0}{\eta^0 \to \gamma\gamma}$$

All of the experiments listed in Table II can be classified as one of three general types:

Type A. Determination of branching ratios by counting relative numbers of gamma rays.

Type B. Kinematic analysis of four gamma ray events.

Type C. Study of the energy spectrum of a single detected gamma ray.

Table II. Neutral Branching Ratio Experiments.

Author	Method	Result
1. DiGiugno et al.[15] (April, 1966)	Lead glass counters (Type C)	R_1 = .416±.022 R_2 = .209±.027 R_3 = .375±.036
2. Wahlig et al.[32] (July, 1966)	Spark chambers (Type B)	$R_4 \leq 0.50$ (90% confidence level)
3. Strugalski et al.[41] (Jan. 1967)	Xenon bubble chamber (Type A)	R_4 = 0.86±0.47
4. Grunhaus[42] (Dec. 1966)	Spark Chambers (Type A)	R_1 = 0.44±.07 R_2 = 0.29±.10 R_3 = 0.27±.10
5. Feldman et al.[43] (May, 1967)	Spark chambers (Type A)	R_1 = .579±.052 R_2 = .177±.035 R_3 = .244±.050
6. Bonany and Sonderegger[44] Sept., 1967)	Spark chambers (Type B)	$R_4 < 0.13$ (95% confidence level)
7. Jacquet et al.[45] (Nov. 1967)	Heavy liquid bubble chamber (Type B)	$R\left(\frac{\pi^0\gamma\gamma}{\text{all modes}}\right) < 0.12$ (95% confidence level)
8. Buniatov et al.[46] (Nov. 1967)	Spark chambers Type (a)	R_1 = .59±.033 R_2 = .41±.033 $R_3 < 0.12$ (95% confidence level)
9. Baltay et al.[47,49] (Dec. 1967)	Deuterium bubble chamber (Type C)	$R_4 < 0.28$ (95% confidence level) R_5 = 0.88±0.16

Table II. (continued)

Author		Method	Result
10.	Bullock et al.[48] (August, 1968)	Heavy liquid bubble chamber (Type A)	$R\left(\frac{\pi^0\pi^0\pi^0}{\pi^+\pi^-\pi^0}\right) = 1.47^{+0.20}_{-0.17}$
11.	Baglin et al.[51] (June, 1969)	Heavy liquid bubble chamber (Type A)	$R\left(\frac{\pi^0\pi^0\pi^0}{\pi^+\pi^-\pi^0}\right) = 1.50^{+0.15}_{-0.29}$
			$R\left(\frac{\gamma\gamma}{\pi^+\pi^-\pi^0}\right) = 1.72\pm0.25$
12.	Cox et al.[52] (March, 1970)	Hydrogen bubble chamber (Type C)	$R_1 = .486\pm.036$
			$R_2 = .392\pm.042$
			$R_3 = .122^{+.052}_{-.044}$
13.	Devons et al.[53,50] (June, 1970)	Spark chambers (Types A, B)	$R_3 < .07$ (90% confidence level)
			$R_5 = 0.75\pm0.09$

In attempting to determine the branching ratio $R\left(\frac{\eta^0 \rightarrow \pi^0\gamma\gamma}{\eta^0 \rightarrow \text{all neutrals}}\right)$ a principal problem has been to separate the decay from background reactions which produce a $\pi^0\pi^0$ system with a mass near that of the η^0. This problem is common to all three types (A, B, C) of experiments listed in Table II and has been handled with varying degrees of credibility.

Experiments of Type A: These experiments measure the η^0 neutral branching ratios by the brute force method of counting gamma rays. In attempting to measure the amount of $\eta^0 \rightarrow \pi^0\gamma\gamma$ one must contend with a substantial uncertainty due to mis-estimates of gamma ray detection efficiency. If the probability of observing a single gamma ray (integrated over the gamma ray energy and over the geometry of the detection system) is q, then the probability of observing n gamma rays when m gamma rays were produced is given by the binomial relationship

$$P_{n/m} = \frac{m!}{n!(m-n)!} q^n(1-q)^{m-n}.$$

If q is not sufficiently large ($q \lesssim .75$) then the number of 4γ events from $\eta^o \to 3\pi^o \to 6\gamma$ may be much greater than the number of 4γ events from $\eta^o \to \pi^o\gamma\gamma \to 4\gamma$. At the same time, the majority of true 4γ events will appear as 2γ events, etc. It is obviously difficult to separate 2, 4, and 6γ decay modes in a situation where two of the three modes appear more like their competitors than themselves. However, if the integrated probability q is large so that the majority of true 6γ decays appear as 5 and 6γ events, etc. and if the statistics are large, experiments of Type A can be quite convincing. Of course the notion of an "integrated probability" q has no meaning if the statistics are not large.

If the integrated detection probability q is large and if the statistics are large, then one can meaningfully discuss the feed-down from true 6γ decays into observed 5, 4, and 3γ events according to the binomial relation for $P_{n/m}$ above. That is, if there are a very large number of detected 5 and 6γ events, then the number of detected 3 and 4γ events expected can be accurately predicted from the relative numbers of 5 and 6γ events. If this is not the case, then one must rely heavily on Monte Carlo calculations to estimate the feed-down which cannot be inferred from the data itself. This difficulty has plagued all of the experiments of Type A listed in Table II. The experiment reported in this thesis is the first experiment of this type (A) which has a sufficiently large integrated probability q and sufficient numbers of 5 and 6γ events to minimize the reliance on Monte Carlo calculations. Table III shows the integrated probability q and the estimated feed-down from true 6γ decays for the experiments of Type A. The feed-down ratios are calculated on the basis of the binomial relation. The Monte Carlo predictions for the experiments which report them are extremely close to the ratios in the table.

Table III. Experiments of Type A.

	Author	Integrated probability q	Number of observed 6γ	Probability of detecting $n\gamma$ from a true 6γ event $n = 6$	5	4	3	2	1	0
1.	Strugalski[41] et al.	.53	4	.02	.13	.27	.31	.20	.07	.01
2.	Grunhaus[42]	.75	17	.18	.36	.30	.13	.03	-	-
3.	Feldman[43] et al.	.55	13	.03	.14	.28	.30	.19	.06	.01
4.	Buniatov[46] et al.	.61	57	.05	.20	.32	.27	.13	.03	-
5.	Bullock[48] et al.	.63	69	.06	.22	.32	.25	.11	.03	-
6.	Baglin[51] et al.	.70	199	.12	.30	.32	.19	.06	.01	-
7.	Devons[53] et al.	.67	~116	.09	.27	.33	.22	.08	.02	-
8.	This experiment	.88	~2500*	.46	.38	.13	.02	-	-	-

* Based on ~27% of data accumulated. See Sec. IV. A. below.

In each of the experiments of Table III the neutral branching ratios were determined by counting relative numbers of gamma rays except in those of Bullock et al.[48] and Baglin et al.[51] These two experiments measured the ratio $R\left(\frac{\pi^0\pi^0\pi^0}{\pi^+\pi^-\pi^0}\right)$ directly in the same sample of film. They calculated the amount of $\eta^0 \to 3\pi^0$ from the number of 5 and 6γ events and estimates of their efficiency for detecting this number. The experiment of Devons et al.[53] did an extensive analysis of the 4γ events (experiment Type B) in addition to counting gamma rays.

<u>Experiments of Type B</u>: These experiments concentrate on analysis

of 4γ events. By kinematic reconstruction, they attempt to resolve $\eta^{o} \to \pi^{o}\gamma\gamma \to 4\gamma$ events from background 4γ events. These background events arise from two sources: (1) production of a $\pi^{o}\pi^{o}$ system with a mass near that of the η^{o} and, (2) $\eta^{o} \to 3\pi^{o} \to 6\gamma$ events where two gamma rays escape detection.

There are three principal difficulties with this type of experiment:

(1) The results depend on the ability to calculate the detection efficiency for 4γ.

(2) Pairing ambiguities: there are six ways of pairing 4γ if we assume a $\pi^{o}\gamma\gamma$ system. For a $\pi^{o}\pi^{o}$ system there are three possible pairs.

(3) The 4γ sample is contaminated by $\eta^{o} \to 3\pi^{o} \to 6\gamma$ events where two gamma rays have escaped detection. Of these experiments, only that of Devons et al.[53] examines 6γ events. The others must estimate the feed-down into 4γ events.

Experiments of Type C: These experiments have the advantage of not being terribly sensitive to q, the probability of observing a single gamma ray. The observed decay is $\eta^{o} \to \gamma + X$ where X may be any number of undetected neutral particles. The observed energy spectrum of the single detected gamma ray in the η^{o} rest frame is compared with that predicted from Monte Carlo calculations. If there is no $\eta^{o} \to \pi^{o}\gamma\gamma$ present one would see a broad peak in E_{γ} from $\eta^{o} \to 3\pi^{o}$ clearly separated from a narrow peak from $\eta^{o} \to \gamma\gamma$. The effect of a substantial amount of $\eta^{o} \to \pi^{o}\gamma\gamma$ is to fill in the valley between the two peaks. Gamma rays from a $\pi^{o}\pi^{o}$ system also fill in the valley. The principal problem is to separate any $\eta^{o} \to \pi^{o}\gamma\gamma$ from the $\pi^{o}\pi^{o}$ background. The expected distribution of observed gamma ray energies from $\eta^{o} \to \pi^{o}\gamma\gamma$ depends (only slightly) on the matrix element for this process and on the gamma ray detection efficiency of the system. Unlike experiments of types A and B, the dependence on gamma ray detection efficiency is linear. Naturally, a high degree of precision is necessary in measuring E_γ. For this reason such an experiment cannot be done with an array of spark chambers.

Three experiments of type C have been reported.[15,47,52] The bubble chamber experiment of Cox et al.[52] involves poor statistics and a questionable treatment of background. The bubble chamber experiment of Baltay et al.[47] is not particularly overwhelming statistically but their background treatment seems convincing. They find no evidence for $\eta^o \rightarrow \pi^o\gamma\gamma$. The experiment of DiGiugno et al.,[15] with greater statistics, finds a very large amount of $\eta^o \rightarrow \pi^o\gamma\gamma$. In this experiment a lead glass Cerenkov counter was used to measure the gamma ray energies.

Although there are a few experiments listed in Table II which find a large amount of $\eta^o \rightarrow \pi^o\gamma\gamma$, the majority find there to be little or none of this decay mode present. The high statistics experiment reported in this thesis confirms the majority findings.

II. EXPERIMENTAL METHOD

A. General Considerations

The η^o mesons are produced for analysis in the reaction $\pi^- p \rightarrow \eta^o n$ by colliding a π^- beam from the Berkeley Bevatron with a stationary proton target (liquid hydrogen). The reaction is studied by an array of neutron detectors and a set of lead plate spark chambers which constitute five sides of a cube surrounding the target (Fig. 1). The neutron is observed by one of 20 large scintillation counters and selected by its time of flight from target to detector. The gamma rays from the decay of the η^o (or associated π^o's) are detected by photographing showers produced in the lead plates of the spark chambers. Anticoincidence counters surrounding the hydrogen target veto any interaction in which charged particles are produced, including those events where the η^o decays by one of its charged modes.

Those neutral processes which can be initiated by a beam of our energy (589 MeV or 716 MeV/c) and which are expected to have sufficient cross section to be non-negligible are:

$$\pi^- p \rightarrow \eta^o n \qquad (1)$$

$$\rightarrow \pi^o n \qquad (2)$$

$$\rightarrow \pi^o \pi^o n \qquad (3)$$

$$\rightarrow \pi^o \pi^o \pi^o n. \qquad (4)$$

The neutral decays of the η^o meson involve only π^o mesons and gamma rays. Both the η^o and π^o decay so rapidly (the π^o into $\gamma\gamma$) that they do not emerge from the target. Thus we observe only

$$\pi^- + P \rightarrow n + \text{gamma rays.}$$

It is from the reconstruction of the observed patterns of gamma ray showers that the branching fractions of the η^o are obtained.

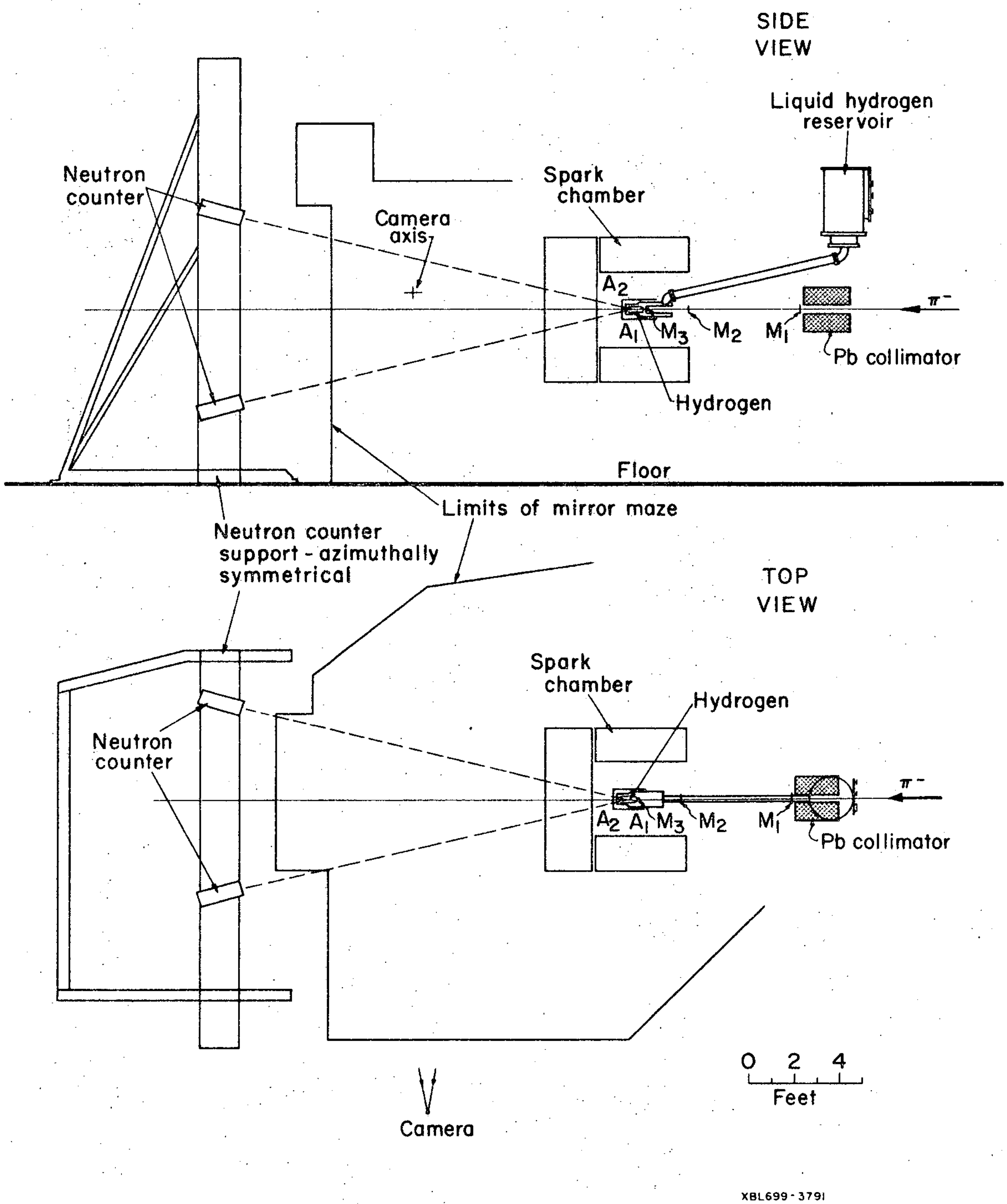

Fig. 1. Experimental layout.

The time of flight of the neutron between target and detector determines whether or not an event is photographed for analysis. The reactions (1) through (4) each have characteristic time of flight spectra, shown in Fig. 2(b). The sum of all these spectra yields the experimental distribution of Fig. 2(a). It is desirable to study the entire distribution. The background processes, (3) and (4), must be understood in detail. The charge exchange reaction (2), with its well determined kinematics and with the characteristic $\pi^o \rightarrow \gamma\gamma$ decay, provides a sensitive test of the detection system and of the analysis procedures. Consequently, no stringent requirements are imposed on the neutron time of flight (such as triggering only on the η^o peak).

Most of the data in this experiment were accumulated with a beam of momentum 716 MeV/c. Data were also taken at two momenta below (654, 686 MeV/c) and two momenta above (745, 772 MeV/c) this central value with the same counter geometry. Data at these momenta, especially the lowest (which is below η^o production threshold), provide valuable information about the background reactions (3) and (4).

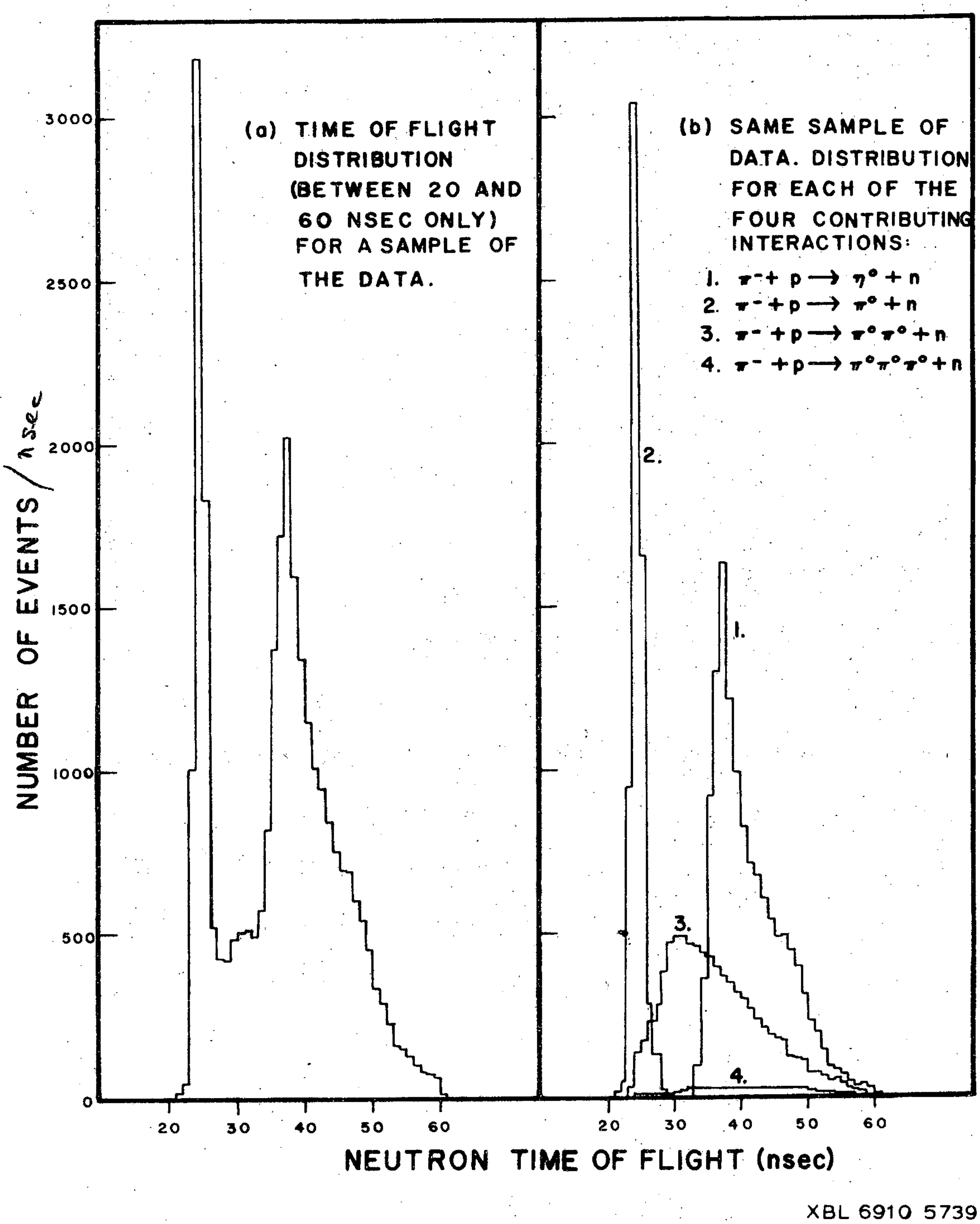

Fig. 2. Experimental time-of-flight distributions for a portion of the data at 716 MeV/c. The distributions in (b) represent approximate fits to the data.

B. Physical Arrangement of Apparatus

This section discusses certain general features of the experimental equipment and its deployment. A more detailed description of each piece of equipment is presented in Sec. III below.

The overall arrangements are shown in Fig. 1. The beam of pions is defined by three plane, circular counters in triple coincidence (M_1, M_2, M_3). The photomultiplier tubes are mounted on opposite sides of the beam to avoid counting off-axis pions through Čerenkov effects in the light guides. The first of the three counters is 1/2-in. thick, producing a very stable output pulse suitable for accurate timing. The third and last counter is a 1/16-in. thick wafer placed extremely close (1.7 in.) to the liquid hydrogen. The beam so defined is roughly the diameter of the last counter (3-in.) and is smaller than the target. The liquid hydrogen target is a cylinder 4-in. in diameter and 8-in. long placed coaxially with the beam. It is enclosed on the exit face and sides by two counters used in anticoincidence (Fig. 3). The exit-face counter (A_2) is a plane, square counter perpendicular to the beam. This counter vetoes events with charged reaction products in the forward direction as well as events where the beam pion passes through the target without interacting. The other veto counter (A_1) is a hexagonal cylinder surrounding the target and is in contact with the first, making a closed system in the forward direction. This counter eliminates charged reaction products at laboratory scattering angles up to 150 deg.

There are five spark chambers, each constituting one face of a cube which encloses a free volume of approximately one cubic meter and which contains the liquid hydrogen vessel. The pion beam enters this cubical volume perpendicular to and through the open face. Except for a hole to

(a)

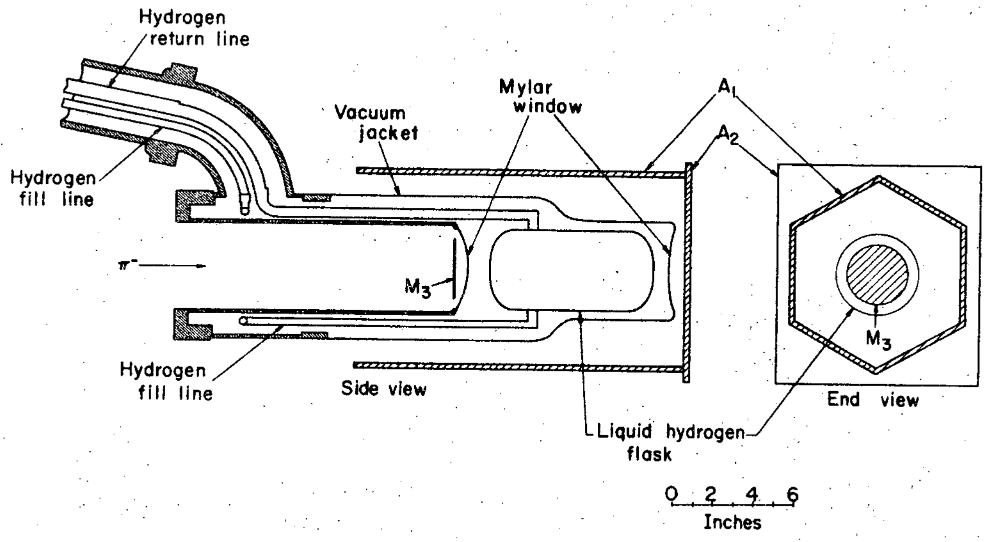

(b)

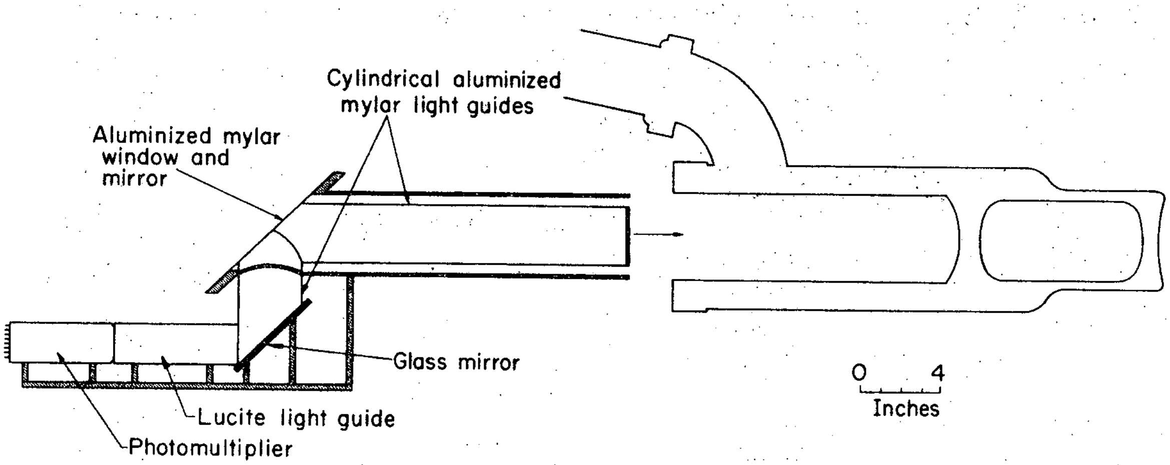

XBL 6910-5779

Fig. 3. Hydrogen target, veto counters, and the beam defining counter M_3.

admit the beam, the open face is guarded by a set of gamma ray detection counters (Fig. 4) to enclose more completely the hydrogen target. They are sandwiches of lead and scintillator, the total thickness being 4.5 radiation lengths. The four side spark chambers each contain ~ 7 radiation lengths. The back chamber, through which the unused beam passes, contains ~ 8 radiation lengths. The total solid angle subtended at the target by the combined system of spark chambers and gamma counters is 3.7 π ster.

Each spark chamber is viewed in orthogonal stereo. A system of 46 mirrors brings all 10 views to a single camera. An array of data lights is photographed with the spark chambers and displays the following information: the event (frame) number, which neutron counter fired, the neutron time of flight, and which gamma counter fired, if any.

Each of the 20 neutron counters is placed at the same polar angle of 13.4 deg. They have different azimuthal angles, are at a distance of 18 ft from the target, and each subtends 1.08 msr in the laboratory system. The entrance face of each neutron detector is covered by a plane counter used in anticoincidence to ensure that the detector does not respond to charged particles.

At this polar angle of 13.4 deg, the counters straddle the kinematic "Jacobian peak" for the reaction $\pi^- p \to \eta^o n$ at 716 MeV/c; that is, they cover the maximum solid angle in the center of mass system for their solid angle in the laboratory. Sacrificed to this geometry is a unique time of flight for neutrons from this reaction. Gained is a large counting rate. Figure 5a shows the laboratory kinematics for the neutron recoiling from the η^o. The hash marks on the curve represent center of mass scattering angles in multiples of 5 deg. The physical arrangement of the neutron

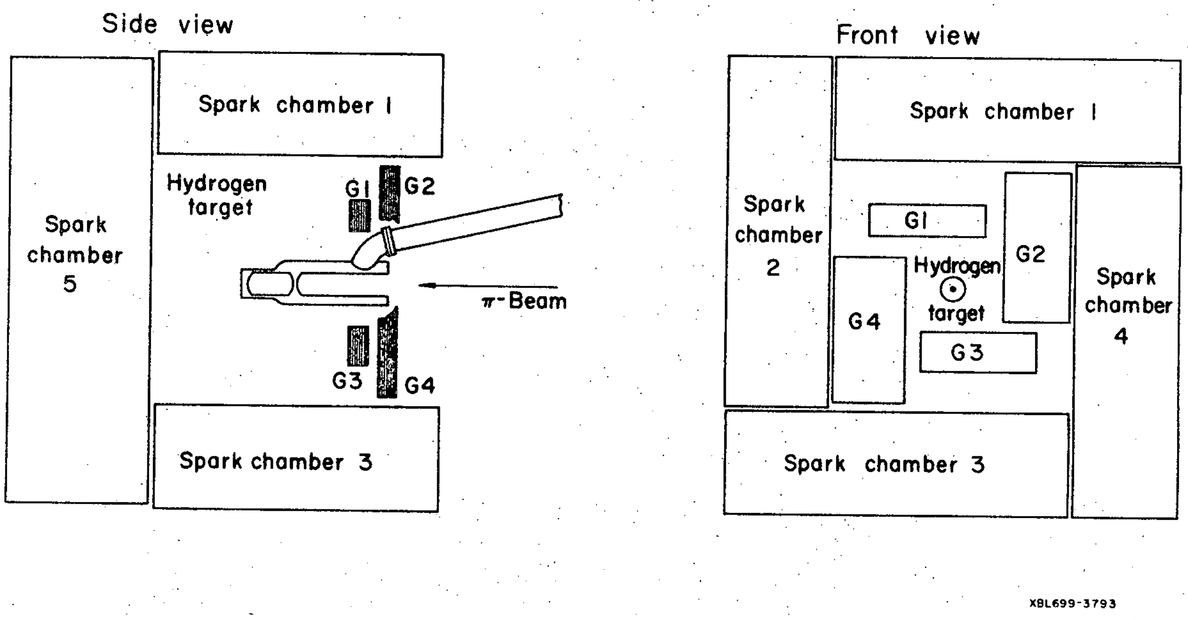

Fig. 4. Arrangement of spark chambers, hydrogen target, and gamma ray detection counters G_i.

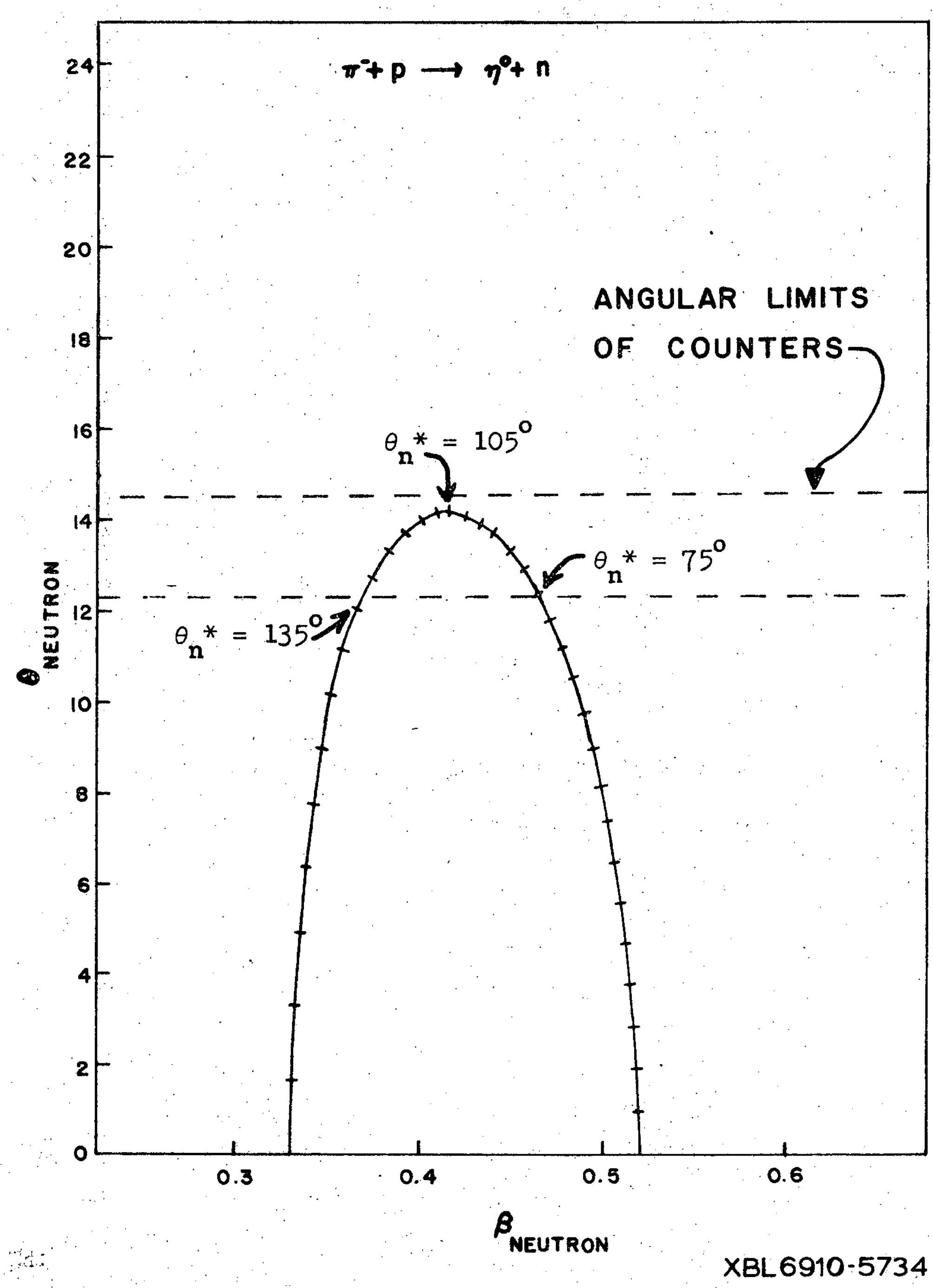

Fig. 5a. Neutron kinematics in the laboratory for $\pi^- p \rightarrow \eta^o n$ at 716 MeV/c.

counters can be seen to cover nearly 60 deg of scattering angle in the center of mass system. Figure 5b shows the laboratory kinematics for neutrons recoiling from systems of various masses (135 to 560 MeV).

During the design phase of the experiment several possible arrangements for the neutron counters were considered. In particular, the possibility of using the counters at a laboratory scattering angle of zero degrees was rejected in favor of placing them at the Jacobian peak. Monte Carlo calculations indicated that the Jacobian peak orientation would give both a larger counting rate and better geometric efficiency for the detection of gamma rays. This geometry would select events with forward scattered η^o and the likelihood of losing gamma rays upstream (where there are no spark chambers) would be minimized. An arrangement with neutron counters at zero degrees would have resulted in a smaller spread of neutron velocities from $\pi^- p \rightarrow \eta^o n$. This advantage would have been somewhat offset by less time-of-flight separation from charge exchange neutrons (see Fig. 2). The fast neutrons at a laboratory angle of zero degrees which have just been discussed are those from interactions where the neutron is produced at zero degrees in the center of mass. There are also slow neutrons at zero degrees in the laboratory and 180 degrees in the center of mass. These are too few in number (due to the adverse solid angle transformation) to be useful.

The same Monte Carlo calculations which led to the choice of a Jacobian peak geometry were instrumental in determining other optimum experimental parameters such as the size and location of the hydrogen target.

Several different central momenta (and correspondingly several different neutron counter deployments) were investigated prior to the

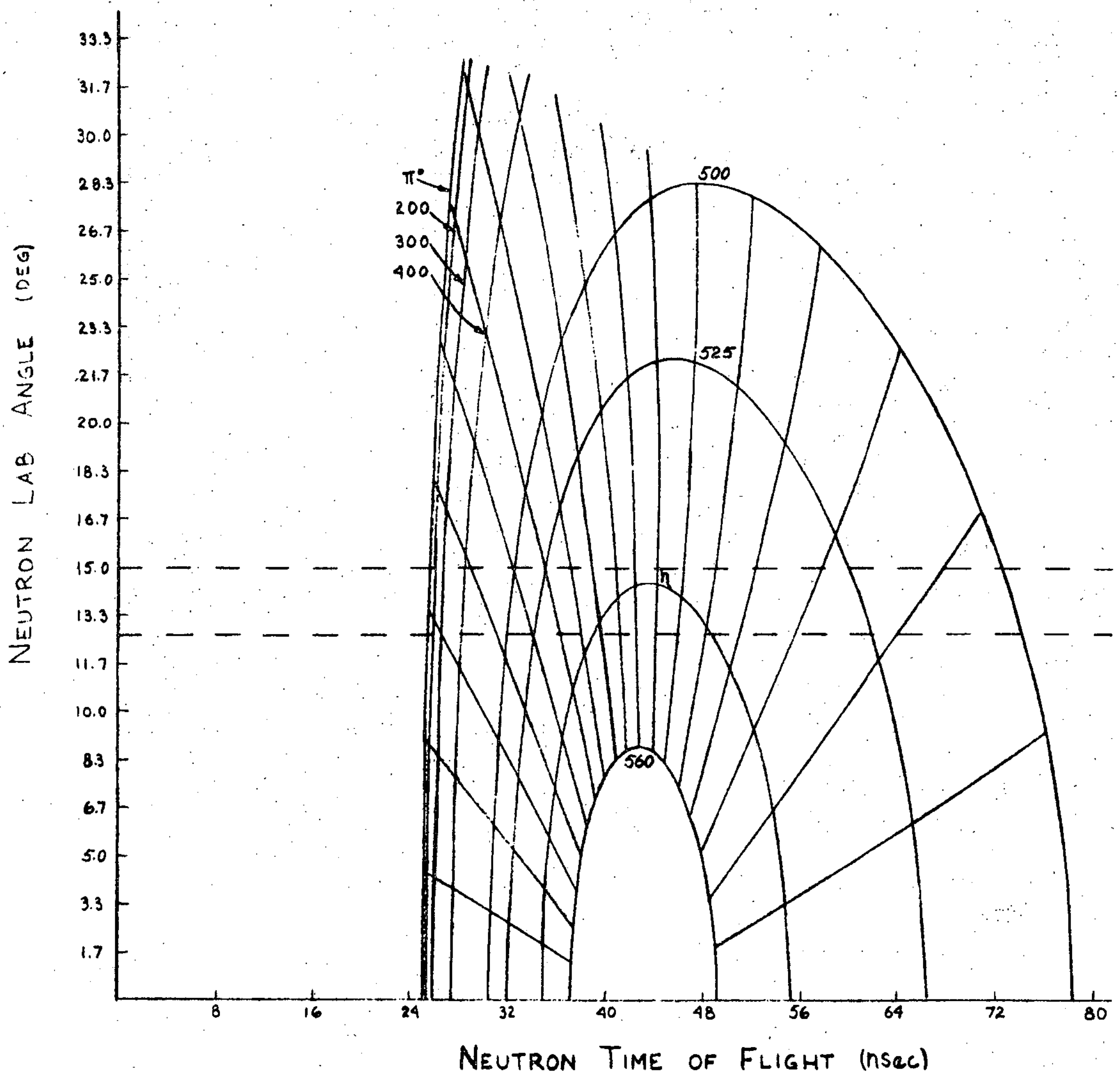

XBL 707-1624

Fig. 5b. Laboratory neutron kinematics for $\pi^- p \rightarrow n$ + "missing mass" at 716 MeV/c for various missing masses. Radial lines indicate constant center-of-mass neutron scattering angles in multiples of 10 deg. Dashed lines indicate approximate angular limits of neutron counters.

beginning of data accumulation. The choice of 716 MeV/c was made experimentally. From threshold the total cross section for η^o production rises sharply with incident pion momentum. At the same time, the center of mass solid angle subtended by the neutron counters decreases with increasing beam momentum. Calculations done during the design phase of the experiment indicated that the solid angle effect should dominate and that the η^o counting rate at 716 MeV/c should actually be greater than at higher momenta with a larger total cross section. In addition, the signal to noise ratio was expected to be vastly superior at 716 MeV/c. Both of these predictions were verified experimentally. The momentum 716 MeV/c, which had been predicted to be optimum, was therefore chosen for the bulk of the data accumulation.

III. THE APPARATUS

A. Beam Description

The pion beam (Fig. 6) collected from a target in the internal proton beam of the Bevatron is quite an ordinary one and deserves no detailed treatment. Field values for the beam elements were determined using the program OPTIK[54] and proved quite close to the final parameters. The momentum defining H-magnet (B2) was wire orbited.

The beam line can be divided into two halves at the momentum slit. The first half serves only to collect particles from the internal aluminum target and to bend those of roughly the proper momentum onto the slit. In addition to its collecting duties, the first quadrupole doublet, Q1, helps focus the particles onto the slit. In this it is aided by a field lens (Q2) in which a brass collimator is buried. The particles are bent onto this collimating slit by an H-magnet, B1. The second half of the beam selects the momentum and focuses the pions onto the hydrogen target. The elements in this half are a bending magnet (B2) followed by a quadrupole triplet (Q3). The beam line is fixed on either side of B2 so that the bend in this magnet determines the central momentum of the beam. The beam line is fixed upstream of B2 by the momentum slit and downstream by the quadrupole axis, a 2-ft. lead collimator with a 4 by 4-in. aperture, and the beam defining counters.

Beam profile studies indicate the angular divergence of the beam to be less than $\pm$ 1 deg. The momentum dispersion is $\Delta p/p = \pm 0.015$.

At the conclusion of data taking the electron and muon contaminations of the beam were measured by a high pressure methane Cerenkov counter. This counter and its use are fully described elsewhere.[55] The optics of the counter allow one to view two separate angular regions of Cerenkov

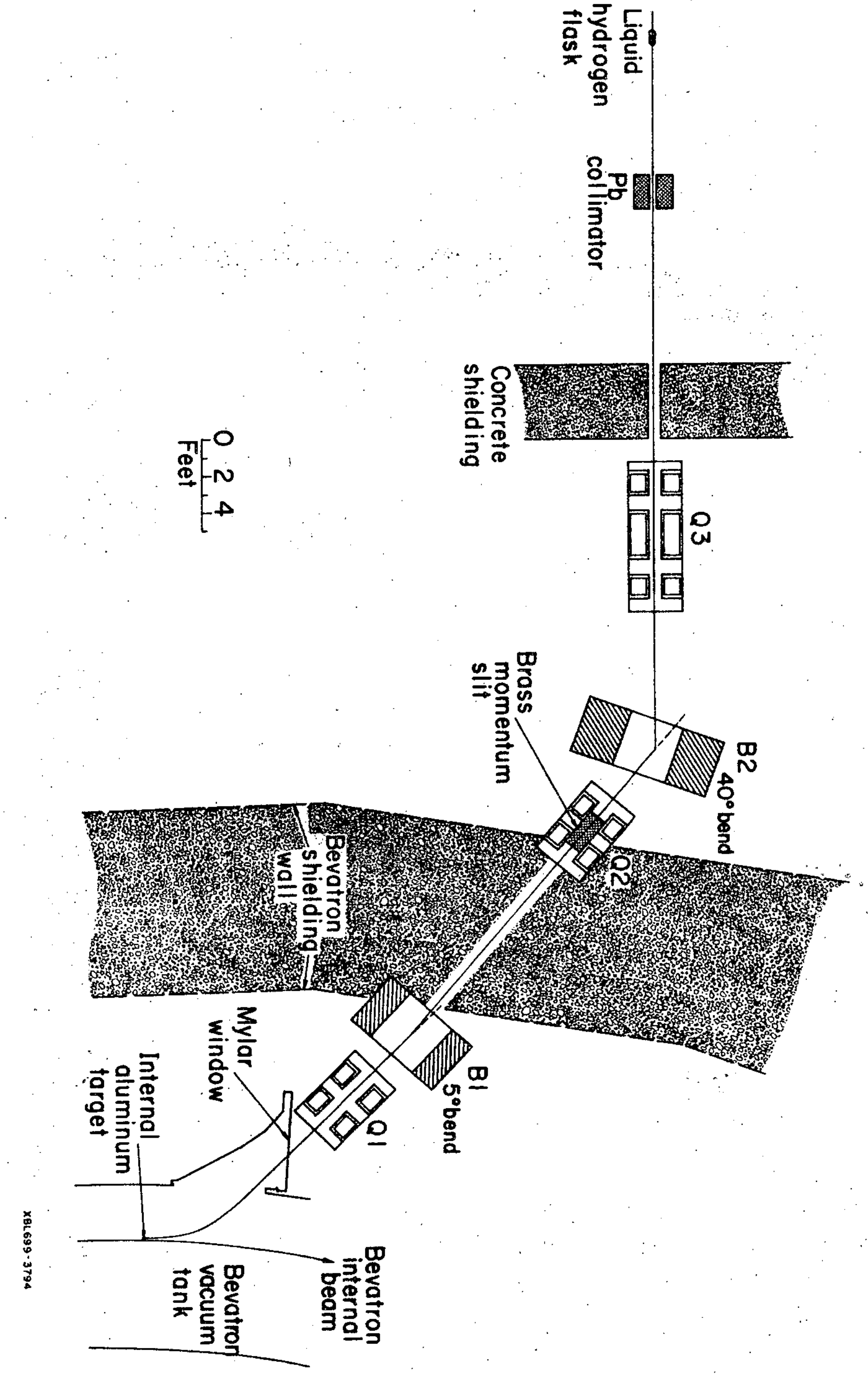

Fig. 6. The pion beam.

light production, $0 \leq \theta \leq 6.6$ deg or $7.4 \leq \theta \leq 13.7$ deg. Summing the light from both regions allows one to use the device as a threshold counter. Examining only the smaller angular region allows one to use the counter differentially and examine each beam component separately. Both results are consistent and show 3% μ^- at all momenta. The electron contaminations are 17, 24, and 33 per cent at 772, 716, and 654 MeV/c respectively. The e^- and μ^- contaminations were not measured for the other two momenta (686 and 745 MeV/c). Not a great deal of data were accumulated at the latter momenta and the e^-, μ^- contaminations do not enter into the data analysis.

The average beam intensity was $\sim 125 \times 10^3$ pions per second during a Bevatron spill of ~ 1.6 seconds. Roughly 20% of the beam particles were vetoed by anti-jamming electronics (see Sec. E below). Thus the net usable flux was about 100×10^3 pions per second or 160×10^3 pions per pulse. The data taking rate was ~ two pictures per Bevatron pulse.

B. Liquid Hydrogen Target

The liquid hydrogen is contained in a cylinder of 0.0075-in. Mylar, 8-in. long and 4-in. in diameter (Fig. 3). This flask is in an evacuated jacket of 0.030-in. spun aluminum having entrance and exit windows of 0.010-in. Mylar through which the beam passes. The aluminum jacket is reinforced on the upstream end where it is joined to a long pipe. This pipe delivers hydrogen from a reservoir and acts as a physical support for the target jacket and the counters surrounding it. (Fig. 1.)

The reinforced section of the aluminum jacket has a re-entrant hole of 4-in. diameter. This hole is introduced into the jacket structure to facilitate placing the last beam counter extremely close to the liquid hydrogen flask. This counter (M_3) has a wafer of scintillator 1.7-in. from the flask and an air light guide through which the beam passes axially (Fig. 3).

Scattering centers other than the hydrogen which could produce logically acceptable events are the last beam counter, the Mylar walls of the hydrogen flask, and the Mylar windows. For processes where $\pi^- + p \rightarrow$ (all neutral final state) we have:

$$\frac{\text{counting rate with hydrogen}}{\text{counting rate without hydrogen}} = 9.95.$$

When the requirement of a detected neutron is added to the requirement of a neutral final state this ratio becomes 11.35. Further, in the region under the η^o peak the ratio is $\gtrsim 35$.

C. Scintillation Counters

All of the scintillation counters are made from "Pilot B" scintillator which is polyvinyltoluene doped with p-terphenyl and p,p'-diphenylstilbene.

The beam defining counters (M_1, M_2, M_3) and the anticounters surrounding the hydrogen target (A_1, A_2) are all viewed by RCA 8575 photomultiplier tubes and, with the exception of M_3, all have light guides of twisted lucite strips. Because M_3 is very close to the hydrogen target and because it is physically buried in the target jacket structure, the beam of pions must pass axially through its light guide. For this reason, the light guide is an air filled cylinder of aluminized Mylar. A thin (.0005-in.) 45-deg mirror of the same material reflects the light to a photomultiplier outside the beam region (Fig. 3).

Each of the three beam defining counters is a plane disc. They descend in size as the beam converges onto the target; M_1, M_2, and M_3 are 4, 3.5, and 3-in. in diameter respectively. M_1 is 1/2-in. thick and produces an output pulse which is very stable in time. M_2 and M_3 are each 1/16-in. thick to minimize scattering.

The veto counter surrounding the hydrogen target (A_1) is a 1/4-in. thick hexagonal cylinder viewed by three tubes (Fig. 3). The veto counter downstream of the target (A_2) is an 8-in. square, 1/4-in. thick. This counter is more than 99.9% efficient, as indicated by the fact that the neutral counting rate with target empty is $\simeq$ 0.07% of the beam rate.

The neutron counters (N_i) are cylinders of scintillator 8-in. in diameter and 8-in. long. Amperex XP1040 photomultiplier tubes (5-in. in diameter) view the scintillator through light guides which are truncated cones of Lucite. The entrance face of each neutron counter is covered by a 10-in. square veto counter (V_i). Here again use is made of twisted strip light pipes.

The gamma ray detection counters which partially cover the open face of the spark chamber cube are four in number (G_1 - G_4). Each is a multi-layer sandwich of 1/4-in. sheets of scintillator alternating with 1/8-in. sheets of lead. There are eight such rectangular sheets of each material. The dimensions of the counters are: G_1 = 5.5 × 20 in., G_2 = 26 × 12.5 in., G_3 = 7 × 20 in., G_4 = 25.5 × 12 in. G_2, G_3, and G_4 are each viewed by two Amperex 58AVP photomultiplier tubes placed directly in contact with the smallest side of the sandwich. G_1 has a single such 5-in. diameter photomultiplier mounted in the same way. The deployment of these counters is shown in Fig. 4.

The gamma ray detection counters are calibrated in such a way that they will respond to a minimum ionizing particle passing through any one of the eight sheets of scintillator. The calibration procedure is to place the counters in the pion beam so that the pions are normally incident on each sheet of scintillator. The counters are then plateaued (i.e. the photomultiplier high voltage is raised until the counting rate is 100%) with the signal attenuated by a factor of eight at the discriminator input. In normal operation, the input attenuation is discarded and the counters will respond to 1/8 of the energy deposited by a minimum ionizing particle traversing eight sheets of scintillator.

D. Spark Chambers and Optics

The lead plate spark chambers and the associated optical system were inherited from a prior experiment. A detailed description can be found in the published results of that experiment.[56] The spark chamber pulsers and discharge gaps have also been described elsewhere.[57]

Each of the four side chambers contains 42 lead and 12 aluminum plates of dimension 4×5 ft. The back chamber, through which the beam passes, contains 48 lead and 13 aluminum plates 6.5 ft square. These plates are separated by optically clear Lucite frames with a gap spacing of 5/16-in. The "lead" plates are in reality a lamination of 1/32-in. lead between two sheets of 1/64-in. aluminum. The use of such very thin lead plates makes the detection efficiency for low energy showers quite good (threshold for detection is $E_\gamma \cong 10$ MeV; probability of detection is $\simeq$ 0.35, 0.75, 0.90, and 0.95 for E_γ = 20, 40, 60, and 80 MeV respectively). A large number of plates is then necessary to achieve the desired number of total radiation lengths (~ 7 in the side chambers, ~ 8 in the back chamber).

The first five plates of each chamber are 3/64-in. aluminum. Gamma rays entering the chambers are extremely unlikely to materialize here, the total thickness being ~ .07 radiation lengths. A particle entering the chambers with a visible track in the first four gaps is usually presumed to be charged. This is particularly useful knowledge for tracks in the back chamber where beam contaminating electrons often cause confusing showers.

Figure 7a shows the arrangement of the five spark chambers in space and on the film. Figure 7b shows an actual photograph. Ten field lenses and 46 mirrors comprise an optical system which brings the 10 views to a

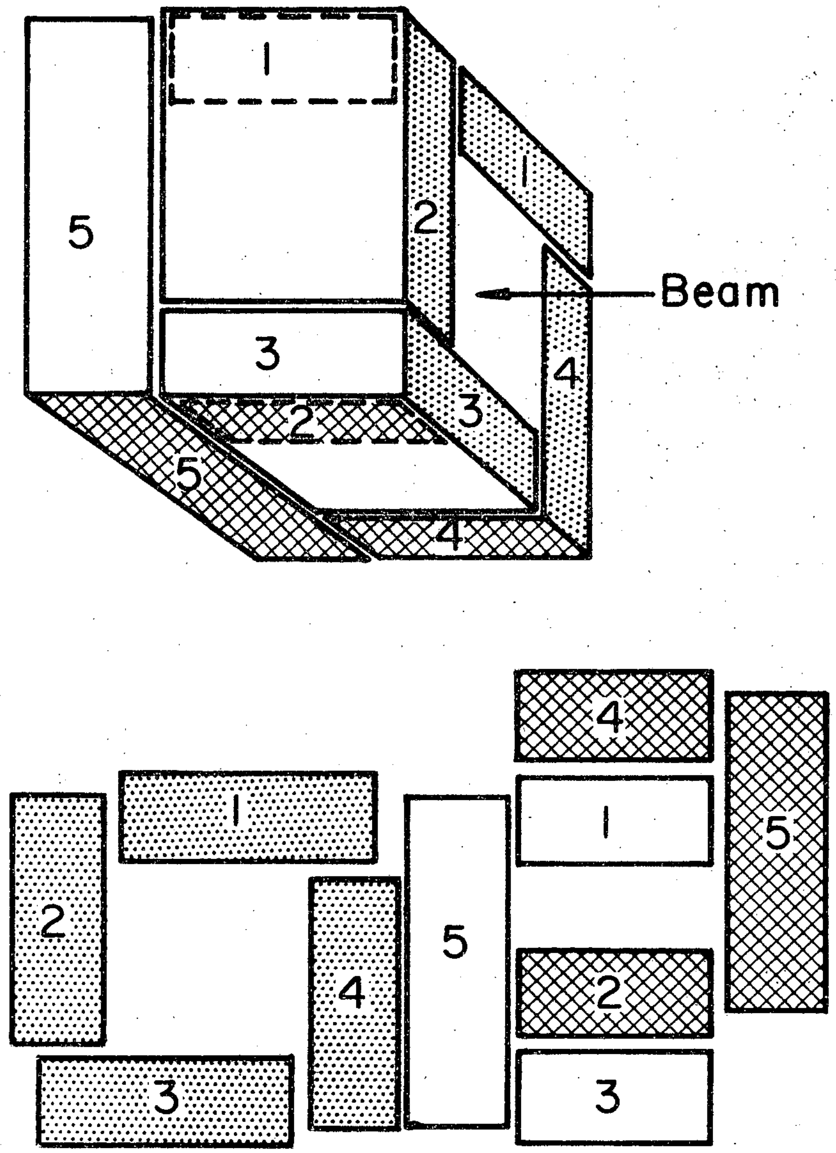

XBL699-3788

Fig. 7a. The arrangement of spark chambers in space (top) and the arrangement of spark chamber views on film (bottom).

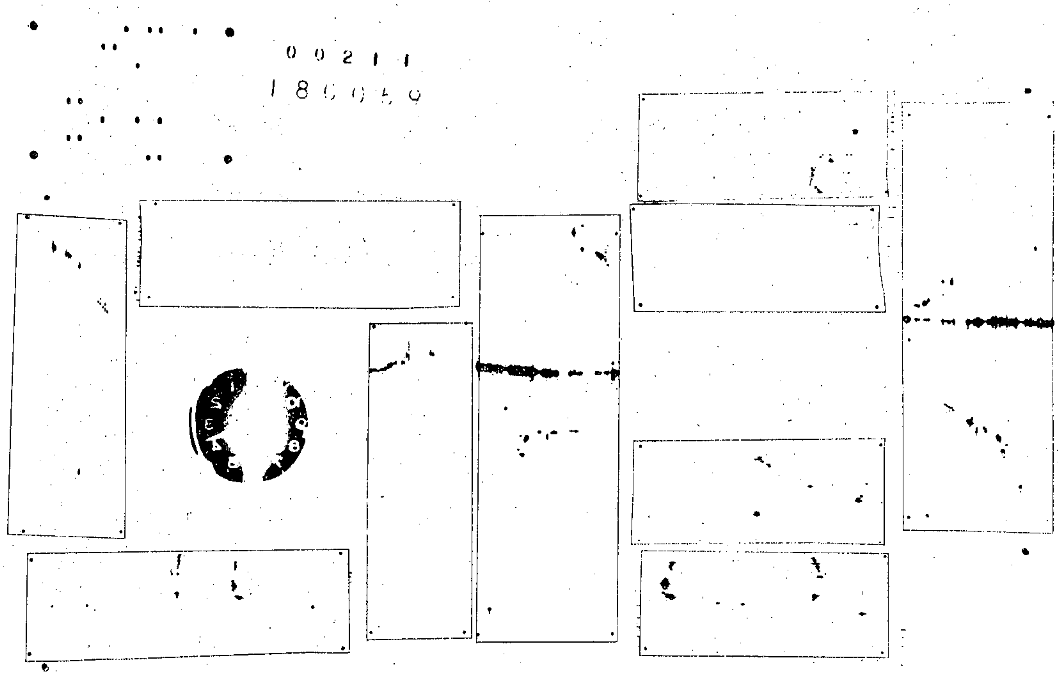

Fig. 7b. Photograph of a six-shower event with a beam track through Chamber 5. The data light array is in the upper left corner.

single Flight Research camera. The array of data lights and a clock are also included in the photograph.

E. Electronics

The neutron counter logic is presented in Appendix C. For the purposes of the following discussion it will be assumed that there is but a single neutron counter and that it has but a single discriminator. In reality there are 20 such counters, each with two discriminators. The final discriminator outputs are fanned in by a series of OR circuits and are indistinguishable at the input of coincidence unit NC (Fig. 8). Similarly, the two veto counters (A_1, A_2) surrounding the hydrogen target are distinct (A_2 views the residual beam as well as the forward angular range and has a special 200 MHz no-dead-time discriminator) but they are always used together and will be represented here as the single counter A.

The first coincidence required is denoted B (for beam) on Fig. 8 and is simply a triple coincidence between M_1, M_2, and M_3. The timing is such that the output of this coincidence unit is determined by M_1 and the beam particle timing is as accurate as the timing from M_1 ($\pm$ 0.25 nsec).

The signal B is then fed into a second coincidence unit M (for monitor) where it may be vetoed by a "DT" (for dead time) pulse. This is a signal generated early by M_1 which is designed to prevent jamming of the system by beam particles too close together in time. M_1 generates a pulse in a special no-dead-time discriminator, DT_1, 52 nsec earlier than in the regular M_1 discriminator. One output of DT_1 is delayed and triggers a similar unit, DT_2. The outputs of DT_1 and DT_2 are then added and when they appear at the input of M they are the DT signal. This pulse begins 68 nsec before M_1 (at M), ends 2 nsec before M_1, begins again 2 nsec after M_1 has died away, and persists for another 500 nsec. Each B signal is then accompanied by its own early and late DT signal which is used as a veto at the M coincidence unit. It cannot eliminate itself but it will

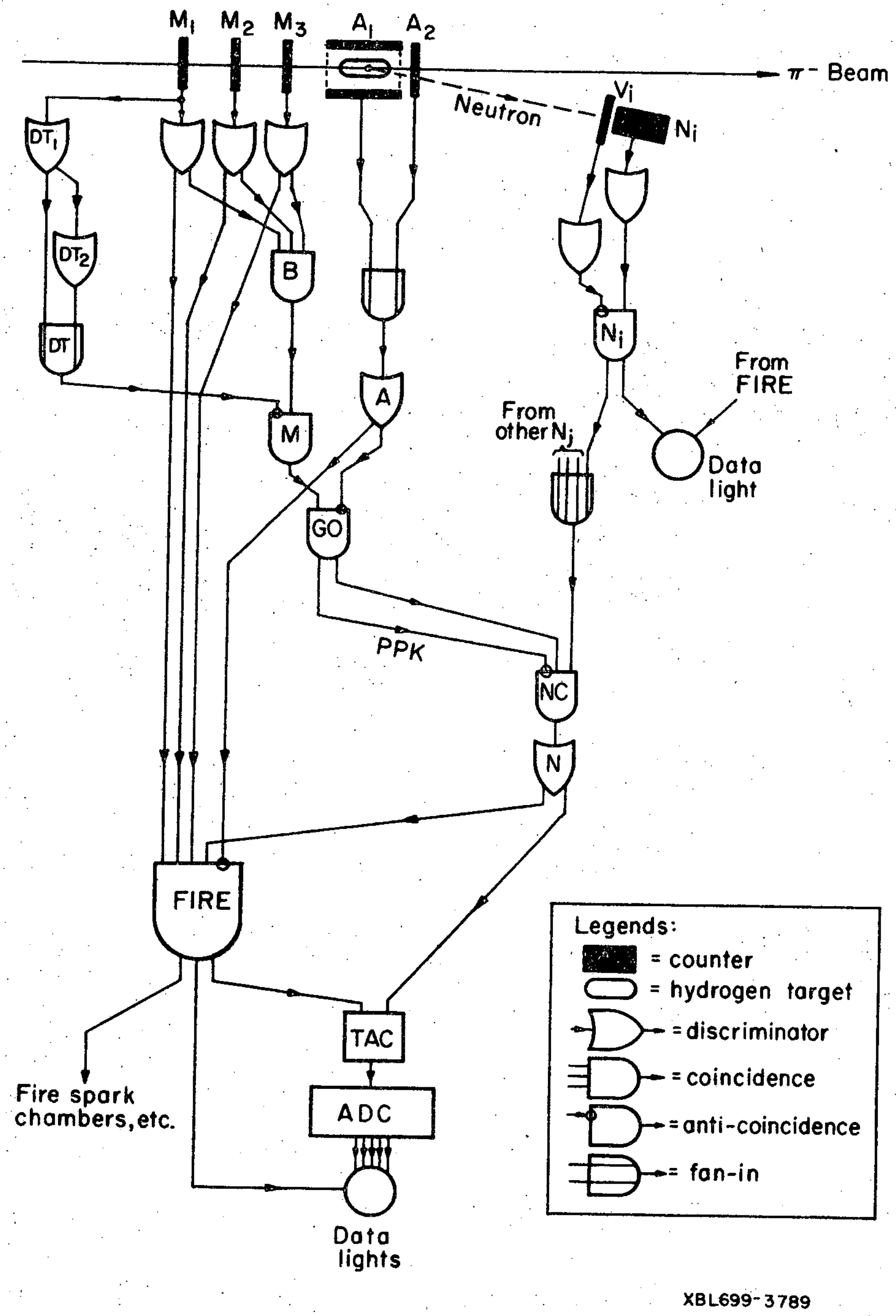

Fig. 8. The electronics.

veto any beam particle nearby in coincident time. This arrangement prevents jamming, reduces the probability of finding beam tracks in the back spark chamber, and lowers the rate of accidental triggering.

After the beam signal, B, has been rendered rate independent at M it is fed into another coincidence unit, GO, where the veto counters ($A = A_1 + A_2$) are in anticoincidence. The output of this unit represents a "neutral final state"; that is, a reaction where a beam particle entered the target region and no charged particles emerged.

The only further requirement necessarily satisfied before triggering the spark chambers is that a neutron must be detected within the proper time limits. The signal N_i (without its private veto, V_i), representing any one of the neutron counters, is required in coincidence with GO at the unit NC (for neutron coincidence). The GO pulse is 140 nsec wide at this unit and arrives well before the neutron signal. Thus the neutron timing is preserved at the output of NC.

Another GO signal, which is clipped to a width of four nsec and which is properly delayed, is used in anticoincidence at NC to veto events where a $\beta = 1$ gamma ray triggers the neutron counter. There is a considerable number of such events and the effectiveness of this "prompt peak killer" (PPK) is shown in Fig. 9. The time region of the spectrum before the prompt peak represents "particles" with $\beta > 1$ and is therefore accidental background. These events are photographed for use in the data analysis.

The output pulse from NC is all that is logically required for triggering the spark chambers. The signal from NC goes to another discriminator, N, to be stretched into a signal of length suitable for the time-to-amplitude converter (TAC). The TAC determines the timing from the overlap of two long (≥ 100 nsec) pulses; in addition to N it must

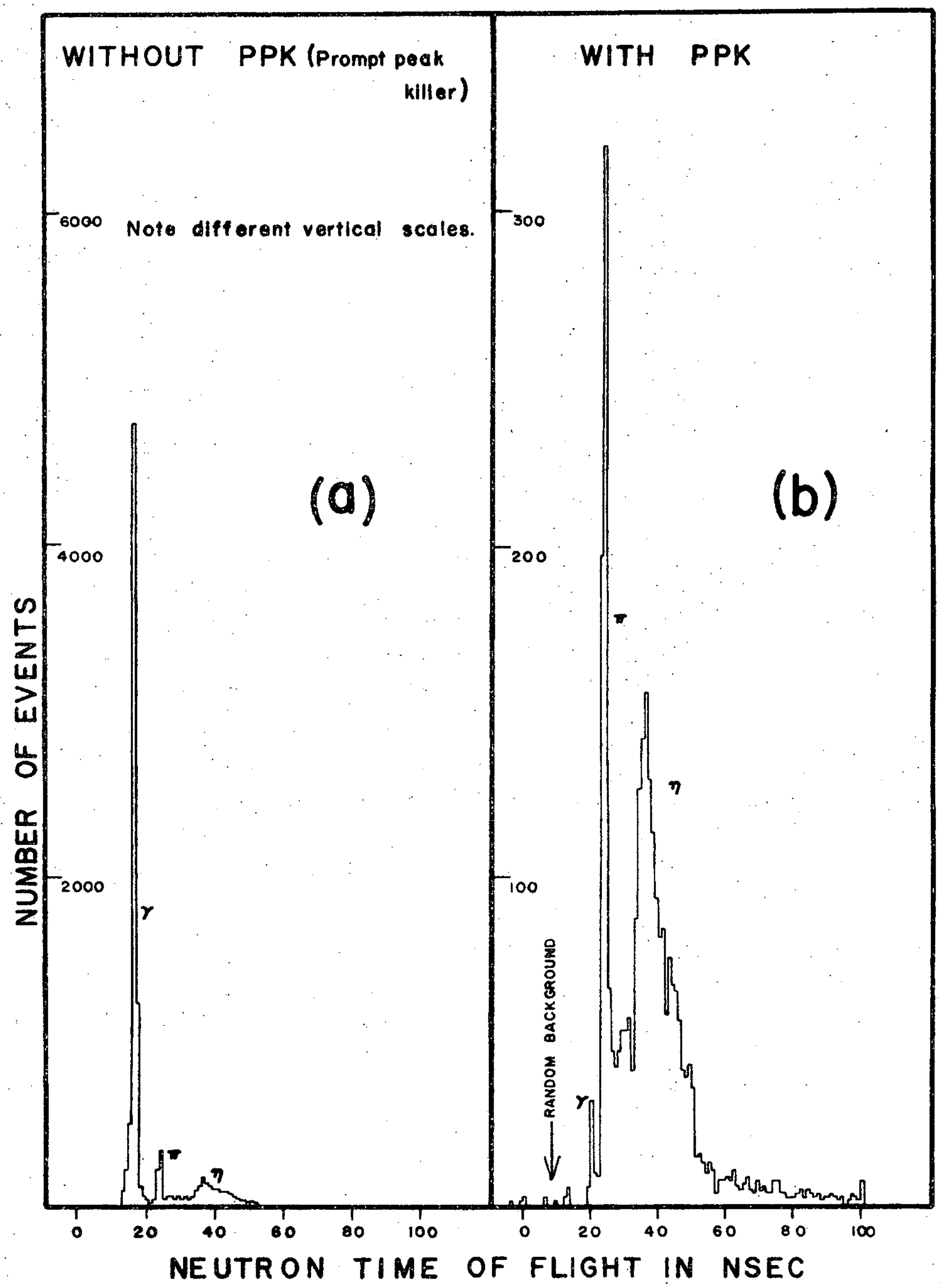

XBL 6910-5738

Fig. 9. Time of flight spectra with (b) and without (a) the "prompt peak killer" for an equal number of incident pions at 716 MeV/c.

receive a signal, such as B, representing the timing of the beam. For this, a circuit which parallels B and which is called FIRE is used. FIRE is a fourfold coincidence between M_1, M_2, M_3, and N with A in anticoincidence. It has its timing determined by M_1 and is logically equivalent to N or NC. FIRE, rather than B, is used for the beam timing in order to avoid extraneous "start" pulses to the TAC. The TAC determines the timing difference between FIRE, which preserves the timing of M_1, and N, which preserves the timing of the individual neutron counter.

The FIRE unit performs a variety of tasks: (1) it fires the spark chambers, the fiducial lights, the event number lights, and the data light array, (2) it advances the camera, (3) it provides one signal to the TAC, and (4) it generates an 80 msec gate to shut the system down during pulsing and recovery. FIRE also provides pulses to test various bits of information for possible display on the data light array; for instance, if any gamma detection counter, G_i, or neutron counter, N_i, has the proper timing relative to FIRE a data light will indicate that this counter detected a particle associated with the event. The counters G_i are not inculded in the logic in any way except by the data light which lights when they are in coincidence with FIRE. The data lights are Xenon flash lamps. When a counter is in coincidence with FIRE the pertinent light is enabled. Each time the spark chambers are fired all the enabled lights receive a high voltage pulse and are flashed.

The TAC output goes to an analog-to-digital converter (ADC) where it is transformed into a binary number which appears on the data light array. The TAC and ADC system has a minimum time resolution of $\pm$ .17 nsec.

IV. DATA ANALYSIS

A. Introduction

It should be emphasized at the outset of the discussion of data analysis that: (1) only 27% of the film taken at the central momentum (716 MeV/c) has been scanned and analyzed, and (2) geometric reconstruction and kinematic fitting have not yet been attempted for any but two-shower events.

The branching ratios are determined from the central momentum data. Data at the other momenta (654, 686, 745, 772 MeV/c) are used to study the background and are not included in the branching ratio determination. The remaining 73% of the central momentum data will be scanned and analyzed in the near future. Even with only 27% of the film scanned this experiment is statistically far more significant than that of any prior experiment (see Table III, page 26).

The long range plans for the data from this experiment also include geometric reconstruction and kinematic fitting. This phase of the analysis depends on a system of three parts: (1) automatic scanning and measuring, (2) computer pattern recognition, and (3) computer reconstruction and fitting. The first and third parts are fully operational; the second is in the final stages of development.

The automatic scanning and measuring is done by SASS,[58] a precision cathode ray tube and photomultiplier system linked to a DDP-24 computer. SASS digitizes the positions of all sparks, fiducial lights, and data box lights for each event. The scanning time is approximately ten seconds per frame. The only information from the SASS scanning that is used in the analysis presented in this thesis is that from the data box. For each event the data box information obtained includes the frame number, the neutron time of flight, which neutron counter fired, and which gamma counter fired, if any.

The computer pattern recognition problem has proved to be a difficult one. The Fortran program DHARMA attempts to recognize showers from the spark co-ordinates digitized by SASS. Although DHARMA appears to be quite reliable for events involving only a few showers, it has difficulty with five and six shower events. For this reason a modified version called DHARMA-H is currently being developed. Each frame is scanned by a human scanner as well as by SASS. The scanner records the origin of each shower referenced to zones of a grid system on the scanning table. The grid zone information also shows how the showers in each view (two views per spark chamber) should be paired. Information from both the hand-scan and the SASS scan is used by DHARMA-H. The program is constrained to find the showers listed by the scanner and determines the origin, direction, and number of sparks for each shower. Thus the human scanner performs the pattern recognition function and the SASS-DHARMA-H combination is nothing more than a relatively sophisticated automatic measuring device.

The geometric reconstruction and kinematic fitting of the events from the DHARMA-H output is performed by the SIOUX which is a standard bubble chamber program developed by the Lawrence Radiation Laboratory Group A. It has been suitably modified for use with the spark chamber data. While DHARMA-H is not yet fully operational, SIOUX can at present operate directly on the hand-scan grid zone information. The grid zones localize the origin of each shower to within an approximately three-inch cubical volume in space. By assuming that the shower originates at the center of the grid zone and that it points directly back to the target some meaningful information about two shower events (e.g., $\pi^- p \rightarrow \eta^o n$ followed by $\eta^o \rightarrow \gamma\gamma$) has been obtained with SIOUX. The kinematic analysis is handicapped by by imprecise directional and no energy information for the showers. The energy will ultimately be determined by the DHARMA-H spark count. Even without this energy information, the SIOUX analysis of the two-shower events (a three constraint fit) has been reasonably successful. Kinematic analysis of more complicated events must wait for DHARMA-H.

B. Method of Analysis

The η^o branching ratios are obtained in this thesis by counting relative numbers of gamma rays (experiment of Type A, see page 24). The film is scanned by human scanners who record the number of showers. The number of gamma rays is taken to be the sum of the number of recorded showers and the number of gamma detection counters which fired. The latter information is provided by the data box lights on each frame.

It is most convenient to display the shower information as a function of neutron time of flight. A distribution of number of events versus time of flight is obtained for each number of gamma rays. Figure 10 shows the scanned data at the central momentum (716 MeV/c) before it has been corrected for scanning efficiency. Figures 11 and 12 show the raw scanned data at the lowest (654 MeV/c) and highest (772 MeV/c) momenta at which data were accumulated. The data at 654 MeV/c contains no η^o as the beam energy is below η^o threshold. Note the characteristic peaks from $\pi^- p \to \pi^o n$ (time of flight ~ 25 nsec) and $\pi^- p \to \eta^o n$. The η^o peak at 716 MeV/c (33 - 53 nsec) is much broader than the η^o peak at 772 MeV/c (29 - 33 nsec) or the charge exchange peaks. This is because the neutron counters straddle the Jacobian peak for $\pi^- p \to \eta^o n$ at 716 MeV/c. Notice also that the efficiency for observing 2γ charge exchange events is much lower than the efficiency for observing 2γ eta events. This will be discussed in Sec. F below.

The raw data distributions shown in Figs. 10 - 12 will be corrected for scanning error. Then the time of flight spectra for non-η^o events are deduced from the data at 654 and 772 MeV/c. These shapes, along with the characteristic η^o shape, are fitted to the 716 MeV/c time of flight spectra to obtain the number of eta decays in a given gamma ray category (i.e.,

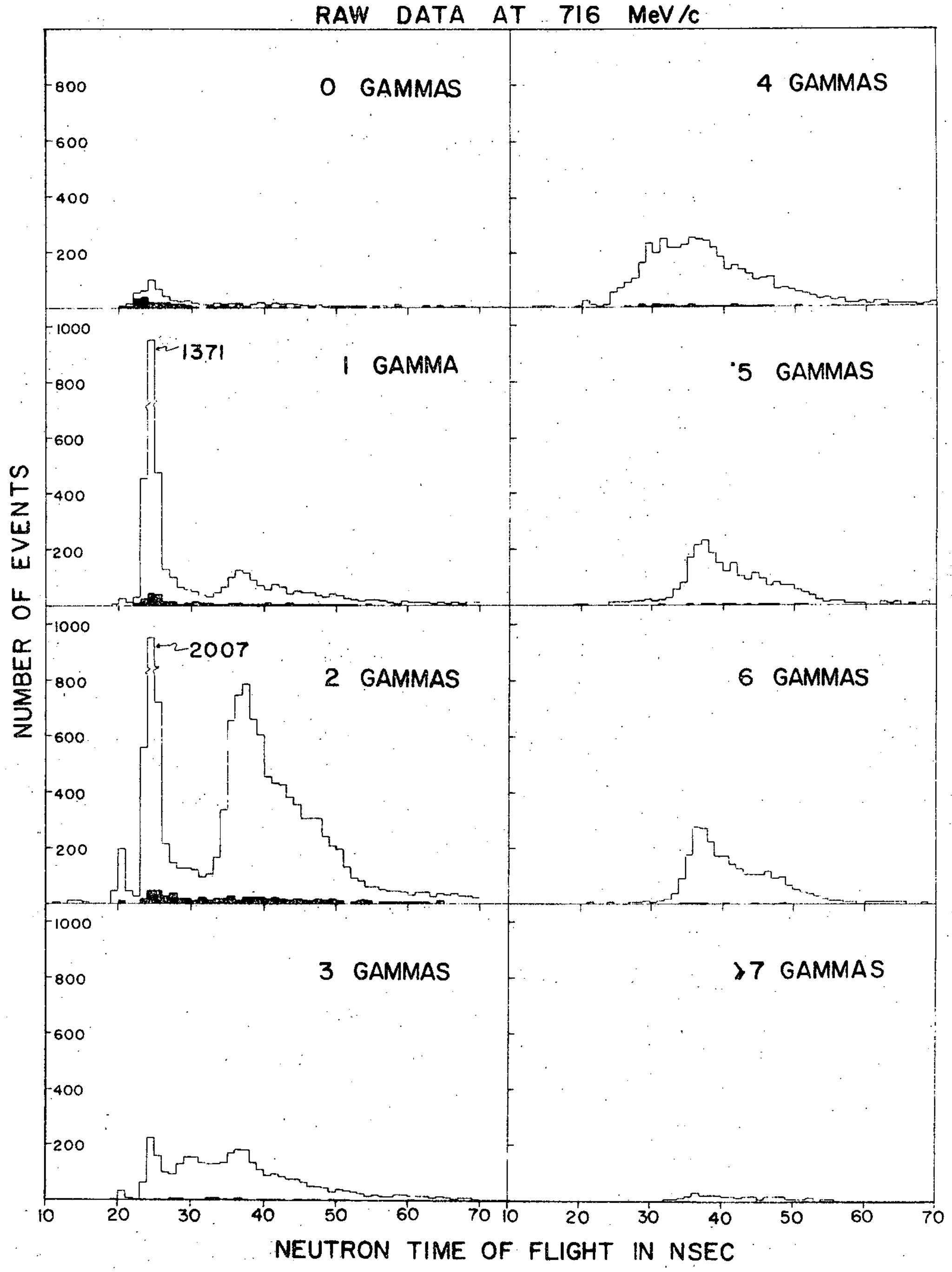

Fig. 10. Raw scanned data at 716 MeV/c. The solid histograms are for the target empty data.

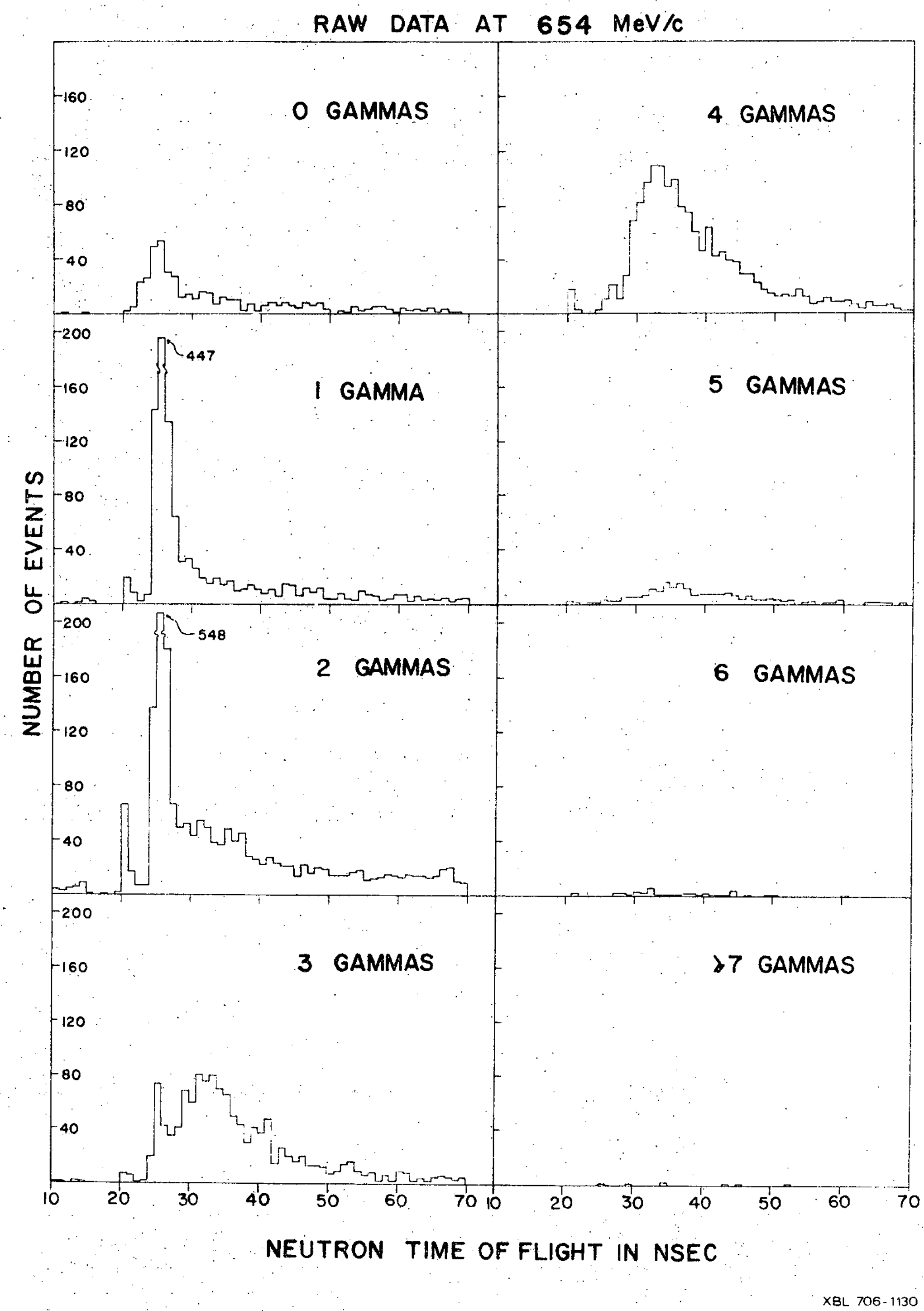

Figure 11. Raw scanned data at 654 MeV/c.

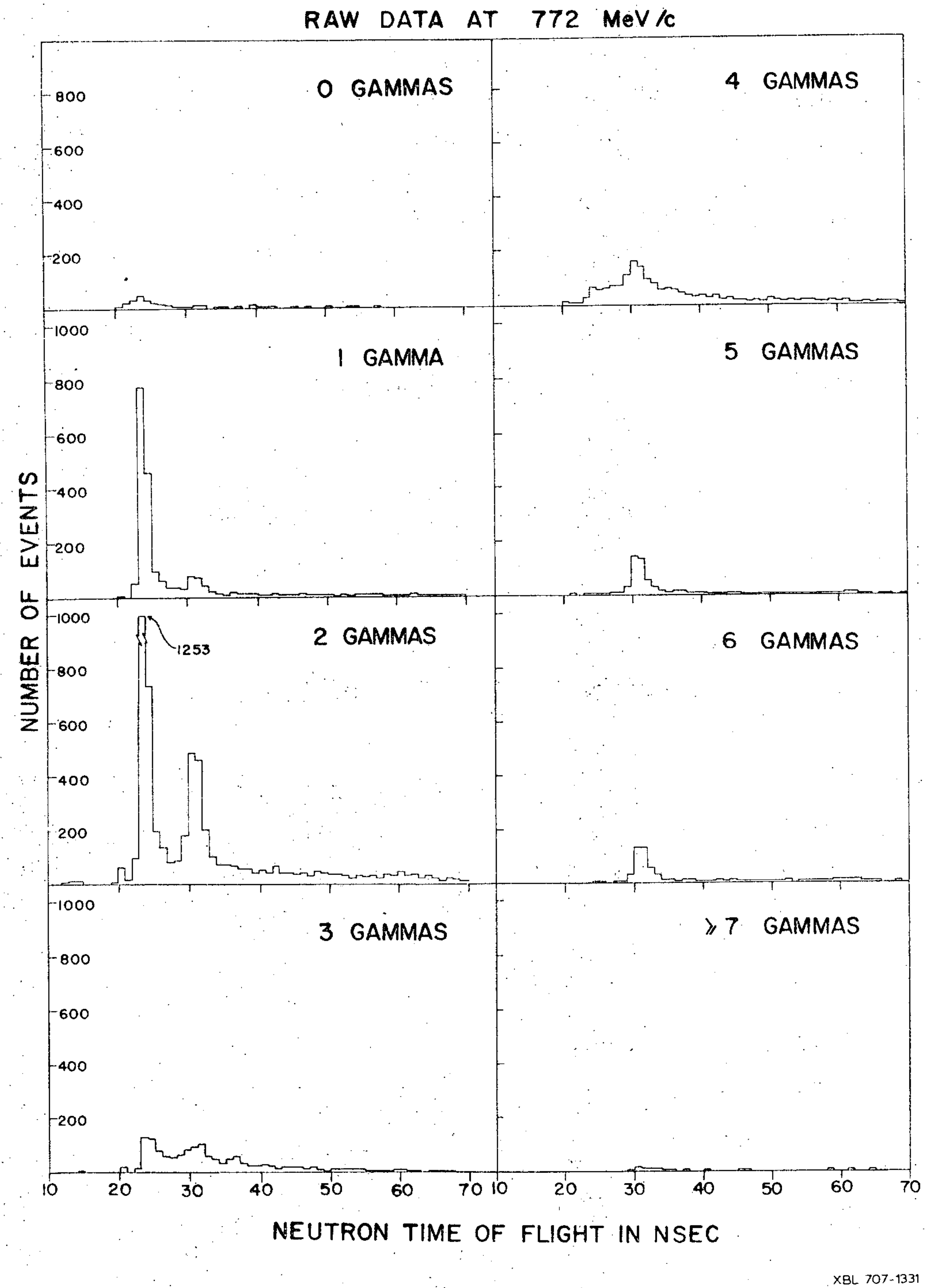

Fig. 12. Raw scanned data at 772 MeV/c.

$\eta^{o} \rightarrow N\gamma$ where N = 0, 1, ...6). These numbers are compared to the predictions for "feed-down" from a true $\eta^{o} \rightarrow M\gamma$ event into an observed $\eta^{o} \rightarrow N\gamma$ event ($M > N$). With the assumption that only the three decays $\eta^{o} \rightarrow \gamma\gamma$, $\eta^{o} \rightarrow \pi^{o}\gamma\gamma$, and $\eta^{o} \rightarrow 3\pi^{o}$ are present, the neutral branching ratios are deduced.

C. Data Accumulated and Information Available

The amount of data accumulated at each beam momentum is shown in Table IV in terms of the total number of incident beam pions. Of the total of ~ 166 000 pictures taken in this experiment ~ 120 000 were taken at the central momentum with the hydrogen target full. Approximately 43% of these 120 000 pictures are η^{o} events.

Table IV. Data accumulated.

Beam Momentum (MeV/c)	Hydrogen target	Number of millions of beam pions for which data was taken	Number of millions of beam pions for which film was was scanned	Number of film frames scanned
654	Full	1431	1431	7227
654	Empty	200	0	0
686	Full	829	0	0
686	Empty	0	0	0
716	Full	9230	2517	32 577
716	Empty	1698	1698	1098
745	Full	857	0	0
745	Empty	0	0	0
772	Full	1469	1035	12 971
772	Empty	200	0	0

All of the information available is written on a magnetic tape called the "Master List." An event is listed by the frame number which appears on the picture in two ways: (1) arabic numberals ("nixie" lights) which are read by the human scanner, and (2) binary coded decimal digit lights in the data light array which are read by SASS. SASS also reads from the data light array the neutron counter which fired, the neutron time of flight, and which gamma counter fired (if any). This information is placed on the Master List.

The human scanner records the position in both spark chamber views of each shower he finds. The scanner also makes certain value judgements (see Sec. D. below) about each shower which he lists in numerical code. Finally, the scanner records the number and type of non-shower tracks (for example, beam tracks) in the chambers. All of this hand-scan information is placed on the Master List.

A library of information about the experimental conditions under which each picture was taken is also available on the Master List. For a given frame number one can determine the beam momentum, whether or not the hydrogen target was full, and whether or not the picture was taken with all the apparatus functioning properly. Equipment malfunctions, whether due to electronic failure or human error, cause the event to be ignored in the analysis. Only a few percent of the frames need to be disregarded for this reason.

D. Film Scanning

Figure 7b, page 49, shows a typical photograph of a six shower event. Figure 7a shows the orientation of the spark chambers in space and on the film. The array of data lights is in the upper left hand corner of the frame. Notice the beam track passing through the center of the rear spark chamber (Number 5). The beam track is, of course, not associated with the event. The active time of the spark chambers is approximately 2.5 microseconds. If a beam pion (or muon) passes through the rear spark chamber between 0 and 1 μsec before the event which triggers the chambers it will appear as a "new" beam track with a spark in every gap. If such a pion passes through the chamber between 1 and 2.5 μsec before the event it will appear as an "old" beam track. Such tracks are disjointed and dispersed; they present a major difficulty in scanning because they may be confused with showers.

Thirty-five per cent of the scanned film frames have a beam track passing through Chamber 5 (~ 14% of the frames have a "new" track and ~ 21% have an "old" track). There are three types of beam tracks observed: non-interacting pions or muons (~ 52%), electrons (~ 22%) and pions which interact in the spark chamber plates (~ 26%). The beam electrons cause showers in Chamber 5. When they are "new" they are very straight and well collimated showers passing completely through the chamber. When they are "old" they may resemble forward produced gamma ray showers. Approximately 60% of the beam pions which interact in the spark chamber scatter elastically. The remaining 40% charge exchange, These events show a beam track which abruptly stops in the chamber. Usually one (and often two) of the showers in the chambers point back to the end point of the beam track. As for the electron tracks, when these charge exchange tracks are "new" they are easy to recognize. When they are old and dispersed they may cause confusion.

New and old non-interacting beam tracks are easily recognized as are new electron tracks and new interacting beam tracks. Old electron tracks (~ 4.6% of frames) and old π^- + Pb charge exchange tracks (~ 3.3% of frames) may be improperly recorded as showers by the scanner. As the tracks become old and dispersed they begin to have the segmented, irregular appearance of showers. Fortunately, as the tracks grow older the individual sparks grow larger and more diffuse. Often an old track looks like a disjointed collections of "blobs." The scanners are taught to exercise special care in the central region of chamber 5 through which the beam passes. It is believed that old tracks are mistaken for showers on less than 1% of the frames. This mis-identification is corrected for in the general treatment of scanning efficiency.

The scanner records the non-shower information (beam tracks) and then examines the data light array to see whether or not a gamma counter fired. He then scans the frame for showers, listing each by the grid zones (two views) where it appears. Following each recorded shower is a coded statement about the shower:

(1) The shower is "normal." That is, it begins in the active region of the chamber, has more than two sparks, and points toward the hydrogen target.

(2) The shower occurs in the region of a corner between two chambers. Such a shower may originate in the dead extremities of one chamber and first appear in another chamber.

(3) The shower has only two sparks.

(4) The shower does not point to the hydrogen target.

(5) The shower is probably a fragment of another shower rather than an independent one.

(6) The "shower" is probably an old beam track fragment.

(7) The shower is probably produced by the same photon which triggered a gamma counter.

Showers of types (1), (2), and (7) are counted as such. The number of triggered gamma counters is added to the number of these showers to obtain the total number of detected gamma rays for the event. In the special case of a shower of type (7) the gamma counter responsible for producing the shower is not counted. In such cases the photon materializes in the gamma counter and produces a shower which spills over into the adjacent chamber. By convention, the shower in the chamber is counted and the triggered gamma counter is not. Figure 4 (page 36) shows the relative positions of the chambers and gamma counters.

The scanners proved to be quite adept at correctly making most of the above value judgements about the showers. For showers of types (4) and (7) their judgement appeared somewhat less reliable. Every event including such a shower was rescanned by a physicist working together with the most competent of the scanners. The Master List was updated accordingly.

The scanners were generally over-zealous in finding showers which do not point back to the hydrogen target. When showers occur near the non-active edges of the chambers the entirety of the shower is not always observed. The observed fragment, which may be only a branch of the whole shower, does not necessarily point towards the target. Showers in the vicinity of the gamma counters also may not point towards the target. The gamma counters (like the spark chambers) contain dead regions, most notably the support brackets, where a photon may materialize without triggering the counter. Such photons may produce showers which appear in the adjacent chambers and point more towards the counters than towards the target. All events containing a shower which the original scanner recorded as not pointing towards the target were re-scanned. If the shower appeared to be correlated with an inactive region of a spark chamber or gamma counter the "vertex problem" label was removed from the Master List.

If a scanner labelled a shower as one involving a "doubly-detected photon" (observed as both a shower in a chamber and as a triggered gamma counter) he did so quite reliably. The mistake which he was likely to make was to fail to recognize such cases. It appears that the scanner is quite likely not to notice the data light indicating a triggered gamma counter. For this reason the SASS reading of the data light array is always used in the analysis to indicate a counter detected photon. A re-scan was done for every event: (1) where a shower appeared in a chamber adjacent to a gamma counter, (2) where the SASS scan indicated that particular counter to have been triggered, and (3) where the scanner did <u>not</u> indicate a doubly-detected photon. The Master List was then corrected accordingly.

After the scanning information was corrected for "vertex problem" and "doubly-detected photon" errors, the number of detected gamma rays for each event was determined. No other corrections were applied to individual events. A neutron time-of-flight distribution is obtained for each number of detected photons (see Figs. 10 - 12). The scanning efficiency correction (to be discussed below) is applied to the distributions themselves rather than to the individual events.

The number of detected photons for each event is taken to be the sum of all "normal" and "corner" showers [types (1) and (2) above] and all triggered gamma counters (determined from the SASS scan of the data lights).

Showers with only two sparks are not counted. Some of these two-spark showers are undoubtedly genuine low energy gamma rays which convert. However, the chambers are quite transparent to low energy ($\lesssim$ 10 MeV) photons. Photons of such energy are copiously produced through Bremsstrahlung in the development of a normal shower. Due to the transparency of the chambers to these photons, they may produce one and two-spark showers a considerable distance away from the mother shower. The directional information associated with two-spark showers is highly unreliable and we must ignore them. The Monte Carlo calculation which we will use to calculate the amount of "feed-down" (from $\eta^o \rightarrow M\gamma$ into an observed $\eta^o \rightarrow N\gamma$) can easily account for an energy cut-off excluding two-spark showers.

"Vertex problem" showers remaining after the re-scan corrections described above are also not counted as showers. Generally these showers point either towards the center of chamber 5 (the remnants of a π^- + Pb charge exchange event) or towards the lead collimator upstream of the hydrogen target (see Fig. 1, page 30). Presumably the latter are associated with an off-axis beam pion stopping or interacting in the collimator.

E. Scanning Efficiency Correction

One complete roll of film taken at 716 MeV/c with the hydrogen target full was triple-scanned to determine the scanning efficiency for this analysis. The corrections discussed in the previous section were applied to each scan. If all three of the scanners agreed on the number of showers, their type, and their grid zone locations the event was taken to be correctly scanned. All of the frames where all three scanners agreed and reported four or more showers were scanned by a physicist. No disagreement with the scanners was found. If a conflict appeared between any two of the three scans for a given event that event was subjected to a special scrutiny. A physicist, working together with the most competent scanner, scanned such events a fourth time. In this case the fourth scan was taken to be correct. There were 2944 frames on the triple-scanned roll of which 1052 had to be scanned a fourth time.

In scanning a true j-gamma event (i.e., an event with (j - g) showers and g triggered gamma counters) the scanner-SASS combination will generally observe the proper number of gamma rays. When a mistake is made it will be made by the scanner rather than SASS. Some small fraction of the time he will fail to notice one or two showers and the event will appear on the Master List as a (j - 1) or (j - 2) gamma event. Similarly, the scanner may mistake one or two old beam track remnants for showers and the Master List will show a (j + 1) or (j + 2) gamma event. Given a true j-gamma event, there is a probability P_{ij} that, after scanning, it will be recorded on the Master List as an i-gamma event. We obtain a matrix of the elements P_{ij} from the triple-scanned film.

We wish to fit the j-gamma time of flight spectrum to find out the number of $\eta^o \to j\gamma$ events present. Suppose, for example, that there are no true $\eta^o \rightarrow 3\gamma$ events. If there are 2000 true $\eta^o \rightarrow 2\gamma$ events in a peak in the time-of-flight spectrum and if there is a $P_{32} = .1$ probability that a scanner will see three showers when only two are present, then a false η^o peak containing 200 events will appear in the three gamma time-of-flight spectrum. In general a strong peak in the j-gamma distribution will be reflected in the $(j \pm 1)$ and $(j \pm 2)$ gamma distributions.

The scanned data must be corrected for scanning error in such a way that neither the shape nor the magnitude of the j-gamma spectrum is reflected in the $(j \pm 1)$ or $(j \pm 2)$ gamma distributions. The technique used in this analysis is to form a matrix of the probabilities P_{ij}, invert it, and apply P_{ij}^{-1} to a vector representing the scanned data. This is done for each bin of the time-of-flight distributions (i.e., each histogram bin). Let us form a vector T_j whose jth component is the true number of j-gamma events for a certain neutron time of flight. Let S_i be a vector whose ith component is the observed number of i-gamma events for the same neutron time of flight. If P_{ij} is the probability that a true j-gamma event is observed as an i-gamma event, then we have

$$S_i = P_{ij}T_j.$$

It is assumed that P_{ij} is independent of neutron time of flight over the region of the time-of-flight spectrum for which the analysis will be performed. The matrix P_{ij} is inverted and the matrix P_{ij}^{-1} is applied to the vector of observed showers to get the number of true showers. This is done for each bin of the time of flight histograms. A further discussion is presented in Appendix D.

Before the scanning efficiency correction matrix is applied to the scanned data a subtraction is made for the target empty data at 716 MeV/c. No target empty film was scanned for 654 or 772 MeV/c. The data at these latter momenta are used principally to infer the shape of the 3 and 4-gamma background distributions. Figure 10 shows the 716 MeV/c target empty data, normalized to the same number of incident beam pions as for the target full data. It is clear that the number of target empty events in the 3 and 4-gamma categories is negligibly small so that the subtraction is not necessary. The majority of the target empty events occur in the 0, 1, and 2-gamma categories. The shape of their time-of-flight distributions indicates that they are quasi-elastic charge exchange events occurring in the target walls.

After the target empty subtraction at 716 MeV/c has been made the scanning correction matrix P_{ij}^{-1} is applied to the vector S_j of the number of observed j-gamma events to obtain the vector T_i representing the true number of i-gamma events. This is done for each bin (1 nsec bin width) of the time-of-flight histograms. No other corrections of any kind are made to the data. Figure 13 shows the results. No target empty subtraction has been made at 654 or 772 MeV/c. Figures 14 and 15 show the data at these momenta after the scanning efficiency correction.

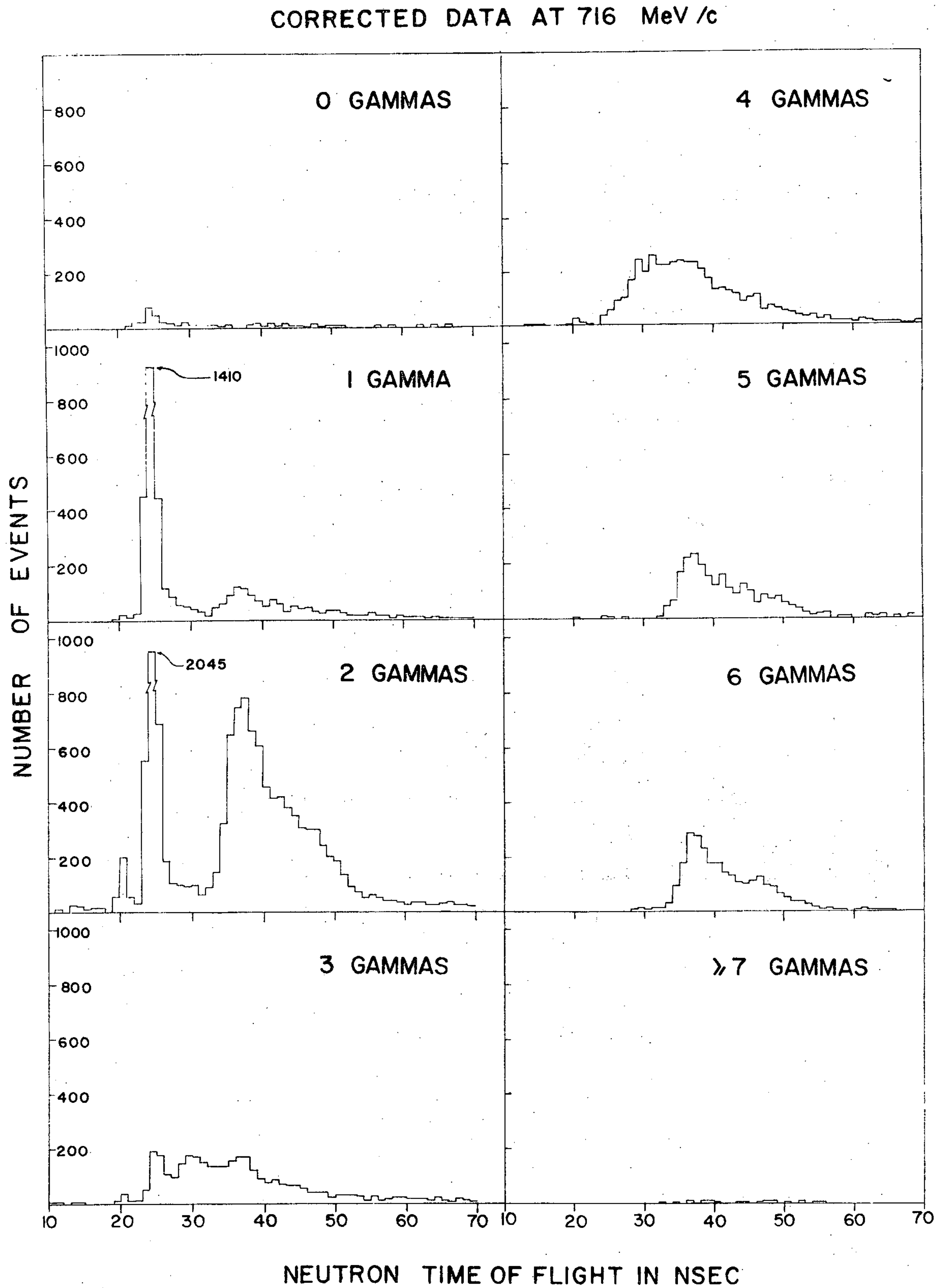

Fig. 13. Data at 716 MeV/c after target empty subtraction and scanning efficiency correction.

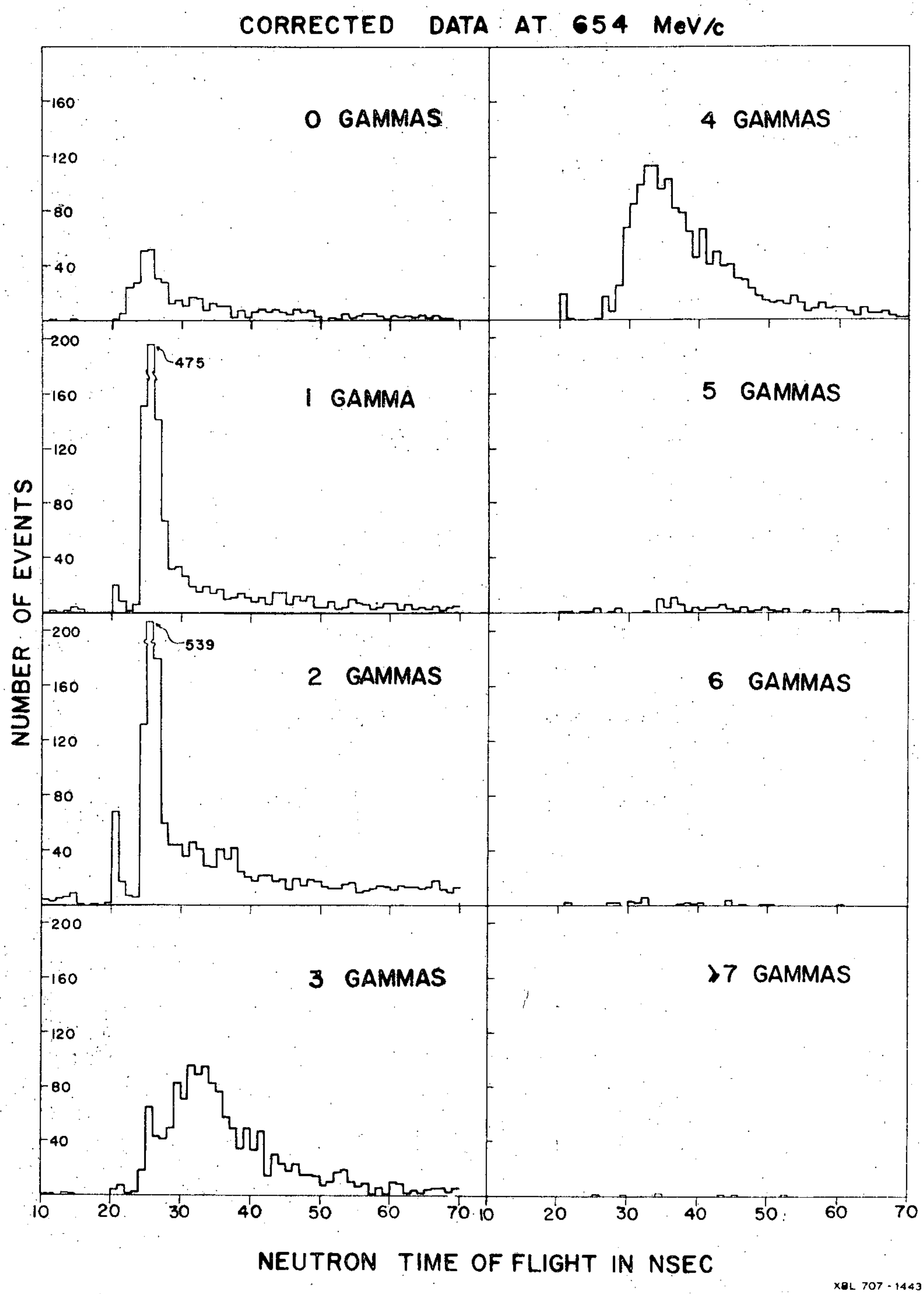

Fig. 14. Data at 654 MeV/c after scanning efficiency correction.

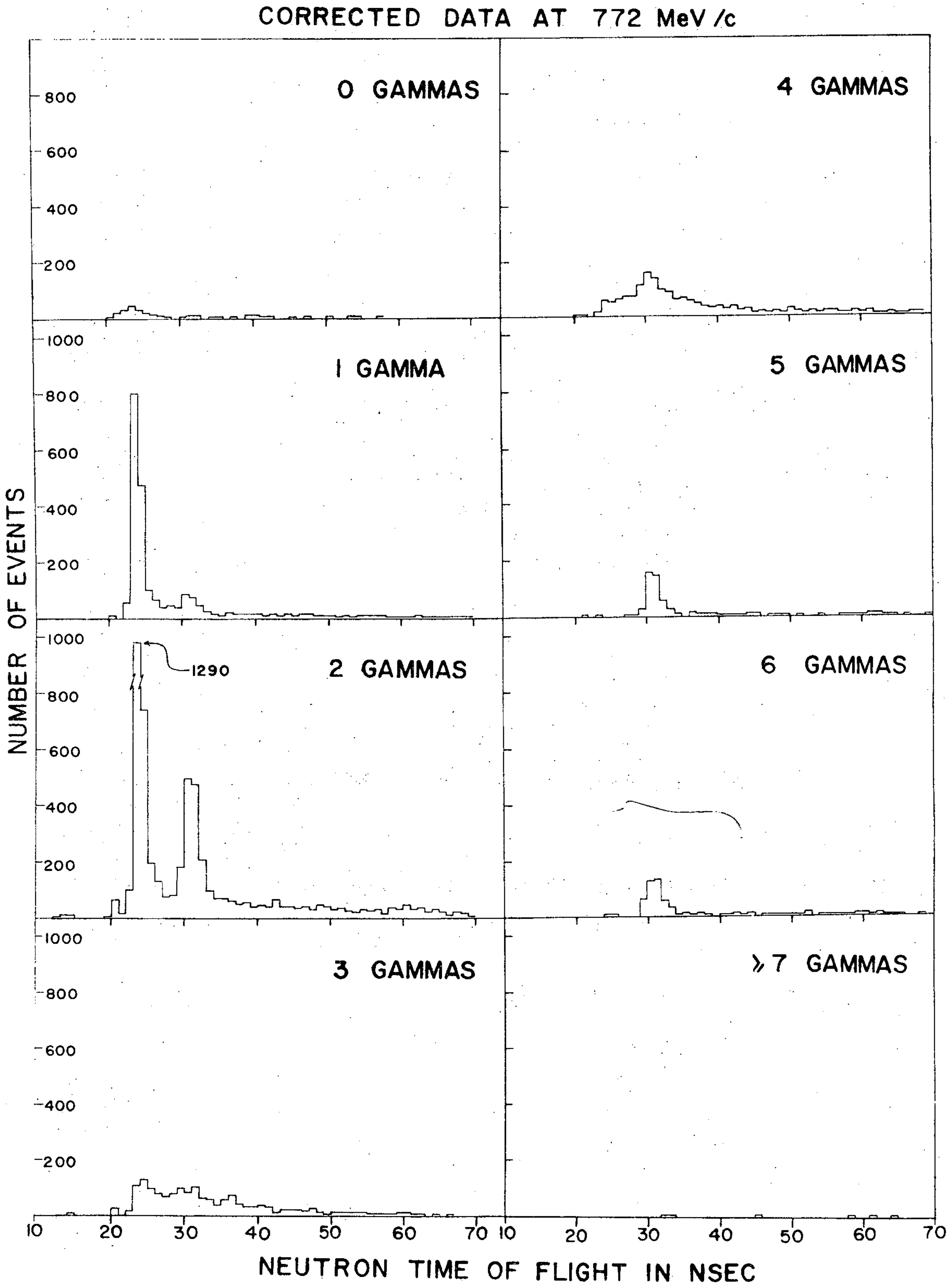

Fig. 15. Data at 772 MeV/c after scanning efficiency correction.

F. General Features of the Data

Examination of Figs. 13 through 15 reveals a number of interesting features. First consider Fig. 13, the corrected time of flight distributions for 716 MeV/c. A strong η^o peak is observed in the 2, 5, and 6-gamma distributions. It is clear that the detection efficiency for $\eta^o \rightarrow 3\pi^o \rightarrow 6\gamma$ is high.

Next consider Fig. 14, the distributions at 654 MeV/c. The threshold beam momentum for η^o production is 686 MeV/c. Since the momentum dispersion of the beam is $\Delta p/p = \pm .015$ we should see no η^o events at 654 ± 9.8 MeV/c. The absence of any clear signal in the 6γ distribution (18 events total) indicates that there are indeed no η^o events present. The small number of 6γ events also implies that there is present very little background of the type $\pi^- p \rightarrow 3\pi^o n$. The threshold beam momentum for this process is 463 MeV/c. Since 654 MeV/c is well above $3\pi^o n$ threshold and since we see very few 6γ events at this momentum we might reasonably expect there to be very little $\pi^- p \rightarrow 3\pi^o n$ present at 716 MeV/c.

Although there are very few 6γ events at 654 MeV/c, there is a considerable number of 5γ events. These 5γ events appear to be true 4γ events plus an extra detected gamma ray. This "feed-up" problem appears elsewhere. Notice, for example, that a charge exchange peak appears in the 3γ distributions at all three momenta (Figs. 13 to 15). This "feed-up" is not attributable to scanning error. It is discussed in Sec. I below; for the present we will simply fit the time-of-flight distributions to determine the number of $\eta^o \rightarrow N\gamma$ events for N = 0, 1, ... 6. The correction for feed-up will be made afterwards.

The 4γ distribution in Fig. 14 shows very clearly the shape of the $\pi^- p \rightarrow \pi^o\pi^o n$ background.

The 5 and 6γ distributions at 716 MeV/c (Fig. 13) indicate that the η^o peak lies between roughly 33 and 62 nsec. Consider the 1 and 2γ distributions at 716 MeV/c with this in mind. It can be seen that there is a small background underneath the $\pi^- p \rightarrow \eta^o n$ peak which diminishes as the neutron time of flight increases. An experimental estimate of this background at 716 MeV/c can be made from the 654 MeV/c data (as discussed in the next section).

Another noteworthy feature of the data is that the feed-down ratio at 716 MeV/c from 2γ to 1γ events is different in the η and charge exchange regions. It is quite small in the η region reflecting the fact that the neutron counters straddle the Jacobian peak for η production and the η's are produced in the forward hemisphere. The feed-down is very large for the charge exchange events. This is because the π^o is produced at large angles in the laboratory (~ 133 deg) and there is a relatively high probability that one of the gamma rays will escape upstream.

G. Determination of the Shapes of the η^o and non-η^o Distributions

The $\pi^- p \to 3\pi^o n$ Shape: The 6γ distribution at 654 MeV/c (Fig. 14) suggests that there is very little $\pi^- p \to 3\pi^o n$ present at that momentum. Anticipating that this is probably also the case at 716 MeV/c, we use the $3\pi^o n$ shape generated by our Monte Carlo program. That is, we assume a phase space distribution for $\pi^- p \to 3\pi^o n$. If we expected this process to be present in any large amount, we would examine the phase space assumption with some care. As matters stand, we expect the contribution from this process to be negligible (and, indeed, it turns out to be negligible) so that we use the phase space shape.

The η^o Shape: Although a Monte Carlo calculation exists which predicts the η^o shape, we prefer to infer this shape from the 5 and 6γ data. If there is very little $\pi^- p \to 3\pi^o n$ present these distributions will contain almost exclusively η^o events.

As mentioned in Sec. A. above, the program SIOUX has been used to make a three constraint kinematical fit to the "two shower" events at 716 MeV/c. These are events with two recorded showers and no triggered gamma counters. In the η^o region they represent ~ 90% of the "two-gamma" events, ~ 40% in the charge exchange region. Figure 16 shows the results of the SIOUX fitting. Histogram (2) shows the time of flight spectrum for all events which fit one of the two processes:

$$\pi^- p \to \eta^o n, \quad \eta^o \to 2\gamma$$

$$\pi^- p \to \pi^o n, \quad \pi^o \to 2\gamma \,.$$

Histogram (3) shows the spectrum for those events which do not fit either of these processes. Figure 16 indicates clearly that nearly all the η^o

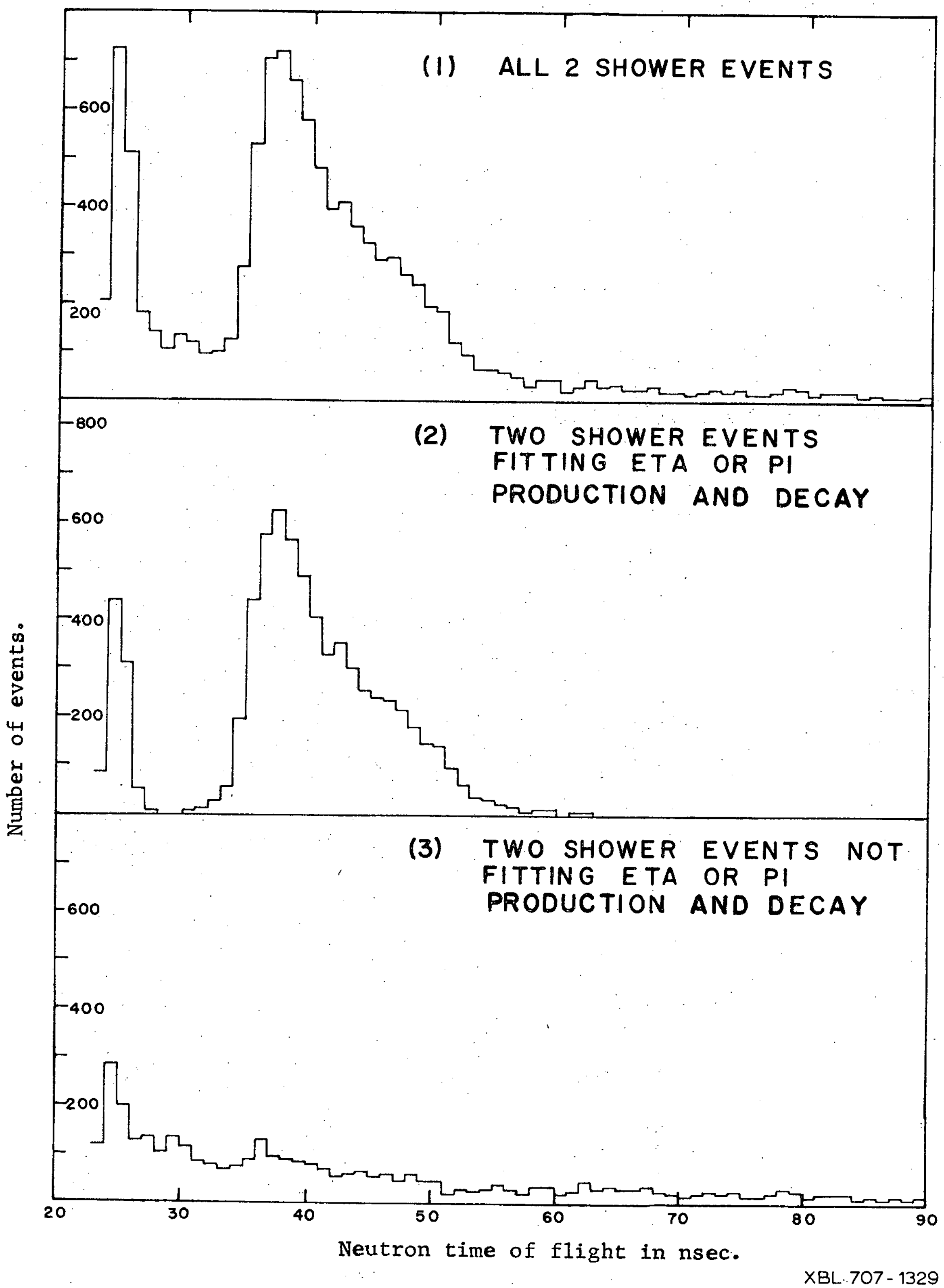

Fig. 16. SIOUX fits to the data at 716 MeV/c.

events fit. The time-of-flight spectrum representing the fitted η^o events may not be quite the proper shape to use in fitting the time-of-flight distributions because of neutron scattering effects (see Appendix E, below). It is probably close to correct, however, and we can use it as a starting place. We make a least squares fit to the 5 and 6γ time-of-flight distributions using the SIOUX fit η^o shape, the phase space distribution for $\pi^- p \rightarrow 3\pi^o n$, and a flat background. A shape representing the process $\pi^- p \rightarrow \pi^o \pi^o n$ is also used in the 5γ fit; this process may appear in the 5γ distribution as feed-up from a true 4γ event.

An excellent fit is obtained to the 6γ distribution with no flat background needed and a trivial amount ($\sim 4\%$) of $\pi^- p \rightarrow 3\pi^o n$. An excellent fit is also obtained to the 5γ distribution which requires nothing but the η^o. No reasonable fit could be obtained to the 5γ spectrum with anything present in addition to the η^o. We subtract the amount of $3\pi^o n$ found from the 6γ distribution and add the 5γ distribution. This is now our "experimental η^o shape." This shape is expected to be the best estimate that we can make. It actually turns out to be quite close to the SIOUX fit shape.

Figure 17 shows the experimental η^o spectrum (deduced from the 5 and 6γ events) and the Monte Carlo prediction. The agreement is reasonably good. Naturally we have more confidence in the experimental spectrum and use it in the fits. Although the Monte Carlo does not predict the exact details of the η^o spectrum, it is very valuable in showing how the spectrum changes shape with changing kinematics. For example, if $\eta^o \rightarrow 3\pi^o$ and we observe only 3 of the 6 gamma rays we might expect this $\eta^o \rightarrow 3\pi^o \rightarrow 3\gamma$ spectrum to be somewhat different than the spectrum for $\eta^o \rightarrow 3\pi^o \rightarrow 6\gamma$. This is because the feed-down depends on the geometry and hence on the kinematics. The predictions of the Monte Carlo for how the η^o shape changes

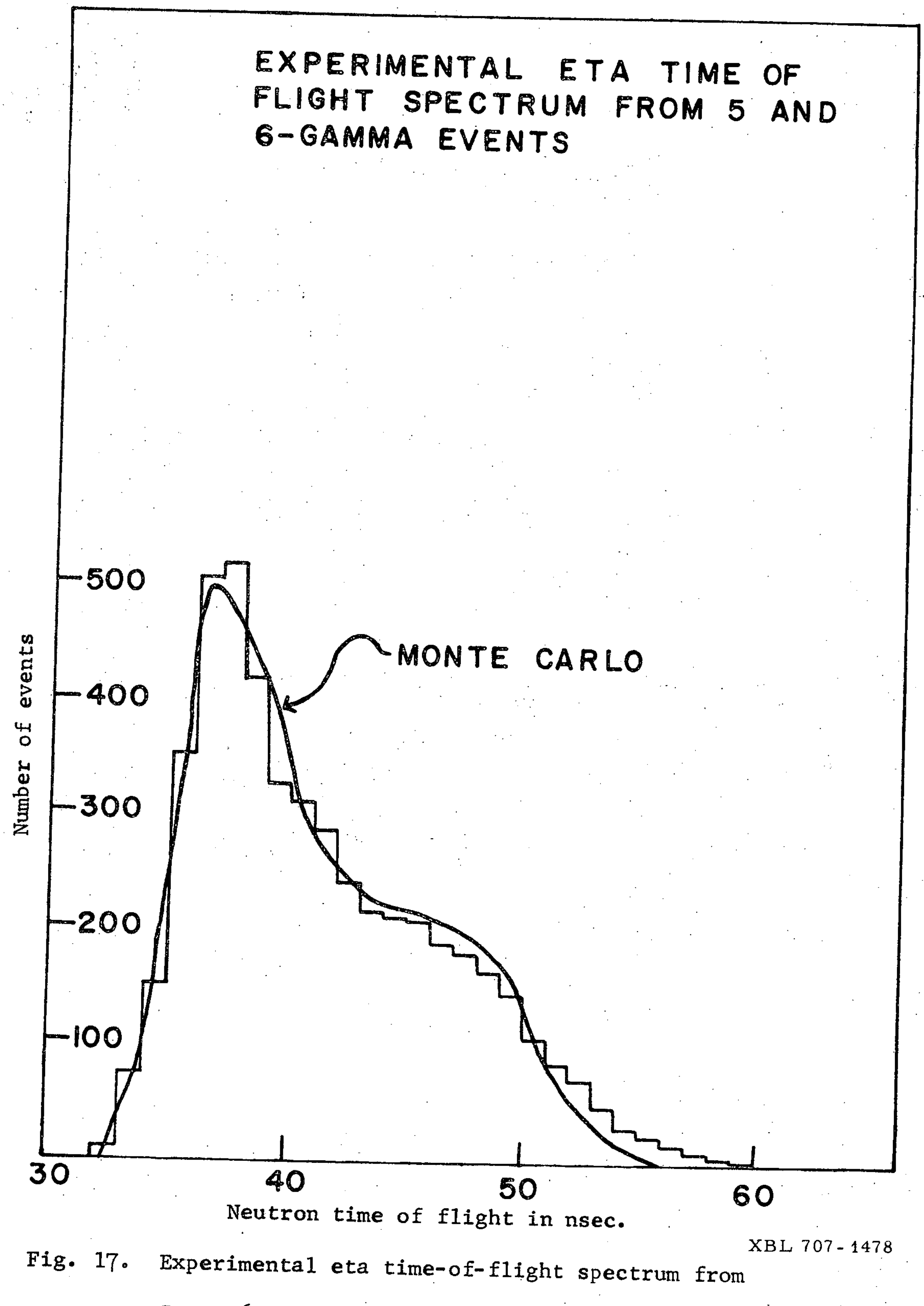

Fig. 17. Experimental eta time-of-flight spectrum from 5 and 6γ events.

with feed-down are insensitive to the exact shape of the η^o distribution. (i.e., they are insensitive to the Monte Carlo parameters). We find that: (1) The shapes for $\eta^o \to 3\pi^o \to 6\gamma$, $\eta^o \to 3\pi^o \to 5\gamma$, $\eta^o \to 3\pi^o \to 4\gamma$, and $\eta^o \to 3\pi^o \to 3\gamma$ are progressively narrower. (2) The shapes for $\eta^o \to (\gamma\gamma) \to 2\gamma$, $\eta^o \to (\gamma\gamma) \to 1\gamma$, and $\eta^o \to (\gamma\gamma) \to 0\gamma$ grow progressively narrower. (3) The shapes for $\eta^o \to 3\pi^o \to (5+6)\ \gamma$, and $\eta^o \to (\gamma\gamma) \to 2\gamma$ are identical and indistinguishable from the total η^o shape. We therefore use the "experimental η^o shape" in the 2γ, 5γ, and 6γ fits. We use our Monte Carlo knowledge of the feed-down shape changes to get modified (slightly narrower) distributions for use in the 0, 1, 3, and 4γ distributions.

<u>The $\pi^- p \to \pi^o\pi^o n$ Shape:</u> Because there is no $\pi^- p \to \eta^o n$ and essentially no $\pi^- p \to 3\pi^o n$ at 654 MeV/c, the 4γ spectrum should be entirely due to events of the type $\pi^- p \to \pi^o\pi^o n$. Figure 18 shows the 4γ time-of-flight distribution at 654 MeV/c. The phase space prediction for the $\pi^- p \to \pi^o\pi^o n$ distribution is shown with the same normalization. There is no agreement whatsoever. The data shows that high π-π mass combinations are favored (slow neutrons). This is not at all surprising; the same effect has been seen before in the reaction $\pi^- p \to \pi^-\pi^+ n$ in the same energy region.[59] It has also been observed at lower energies in the reaction $\pi^- p \to \pi^o\pi^o n$ (but <u>not</u> in the $\pi^- p \to \pi^-\pi^o p$).[60] Because this phenomenon is seen in $\pi^- p \to \pi^+\pi^- n$, and in $\pi^- p \to \pi^o\pi^o n$ but not in $\pi^- p \to \pi^-\pi^o p$, it is presumed to be an I = 0 effect. In the Kirz, Schwartz, and Tripp[59] investigation of $\pi^- p \to \pi^+\pi^- n$ the effect was seen quite strongly in the same energy region as in this experiment. If that experiment was able to see strongly an I = 0 effect in a final state which was a mixture of I = 0 and I = 1, then we should expect to see a large effect in our pure I = 0 reaction (we assume that I = 2 is negligible).

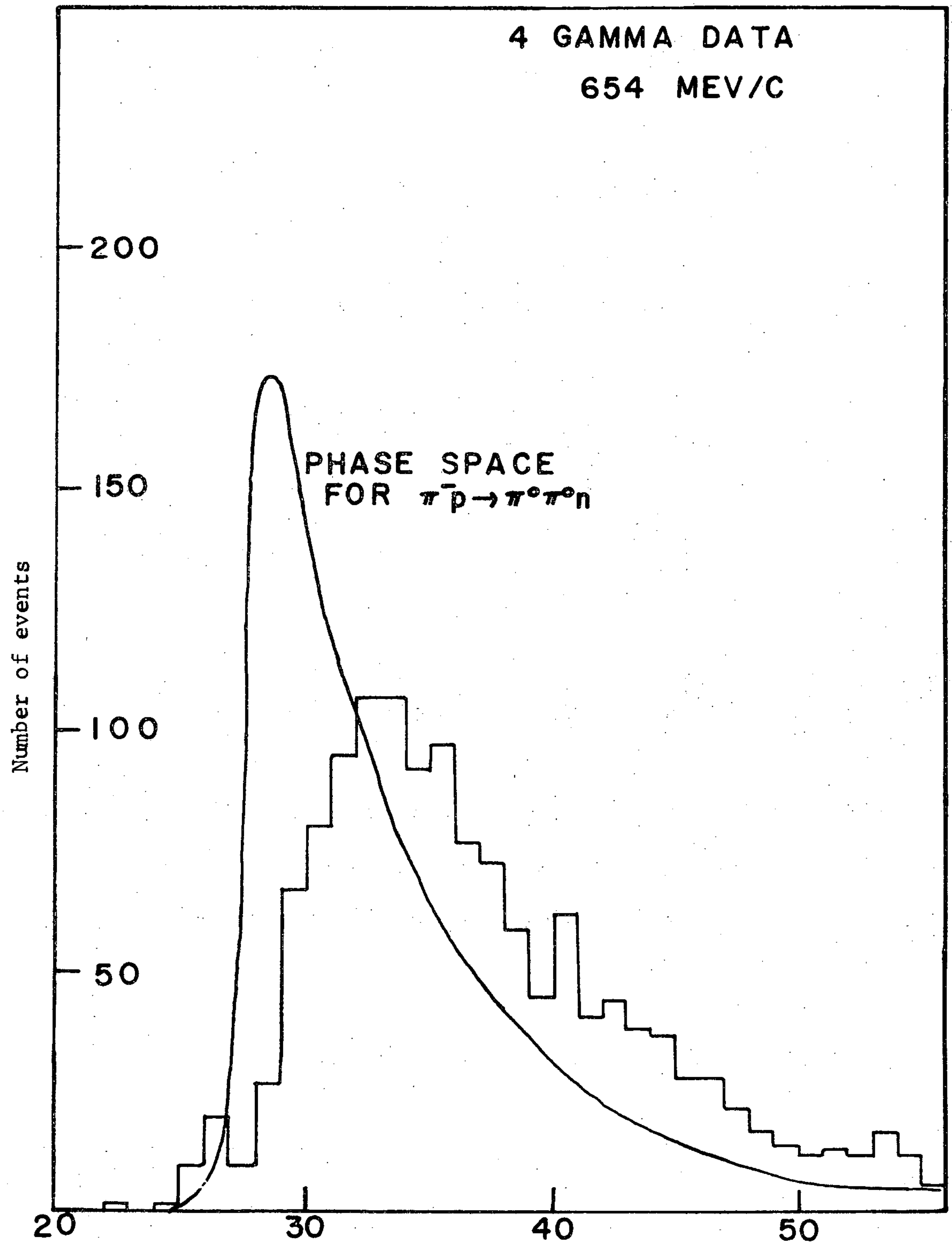

XBL 707-1481

Fig. 18. Comparison of the phase space prediction with the observed spectrum for $\pi^- p \rightarrow \pi^o \pi^o n$. The two distributions are normalized to the same total number of events.

Clearly the phase space shape for $\pi^- p \to \pi^o \pi^o n$ cannot be used to represent the experimental spectrum. We must infer the shape of the $\pi^o \pi^o n$ background at 716 MeV/c from the data at 654 and 772 MeV/c. Examination of Figs. 13 and 14 will show that the $\pi^- p \to \pi^o \pi^o n \to 3\gamma + n$ and $\pi^- p \to \pi^o \pi^o n \to 4\gamma + n$ spectra are not the same at 654 MeV/c. At 716 MeV/c they are closer to one another and at 772 MeV/c they appear to agree. That the 3γ and 4γ distributions are not the same is not surprising; once again, they may represent different kinematical classes. The procedure for obtaining the 3γ distribution is as follows: (1) the 3γ distribution at 654 MeV/c has the estimated charge exchange peak "feed-up" subtracted. (2) The 3γ distribution at 772 MeV/c has the charge exchange feed-up subtracted and the $\eta^o \to 3\pi^o \to 3\gamma$ feed-down subtracted. (3) The two distributions are smoothed out and normalized. (4) They are compared. Figure 19 shows them superimposed. The 772 MeV/c 3γ distribution has been shifted 3 nsec. (i.e., 3 bins) towards longer time-of-flight in order to place it close to the 654 MeV/c distribution. The similarity in shape is startling. The two distributions are averaged in this position. This is the $\pi^- p \to \pi^o \pi^o n \to 3\gamma + n$ "shape" to use at 716 MeV/c. One might naively think that this shape should be located in time midway between the 654 and 772 MeV/c positions. To make the peak of this distribution correspond with the peak in the 716 MeV/c data distribution, however, it is necessary to locate it 0.5 nsec towards the 772 MeV/c position from the center (i.e., 1 nsec from the 772 MeV/c position and 2 nsec from the 654 MeV/c position).

The shape for $\pi^- p \to \pi^o \pi^o n \to 4\gamma + n$ is obtained in similar fashion. In this case there is no charge exchange feed-up correction. The 654 MeV/c 4γ distribution is smoothed. An estimate of $\eta^o \to 3\pi^o \to 4\gamma$ feed-down is subtracted from the 4γ distribution at 772 MeV/c; then this distribution

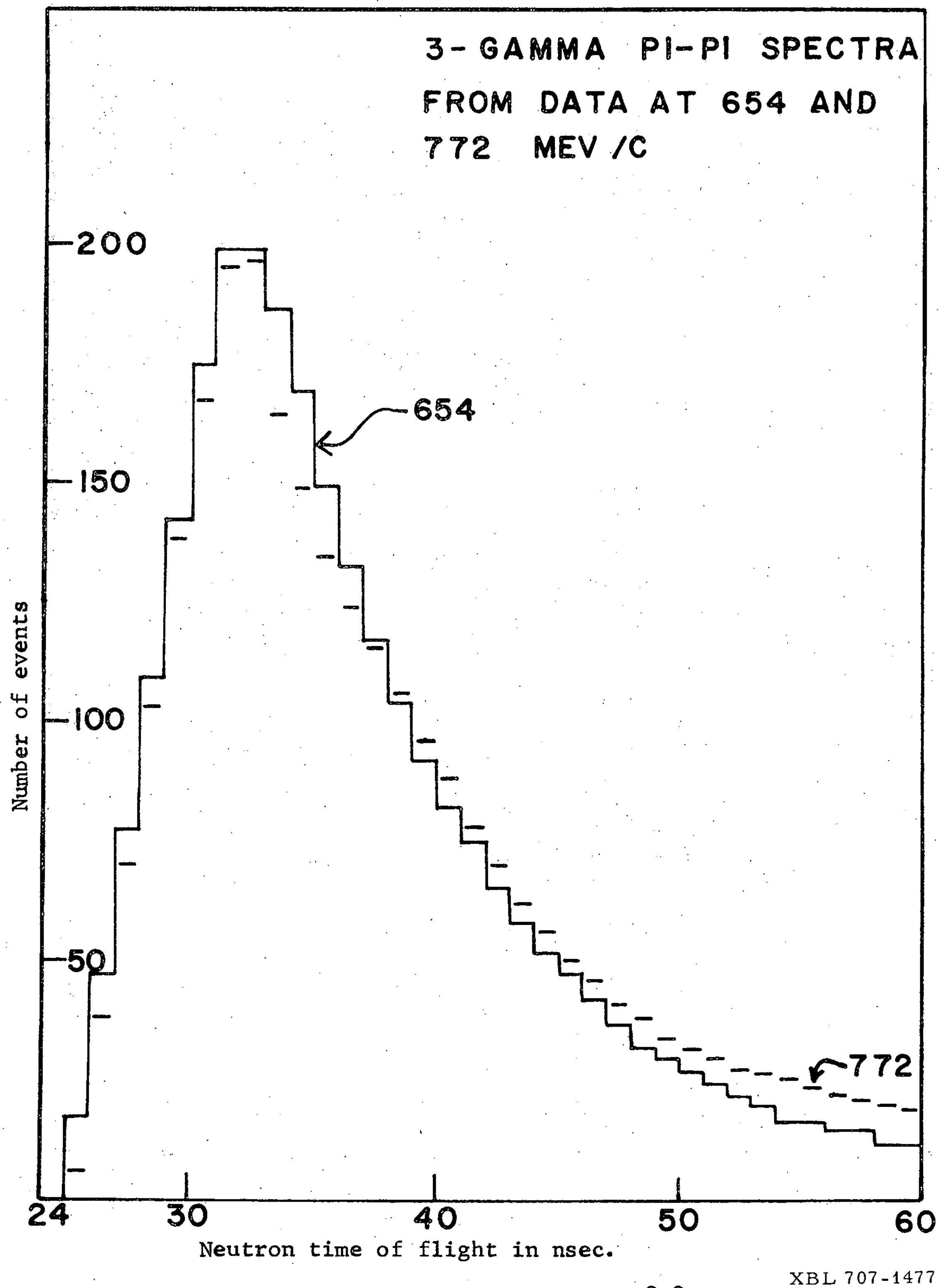

Fig. 19. Comparison of the 3γ spectra from $\pi^- p \to \pi^0\pi^0 n$ at 654 and 772 MeV/c. The 772 MeV/c spectrum has been shifted 3 nsec.

is smoothed. The two distributions (654 and 772 MeV/c) are similarly normalized and compared. Figure 20 shows the two superimposed; here the 772 MeV/c distribution has been shifted 4 nsec towards longer time of flight. Again the resemblance is striking. The two distributions are averaged in this position and then shifted 2 nsec towards shorter time of flight (i.e., halfway between the 654 and 772 MeV/c positions). Comparisons with the data distribution indicates that the peak in the $\pi^o\pi^o n \rightarrow 4\gamma + n$ shape does not coincide with the peak in the data distribution. Agreement is achieved by re-binning the 4γ data distribution 0.5 nsec (1/2 bin width) towards shorter time of flight. This means that the $\pi^o\pi^o n \rightarrow 4\gamma + n$ shape is effectively 0.5 nsec closer to the 654 MeV/c position than the center between 654 and 772 MeV/c.

The Shape of the Background under the 0, 1, and 2γ Distributions: To gain some insight into the background under the 0, 1, and 2γ distributions, let us re-examine Fig. 16. The failing events shown in histogram (3) form a continuum which decreases with increasing neutron time of flight. These events are the background under the "two-shower" η events and they must represent the major part of the background under the "2γ" η events.* These events are from charge exchange where the neutron has scattered in the spark chamber plates before reaching the neutron counters. A discussion of neutron scattering is presented in Appendix E. It turns out that neutron scattering is only noticeable for the charge exchange events, where it is a large effect. The effect of neutron scattering is seen as a long tail on the charge exchange peak. This tail is only present in the 0, 1, and

* We distinguish between "two-shower" events where two photons were observed as showers in the spark chambers and "2γ" events where two photons were detected by the system of counters and spark chambers.

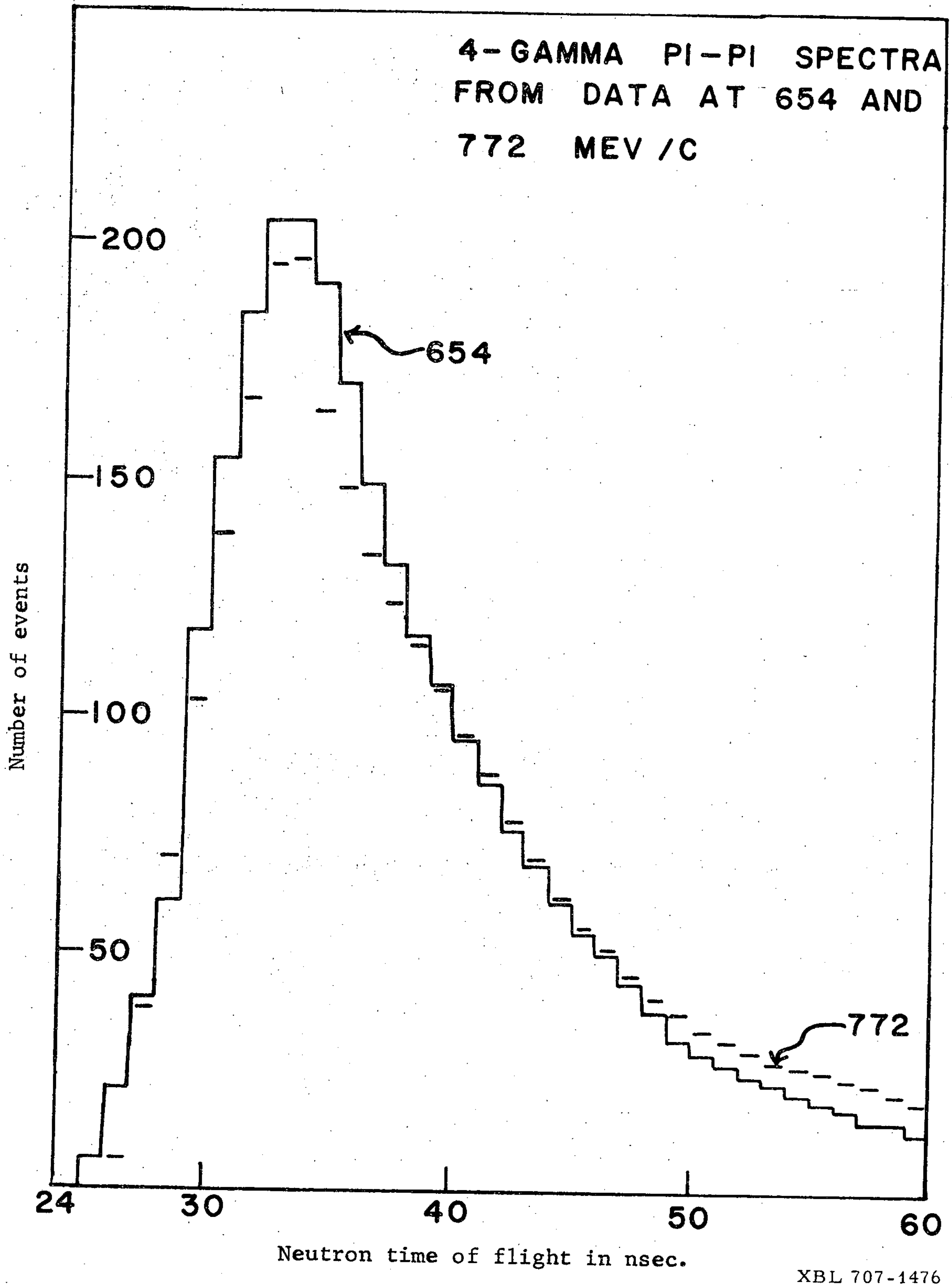

XBL 707-1476

Fig. 20. Comparison of the 4γ spectra from $\pi^- p \rightarrow \pi^o \pi^o n$ at 654 and 772 MeV/c. The 772 MeV/c spectrum has been shifted 4 nsec.

2γ distributions (actually, it may also be present in small amounts in the 3γ distribution due to feed-up). Figures 13 to 15 show that there is no evidence for such a background in any of the other gamma ray categories. The actual form of the neutron scattering tail depends on the charge exchange kinematics. For this reason the 0, 1, and 2γ backgrounds are treated separately. In fact the "two-shower" background in histogram (3) of Fig. 16 is not the same as the "two-gamma" background.

The shapes of the 0, 1, and 2γ backgrounds at 716 MeV/c are taken directly from the 654 MeV/c distributions. An estimate of the $\pi^- p \rightarrow \pi^o \pi^o n \rightarrow 2\gamma + n$ feed-down is subtracted from the 2γ distribution. Then the 0, 1, and 2γ distributions are smoothed and shifted 1 nsec towards shorter time of flight (in going from 654 to 716 MeV/c the charge exchange peak shifts 1 nsec in this direction). These are then the shapes to use in the fits to the 716 MeV/c distributions.

H. Least Squares Fits to the Time-of-Flight Distributions

The fitting is done only for the 716 MeV/c data distributions The time-of-flight region for the fitting is chosen to avoid the charge exchange region. We are not interested in this process. A least square fit is made to the distribution for each gamma ray category using the shapes described in the previous section. The number of η events is determined in this fashion for the 0, 1, 2, 3, and 4γ categories. The 5 and 6γ distributions are not fitted because we used them to determine the shape of the η peak. The number of η events in the 5γ category is simply the number of observed events. The number in the 6γ category is the number of observed events minus the amount of $\pi^- p \rightarrow 3\pi^0 n \rightarrow 6\gamma + n$ determined in the previous section.

Table V shows which of the distributions were used in each of the fits. For a given gamma ray category, the distributions used are for those processes which are expected to contribute directly and those which are expected to contribute through feed-up or feed-down. For example, consider the 3γ category: There are no processes which contribute directly (i.e., there are no processes present which produce 3γ rays). There may be η present through feed-up from the 2γ decay or through feed-down from either the $\pi^0\gamma\gamma$ or $3\pi^0$ decays. There may be $\pi^0\pi^0 n$ present through feed-down from 4γ events and there may be some 2γ scattered neutron background present through feed-up. The distribution used for the η in fitting the 3γ data is the 2γ eta distribution; this is because it is known (and will soon become obvious to the reader) that most of the events in the 3γ eta peak are due to feed-up.

The numerical results of the fits appear in Table VI. The number of events listed for the 5 and 6γ categories are the numbers obtained while

Table V. Distributions used in the least squares fits.

Number of Gamma Rays	η^o	$\pi^o\pi^o n$	Flat Background	Scattered neutron background
0	X		X	X
1	X	X	X	X
2	X	X	X	X
3	X	X	X	X
4	X	X	X	

Table VI. Numerical results of the least squares fits.

Number of γ rays	Number of η^o events found	Number of $\pi^o\pi^o n$ events found	Number of $3\pi^o n$ events found	Number of scattered neutron background events found	χ^2 per degree of freedom for the fit
0	-	-	-	80±12	4.224
1	772±45	-	-	544±40	1.601
2	7210±101	986±59	-	-	2.593
3	574±77	1908±81	-	-	0.981
4	819±86	2898±99	-	-	0.324
5	2236±70	-	-	-	-
6	2477±73	-	99±34	-	-

determining the "experimental η shape" (see the previous section). None of the fits found a non-zero contribution from a flat background (we considered the possibility that a randomly distributed background might be present).

Figures 21 to 24 show the results of the fitting procedure. The data distribution is shown as the closed histogram. We can see from Fig. 23 that the fitting procedure did not find all the 3γ eta events. The number of 3γ eta events listed in Table VI includes the excess 90 events in the η peak region not found by the fit.

There are several inconsistencies in the relative numbers of events found. The number of $\pi^o\pi^o n$ events found in the 2γ category is too large and the number of background events (zero) is too small. Based on the number of 3 and 4γ $\pi^o\pi^o n$ events we would expect to see ~ 475 2γ events from feed-down. The fitted number is nearly twice that. At the same time no background is found which is ridiculous. In fact, another fit was found which was almost as good ($\chi^2/F = 2.615$) and which reversed the above results: it found very nearly the same number of η^o events, no $\pi^o\pi^o n$ events, and 980 background events. We seem to be able to fit the 2γ distribution with either background or $\pi^o\pi^o n$, almost interchangeably; about half of each would lead to complete consistency among all the fitted numbers. The estimate of the 2γ background at 716 MeV/c from the 654 MeV/c data is the only realistic one we can use. Just to see what happens we have changed the shape of this background until we are able to obtain a better fit. Without changing the 2γ background very noticeably we were able to find a good fit ($\chi^2/F = 0.976$) with 7133±118 η^o events, 499±258 $\pi^o\pi^o n$ events, and 615±313 background events. These numbers of fitted events for the $\pi^o\pi^o n$ and background are completely consistent with the numbers found in other

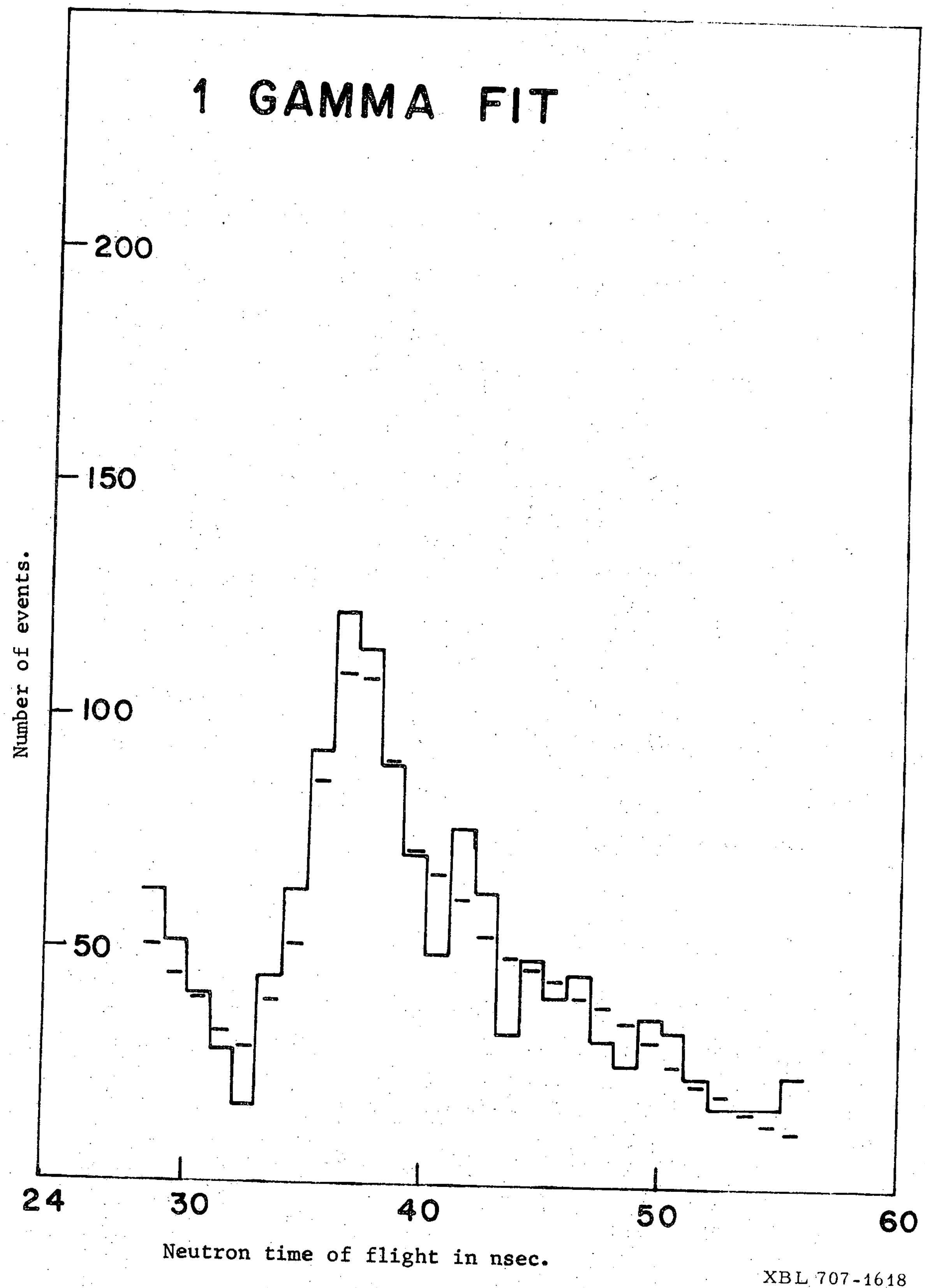

Fig. 21. The 1γ fit. The fitted distribution is the open histogram.

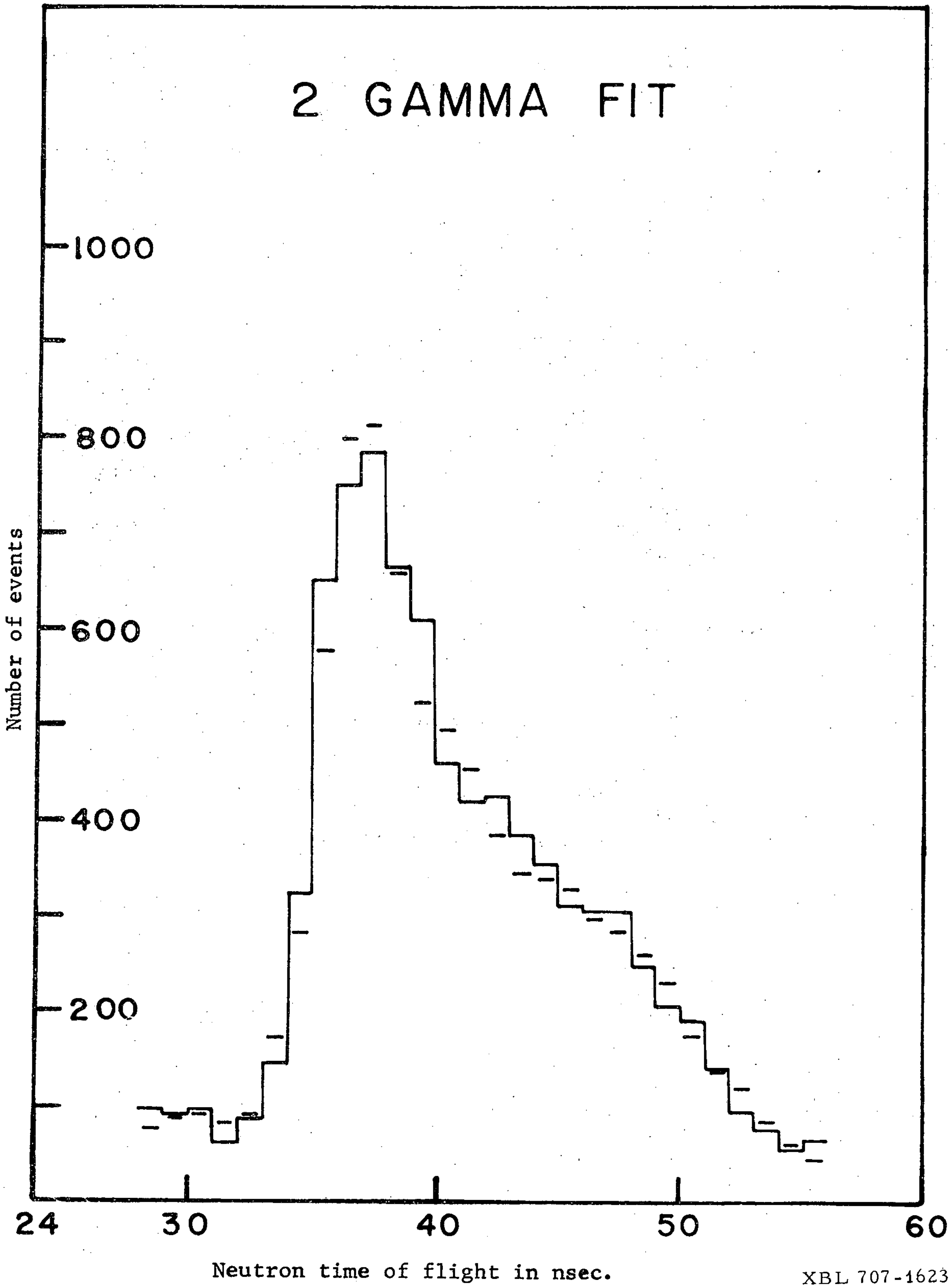

Fig. 22. The 2γ fit. The fitted distribution is the open histogram.

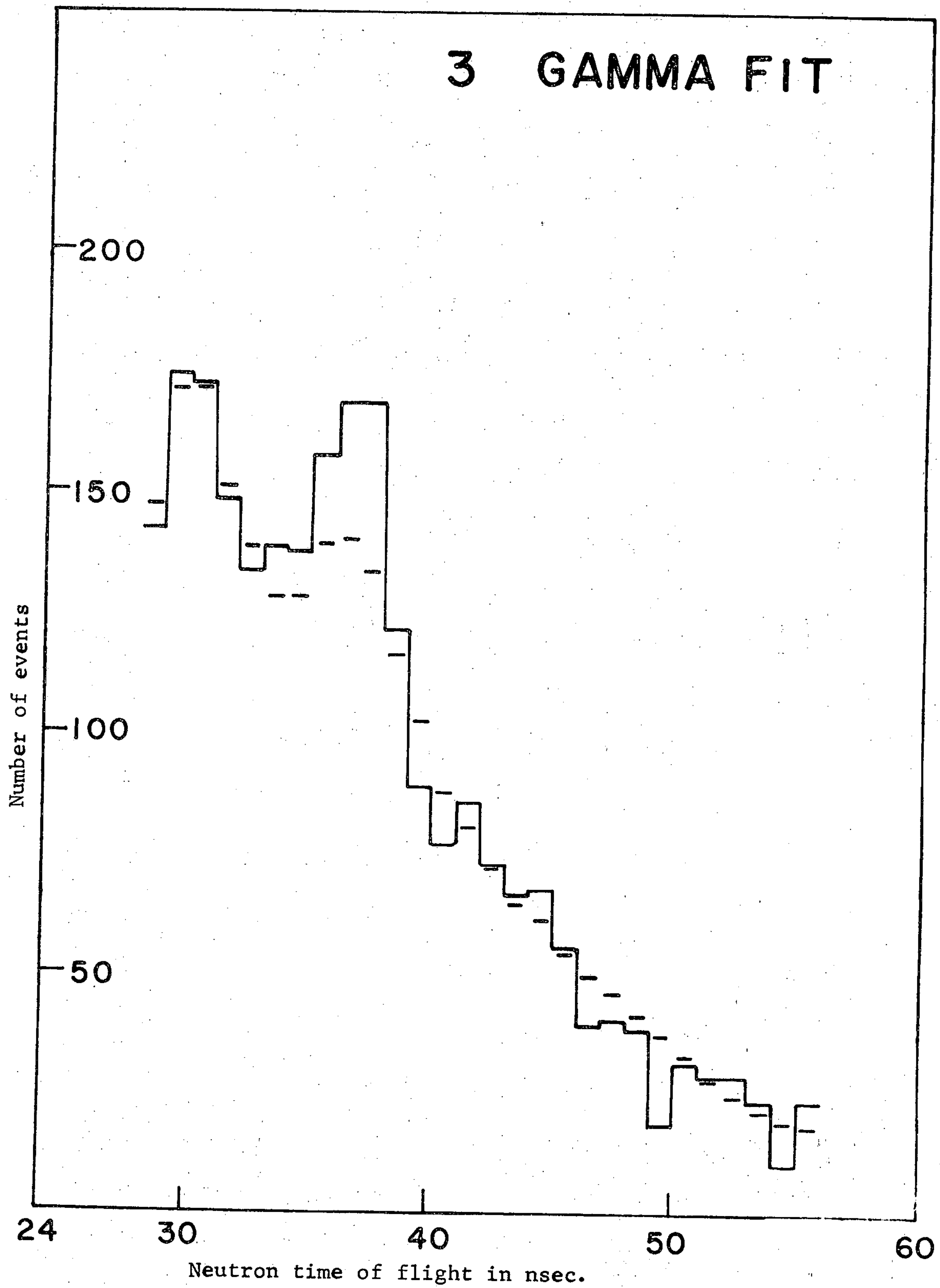

XBL 707-1622

Fig. 23. The 3γ fit. The fitted distribution is the open histogram.

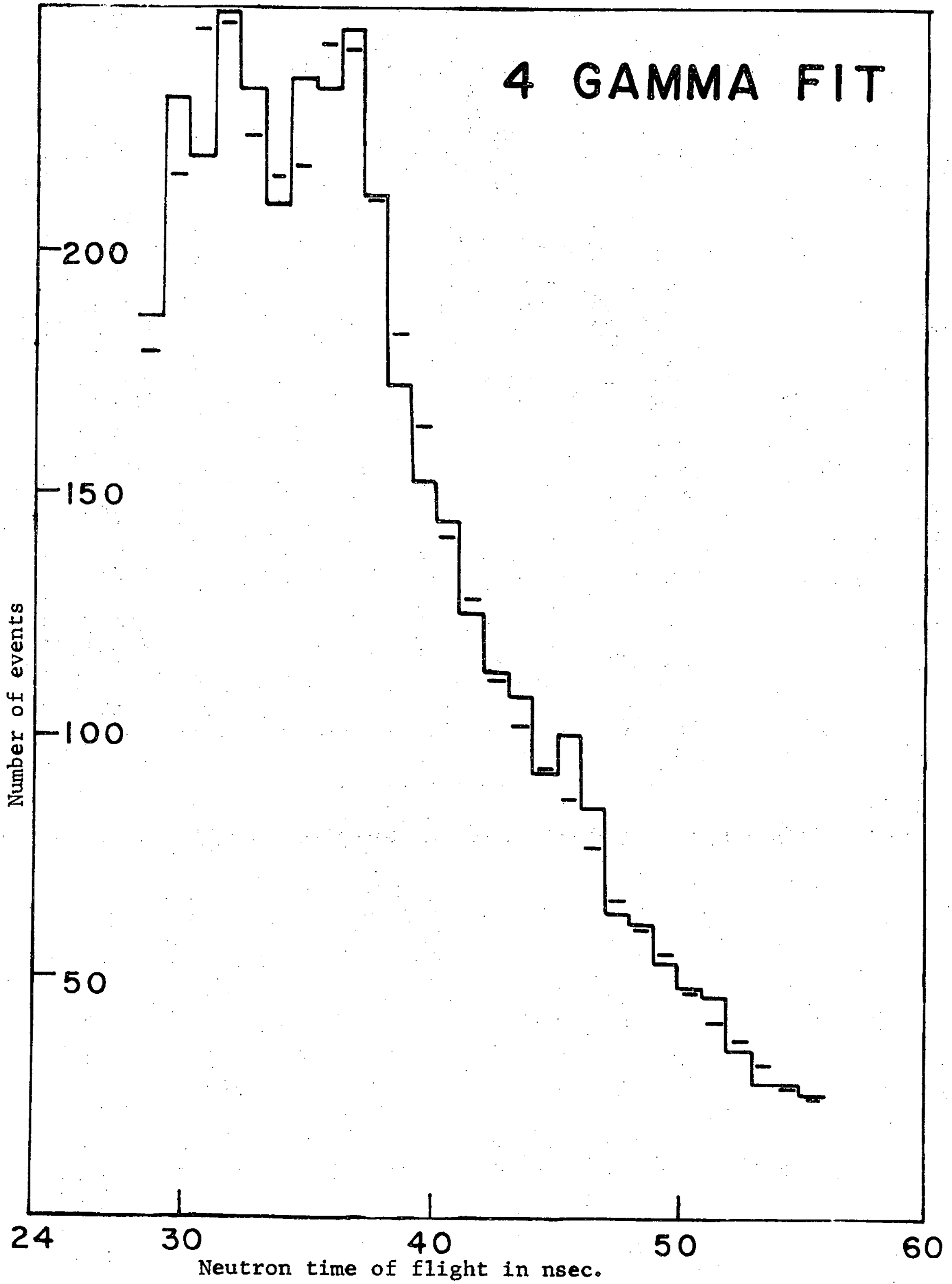

XBL 707-1621

Fig. 24. The 4γ fit. The fitted distribution is the open histogram.

categories of gamma rays. Notice that the number of η^o has not changed appreciably. In calculating the branching ratios we will use the number of $\eta^o \rightarrow 2\gamma$ from the fit listed in Table VI rather than the number we obtained by forcing the fit.

The fit to the 3γ distribution is not overly satisfying as we can see from Fig. 23. A much better fit was achieved by using a narrower η shape (i.e., the shape for $\eta^o \rightarrow 3\pi^o \rightarrow 3\gamma$). However, we can see from the number of events listed in Table VI that the 3γ η events are mostly feed-up from the 2γ events. If there are 2477 6γ events and 2236 5γ events, then we would expect 862 4γ events and 172 3γ events through feed-down from $\eta^o \rightarrow 3\pi^o$ decay. The observed number of 4γ events is completely consistent with this estimate; the number of 3γ events is much too large. If there were a large number of $\eta^o \rightarrow \pi^o\gamma\gamma$ decay events, they would appear mostly in the 4γ category. Consequently we are forced to the conclusion that the 3γ η events are mostly feed-up from 2γ events. So we have used the 2γ η shape which is broader and does not give as good a fit. Perhaps the feed-up mechanism is selective and the shape of feed-up events is narrower. At any rate, the events in the peak region could only be eta events so we add them to the number found in the fit.

The feed-up problem has confused things in the 3γ data. We shall therefore compute the amount of the $\eta^o \rightarrow \pi^o\gamma\gamma$ decay mode which is present (if any) from the 4γ data alone. The effect of adding the unfitted 90 events to the 3γ total will then be only to increase the number of $\eta^o \rightarrow \gamma\gamma$ events from 8320 to 8410; it will have no effect on the estimate of the amount of $\eta^o \rightarrow \pi^o\gamma\gamma$.

Figure 25 shows the results of the fits described above. Over the region for which the fits were done (shown by the dashed vertical lines)

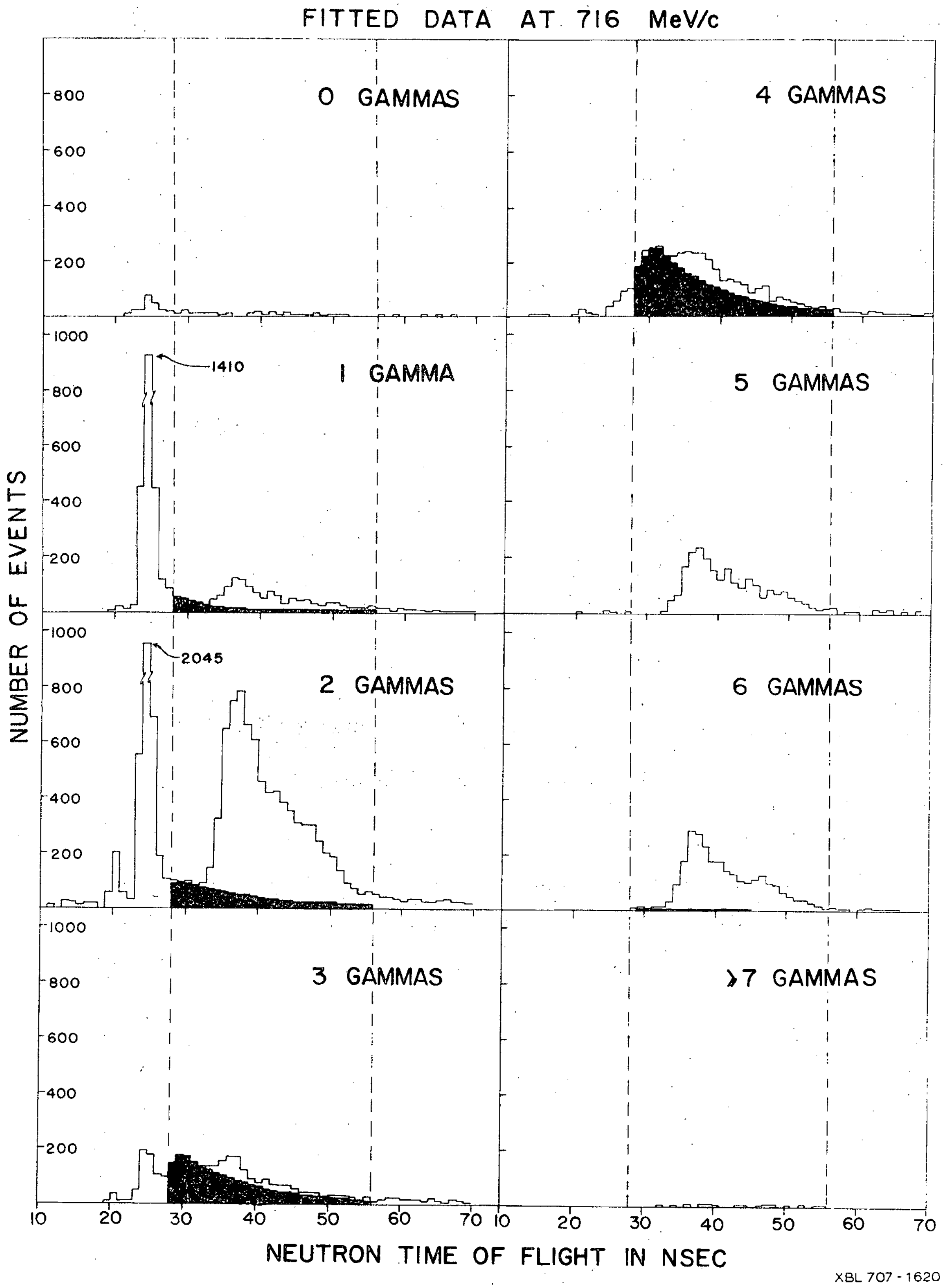

Fig. 25. The fitted data at 716 MeV/c. The vertical dashed lines indicate the region over which the fit was performed.

the numbers of non-eta events found are shown as a shaded histogram. The open histogram is simply the total experimental time-of-flight spectrum, exactly as in Fig. 13. Thus the number of η events found in each category is approximately the number between the two histograms (over the time of flight region for which the fits were done).

I. Feed-up Correction

As we have noted above we seem to have a probability of observing an extra gamma ray. This is most noticeable in the charge exchange region. At all three momenta shown in Figs. 13 to 15 there is an obvious charge exchange peak in the three gamma distribution (the π^0 decays into two gamma rays). This peak is .11, .08, .07 of the two gamma charge exchange peak at 654, 716, and 772 MeV/c respectively. Another place where feed-up is noticed is in the 5γ spectrum at 654 MeV/c. There are no 6γ events at 654 MeV/c so we presume that all observed 5γ events are feed-up from the 4γ events. The number of 5γ events is .05 of the number of 4γ events. Curiously, there appears to be no feed-up at all in the 5γ events at 716 and 772 MeV/c. The region just before the η^0 peak in the 5γ distribution, where we would expect feed-up from the $\pi^- p \rightarrow \pi^0\pi^0 n \rightarrow 4\gamma$ events, is unpopulated. Another place where we can see feed-up is in the 7γ categories (presumed to be feed-up from 6γ events because we do not observe any 8γ events). There are 76 ± 156 7γ events at 716 MeV/c and 56 ± 84 at 772 MeV/c. The big errors reflect the uncertainties in the scanning correction matrix for 7γ events. The sample of data from which this matrix was derived did not include a statistically large number of 7γ events. Using the above numbers we find feed-up of .03 and .09 at 716 and 772 MeV/c respectively. Finally, as discussed before, there is feed-up in the η^0 peak from 2 to 3γ. We estimate this feed-up by taking the difference of the number of η^0 events found in the 3γ categories and the number predicted as feed-down from 6γ, assuming no $\pi^0\gamma\gamma$ decay to be present. This is .055 at 716 and .05 at 772 MeV/c.

The obvious way to find out about the feed-up is to examine the large number of charge exchange events in the 3γ category. Several hundred such frames were examined. In most of these there was a shower which one could identify as the probable culprit.

There appear to be two principal mechanisms by which this feed-up can be produced. Both involve the gamma counters. First, there is the doubly-detected photon. Despite all the care exercised (see Sec. D, above) we do not seem to be able to eliminate this problem entirely. There are events about which a decision simply cannot be made. The other major mechanism involving the gamma counters is double gamma counter triggers. A gamma ray may materialize in one gamma counter and produce a shower which spills over into an adjacent counter. The result is that two gamma counters are triggered by one photon. A third, and less important, mechanism is fragmentation of showers. In some instances it is extremely difficult to tell whether a small shower near a larger one is part of the large shower or not. Finally, there are occasions when the remains of an old beam track may be mistaken for a shower.

Unfortunately, even though we know where most of the feed-up gammas come from, there is not much we can do about it. It is one thing to throw out a shower when you know the frame contains an extra one; it is another to make such a decision when you have no such information. If we were to take a hard line we could get rid of all the feed-up; at the same time we would be missing a large number of true showers. There are a large number of instances where we see two showers close together in the chambers. The Monte Carlo calculations also tells us that the probability of seeing two gamma rays close together is not negligible. Thus there are many events where we expect two adjacent gamma counters to trigger or where we expect there to be a visible shower near a triggered gamma counter. If we were to make a set of scanning rules which were stringent enough to eliminate the feed-up we would eliminate a lot of good data as well. Since the ultimate intention is to kinematically fit the events, we have adopted the point of view that it is better to let the fitting procedures throw away the feed-up gammas.

A certain amount of feed-up is impossible to get rid of because it is actually present in the form of a gamma ray shower which points back to the hydrogen target. Because the spark chambers have an active time of ~ 2.5 microseconds there is a non-zero probability that we may observe showers from a prior event. The vast majority of such showers will be from charge exchange reactions. Approximately 75% of the charge exchange reactions at 716 MeV/c have only one visible shower. (We do not expect to observe photons from an earlier event in time which trigger the gamma counters since the triggered gamma counter must be in fast coincidence with the beam.) Thus there is some likelihood that we may see feed-up which is due to a one shower charge exchange event from an earlier time. A roll of film was taken to study this effect under precisely the same beam conditions as a regular data roll. During the beam spill the chambers were pulsed at random. The film was normalized to the regular roll by comparing the number of accidental beam tracks. A single accidental shower was found in 2% of the frames. Two accidental showers were found in 0.5% of the frames and three in 0.2% of the frames. No frames were found with more than three accidental showers. The relative numbers of 1 and 2γ accidental events is consistent with these being due to charge exchange reactions. There were no frames with an accidental gamma counter triggered.

We see that there is a 2% feed-up which we cannot avoid no matter how we scan the film. This is another argument in favor of not trying to scan so restrictively as to minimize the feed-up. We can never go below 2%.

Recall that no feed-up was observed from the 4γ events at 716 and 772 MeV/c. A 2% feed-up is not inconsistent with this finding as the statistics involved are poor. We actually see no evidence anywhere in the data for feed-up of 2γ. Once again, this would be difficult to observe because of the small numbers of events involved.

The relative numbers of $\eta^o \to N\gamma$ decays found in the least square fits to the time of flight distributions must be corrected for feed-up. It is difficult to determine the exact amount of feed-up to correct for. Since the feed-up is attributable to a large number of different sources, it is difficult to estimate exactly how it changes with the number of gamma rays involved. We will assume that the feed-up is the same regardless of the number of gamma rays involved. Further, we will take the feed-up to be 5% which is an average of all the different feed-up effects that we see. (We will, however, not use 5% as the 6 into 7γ feedup; instead we will use the observed number of 76 events).

Table VII shows the relative numbers of gamma rays from η decay before and after the feed-up correction. It must be emphasized that the feed-up correction makes very little difference in the results. The number of $\eta^o \to \pi^o\gamma\gamma$ decays is calculated from the 4γ η^o events only. We do not use the 3γ events because of the feed-up ambiguity. Secondly, there is no possibility of confusing the $\eta^o \to \gamma\gamma$ and $\eta^o \to 3\pi^o$ decay modes; events from $\eta^o \to \gamma\gamma$ cannot feed up into $\eta^o \to 3\pi^o$ events. Since we find there to be no evidence for $\eta^o \to \pi^o\gamma\gamma$, the total numbers of $\eta^o \to \gamma\gamma$ or $\eta^o \to 3\pi^o$ events are not in any noticeable way changed by the feed-up correction. The only place that the feed-up correction enters into the results is through the estimate of the predicted number of $\eta^o \to 3\pi^o \to 4\gamma$ events. The feed-up correction changes the relative numbers of 4, 5, and 6γ events from the decay $\eta^o \to 3\pi^o$. The upper limit we will quote for $\eta^o \to \pi^o\gamma\gamma$ depends to some degree on the feed-up correction. This dependance is not very significant as we will see below.

Table VII. Feed-up correction for η events.

Number of gamma rays	Number of η^o events before feed-up correction	Number of η^o events after correction
0	0	0
1	772 ± 45	813 ± 47
2	7210 ± 101	7550 ± 106
3	574 ± 77	204 ± 81
4	819 ± 86	851 ± 91
5	2236 ± 70	2309 ± 74
6	2477 ± 73	2437 ± 77

J. Determination of the Branching Ratios

We now know the number of events of the type $\eta^o \to N\gamma$ for N = 0, 1, ...6. We assume, in calculating the branching ratios, that only the modes $\eta^o \to \gamma\gamma$, $\eta^o \to \pi^o\gamma\gamma$, and $\eta^o \to 3\pi^o$ are present. Events with 0, 1, and 2 detected γ are clearly $\eta^o \to \gamma\gamma$ decays. Five and 6γ events are clearly from the $\eta^o \to 3\pi^o$ decay. Three and 4γ events are either $\eta^o \to \pi^o\gamma\gamma$ events or feed-down from $\eta^o \to 3\pi^o$ events. We must estimate the number of 4γ events from $\eta^o \to 3\pi^o$ feed-down and compare that with the number we see. The excess over the number of expected feed-down events will indicate the amount of $\eta^o \to \pi^o\gamma\gamma$ present.

There are two approaches we can use to determine the feed-down. The first is by Monte Carlo calculation. We have a fairly elaborate Monte Carlo calculation which takes into account the spark chamber geometry and a detailed semi-empirical model for shower production.[56] Another approach is simply to assume: (1) that there is some (unknown) average gamma ray detection efficiency, q, for a given type of decay, and (2) that the probability for a given gamma ray escaping, (1 - q), does not depend on what happens to any of the other gamma rays. If both these assumptions are true then the probability of observing n gamma rays when m were produced is:

$$P_{n/m} = \frac{m!}{n!(m-n)!} \; q^n (1-q)^{(m-n)} \; .$$

Now assumption number (1) above must always be true; the average detection probability is simply the fraction of gamma rays detected. The main question regards the second assumption. It is obvious that this should not be exactly true. For example, if two of the six gamma rays from $\eta^o \to 3\pi^o$ have escaped upstream, the probability of a third one escaping in the same way will be much less. But, if the feed-down is small enough, it may well be that assumption (2) is approximately true and that the above relationship for $P_{n/m}$ is also approximately true. The Monte Carlo calculation takes into account all the nonuniformities in the spark chambers; it should be a good place to check the feed-down predictions for $P_{n/m}$.

It turns out that, for any process we observe, we can always find a q such that the above relationship $P_{n/m}$ describes the feed-down accurately. This is not a trivial relationship to satisfy. For example, the Monte Carlo prediction for feed-down from $\eta^o \rightarrow 3\pi^o$ at 716 MeV/c is that we should see 43.4%, 39.7%, 14.1%, 2.5%, and 0.3% of the events at 6, 5, 4, 3, and 2γ events. The predictions of the binomial coefficient $P_{n/m}$ with $q = 0.87$ are 43%, 39%, 15%, 3%, and 0% in the same sequence of gamma categories. The agreement is very good. Other processes described by the Monte Carlo agree as well with the binomial coefficient predictions.

In Sec. G, where the shapes for the fits to the time of flight distributions were described, it was often mentioned that various feed-down "estimates" were made in finding the background distributions. These estimates were made from a table of coefficients $P_{n/m}$. For example, if there are N_4 4γ events (from $\pi^- p \rightarrow \pi^o\pi^o n$) and N_3 3γ events, then we look in the table for a q such that

$$\left(P_{4/4}\right) \Big/ \left(P_{3/4}\right) = N_4 \Big/ N_3 \quad .$$

Then the numbers N_2, N_1, and N_0 can be determined from the coefficients $P_{2/4}$, $P_{1/4}$, and $P_{0/4}$.

In calculating the branching ratios we prefer to use the Monte Carlo calculation because we are aware of the weakness of the assumption (2) above. The resulting inaccuracy in the binomial coefficient is probably only ~ 1% of the total number of decays but we are trying to make calculations on this level of accuracy.

The Monte Carlo predictions for $\eta^{o} \to 3\pi^{o}$ feed-down are as follows (we assume that for the number of 6γ events the Monte Carlo and data agree):

$$N_6 = 2437$$
$$N_5 = 2229$$
$$N_4 = 792$$
$$N_3 = 140$$
$$N_2 = 17$$

Comparing these numbers with Table VII we see that the number of observed 4γ decays is consistent with feed-down from $\eta^{o} \to 3\pi^{o}$. We do not concern ourselves with the 3γ events because of the feed-up introduced ambiguity. Thus we see that the amount of $\eta^{o} \to \pi^{o}\gamma\gamma$ is consistent with zero.

Under the assumption that there is no $\eta^{o} \to \pi^{o}\gamma\gamma$ present, we now calculate the $\eta^{o} \to \gamma\gamma$ and $\eta^{o} \to 3\pi^{o}$ branching ratios. We assume that all the 4, 5, and 6γ events are from $\eta^{o} \to 3\pi^{o}$. We also assume that the Monte Carlo predictions are correct so that there are 140 $\eta^{o} \to 3\pi^{o} \to 3\gamma$ and 17 $\eta^{o} \to 3\pi^{o} \to 2\gamma$ events. Thus we have 8410 ± 129 $\eta^{o} \to \gamma\gamma$ events and 5754 ± 151 $\eta^{o} \to 3\pi^{o}$ events. Then the branching ratios are

$$R\left(\frac{\eta^{o} \to \gamma\gamma}{\eta^{o} \to \text{all neutrals}}\right) = 0.594 \pm 0.012$$

$$R\left(\frac{\eta^{o} \to 3\pi^{o}}{\eta^{o} \to \text{all neutrals}}\right) = 0.406 \pm 0.012.$$

The above branching ratios must be corrected for systematic effects. There is a probability (~ .009) that an individual gamma ray will convert prematurely in the target walls and veto the events. Also, a decay involving a Dalitz pair will cause the event to be vetoed. The combination of these two effects is expected to veto $(3.4\pm0.5)\%$ of the $\eta^o \to \gamma\gamma$ decays and $(8.8\pm1.4)\%$ of the $\eta^o \to 3\pi^o$ decays. The corrected branching ratios are

$$R\left(\frac{\eta^o \to \gamma\gamma}{\eta^o \to \text{all neutrals}}\right) = 0.580\pm0.013$$

$$R\left(\frac{\eta^o \to 3\pi^o}{\eta^o \to \text{all neutrals}}\right) = 0.420\pm0.015.$$

Finally, we calculate an upper limit on the amount of $\eta^o \to \pi^o\gamma\gamma$ present. To do this we must estimate the error on our Monte Carlo prediction for the number of 4γ events expected as feed-down from the $\eta^o \to 3\pi^o$ decay. The Monte Carlo prediction for the $\eta^o \to 2\gamma$ feed-down is 87.5% two-gamma and 12.5% one-gamma events. We actually observe 90% and 10% respectively. This corresponds to the binomial coefficients for $q_{2\gamma} = .950$. The Monte Carlo prediction implies a $q_{2\gamma} = .935$. That means the Monte Carlo has made an "error" of 1.5% in determining the "average detection efficiency per gamma ray." The Monte Carlo feed-down prediction for $\eta^o \to 3\pi^o$ is very close to that of the binomial coefficient prediction for $q_{6\gamma} = .87$. Using the binomial coefficients for $q = .87\pm.015$, we deduce an error for the Monte Carlo prediction. The result is that the Monte Carlo predicts there to be 792 ± 221 4γ events from the $\eta^o \to 3\pi^o$ decay. We observe 851 ± 91 4γ events. We conclude that there are 59 ± 239 4γ events from the mode $\eta^o \to \pi^o\gamma\gamma$. We know from the Monte Carlo that 61% of the $\eta^o \to \pi^o\gamma\gamma$ decays appear as 4γ events. Thus we have, finally, 97 ± 392 decays of the type $\eta^o \to \pi^o\gamma\gamma$. Or, with 95% confidence, we have that the number of $\eta^o \to \pi^o\gamma\gamma$ events is less than 881. This means that

$$R\left(\frac{\eta^o \to \pi^o\gamma\gamma}{\eta^o \to \text{all neutrals}}\right) < 0.061 \text{ with 95\% confidence.}$$

Had we used the numbers which were uncorrected for feed-up, this upper limit would have been 0.058. The feed-up correction has made a negligible difference as indicated above.

V. CONCLUSIONS

We find that our data are consistent with zero decays of the type $\eta^o \to \pi^o\gamma\gamma$. With the assumption that only the decays $\eta^o \to \gamma\gamma$ and $\eta^o \to 3\pi^o$ are present, we find

$$R\left(\frac{\eta^o \to \gamma\gamma}{\eta^o \to \text{all neutrals}}\right) = 0.580 \pm 0.013$$

$$R\left(\frac{\eta^o \to 3\pi^o}{\eta^o \to \text{all neutrals}}\right) = 0.420 \pm 0.015 \quad .$$

Furthermore, we find that, with 95% confidence

$$R\left(\frac{\eta^o \to \pi^o\gamma\gamma}{\eta^o \to \text{all neutrals}}\right) < 0.061.$$

This limit is as low as any previously published.[44] The present experiment has a much more complete picture of the η decay scheme. Consequently it is less subject to systematic errors and relies less heavily on Monte Carlo calculations.

If we combine the $\left(\frac{\eta^o \to 3\pi^o}{\eta^o \to \text{neutrals}}\right)$ branching ratio found in this experiment with the "all neutrals" and $\pi^+\pi^-\pi^o$ branching ratios representing the current world averages,[14] we find that

$$R\left(\frac{\pi^o\pi^o\pi^o}{\pi^+\pi^-\pi^o}\right) \cong 1.31 \pm 0.10.$$

This value is low enough to suggest that the linear matrix element may be inadequate but not so low as to imply a $\Delta I = 3$ transition.

ACKNOWLEDGEMENTS

I would like to express my sincere appreciation to Professor A. C. Helmholz who has been my advisor, research director, and the chairman of my dissertation committee. I am also indebted to Professor Burton J. Moyer for his support over the years.

The data accumulation for this thesis was performed under the guidance of Drs. Robert W. Kenney and Michael A. Wahlig. The data analysis was performed under the guidance of Drs. Morris Pripstein and Orin Dahl. I am indebted to all these gentlemen, from each of whom I have learned a great deal.

My fellow graduate students, Roger Chaffee, Ivan Linscott, and Jerry Nelson have all contributed copiously of their time and ingenuity. Without their assistance this thesis could not have been completed.

I am also indebted to the scanning and measuring group under the direction of Miss Ellen Epstein and Mr. Robert Hogrefe. Mr. Thomas Dodson scanned most of the difficult film.

I am also grateful to Miss Miriam L. Machlis who has cheerfully typed several versions of this manuscript and patiently corrected any grammatical errors.

This work was done under the auspices of the U. S. Atomic Energy Commission.

APPENDICES

A. Radiative Decay Modes

If $\underline{k} = k\hat{k}$ is the momentum of a gamma ray and $\underline{e}$ is its polarization vector ($\underline{k} \cdot \underline{e} = 0$) then electric moments appear as terms in $(k\underline{e})$ in a matrix element and magnetic moments appear as terms in $(\underline{k} \times \underline{e})$. If $\sum_e$ represents a sum over gamma ray spins then we have for any vectors $\underline{A}$ and $\underline{B}$

$$\sum_e (\underline{A} \cdot \underline{e})(\underline{B} \cdot \underline{e}) = \underline{A} \cdot \underline{B} - (\underline{A} \cdot \hat{k})(\underline{B} \cdot \hat{k}) \tag{1}$$

$$\sum_e (\underline{A} \times \underline{e}) \cdot (\underline{B} \times \underline{e}) = \underline{A} \cdot \underline{B} + (\underline{A} \cdot \hat{k})(\underline{B} \cdot \hat{k}). \tag{2}$$

With these relationships we can form the simplest matrix elements with the correct angular momentum properties for a given radiative decay.

Case 1. $\eta^o \to \gamma\gamma$

The building blocks for the matrix elements for this process are:

$\underline{k} = \underline{k}_1 = - \underline{k}_2$ where $\underline{k}_i$ is the momentum of gamma ray γ_i

$$\left.\begin{matrix} k_1\underline{e}_1 \\ \\ k_2\underline{e}_2 \end{matrix}\right\} \text{electric moments}$$

$$\left.\begin{matrix} \underline{k}_1 \times \underline{e}_1 \\ \\ \underline{k}_2 \times \underline{e}_2 \end{matrix}\right\} \text{magnetic moments}$$

The matrix element must be symmetric in γ_1, γ_2. Because $J^P = 0^-$ and the photons have negative intrinsic parity, we want the matrix element to be a scalar form with negative parity. It must therefore have orbital angular momentum $\ell = 1$; that is, there must be one vector $\underline{k}$ in the matrix element to represent the single unit of orbital angular momentum. The simplest matrix element with these properties is

$$M = f(k)k_1\underline{e}_1 \cdot (\underline{k}_2 \times \underline{e}_2)$$

$$= f(k)k_1(\underline{e}_2 \times \underline{e}_1) \cdot \underline{k}_2$$

$$= f(k)k\ \underline{k} \cdot (\underline{e}_1 \times \underline{e}_2)\ .$$

Here we have used $\underline{k}_1 = -\underline{k}_2 = \underline{k}$. $f(k)$ is a model dependent form factor. Notice that the above amplitude is symmetric in γ_1 and γ_2.

The transition rate $\Gamma_{\gamma\gamma}$ will depend on the square of the matrix element summed over the undetected final state polarizations

$$\Gamma_{\gamma\gamma} \sim \sum_{e_1, e_2} |M|^2 = \sum_{e_1, e_2} |f(k)|^2 k^2 \left[\underline{k} \cdot (\underline{e}_1 \times \underline{e}_2)\right]^2 \ .$$

Using the relations (1) and (2) above, we find

$$\Gamma_{\gamma\gamma} \sim 2|f(k)|^2 k^4.$$

<u>Case 2.</u> $\eta^o \to \pi^+\pi^-\gamma$

Here we need to construct a scalar form with positive total orbital parity. Consider the pions as a sub-system with internal orbital angular momentum ℓ. The $\pi\pi$ system has orbital angular momentum L relative to the γ. Since the η^o has C = +1 and the γ has C = -1, the $\pi\pi$ system must have C = -1. This implies that ℓ is odd $\left(C(\pi^+\pi^-) = (-1)^\ell \right)$. To get the proper parity we must then have L odd also $\left\{ P(\eta^o) = -1 \text{ and } P(\pi\pi\gamma) = (-1)^3(-1)^\ell(-1)^L \right\}$.
The simplest situation is $\ell = L = 1$.

Let

$\underline{q}$ = momentum of π^+ in $\pi\pi$ rest frame

$\underline{k}$ = momentum of γ in η^o rest frame

$\underline{e} = \gamma$ spin.

The possible building blocks for the matrix element are then

$\underline{q}$, the π^+ momentum

$(\underline{k} \times \underline{e})$, magnetic moments

$(k\underline{e})$, electric moments.

Since $\ell = 1$ we must have one factor of $\underline{q}$ in the matrix element. $L = 1$ implies the presence of one factor of $\underline{k}$. Hence we have, where $f(k,q)$ is a model dependent form factor,

$$M = f(k,q)\underline{q} \cdot (\underline{k} \times \underline{e}).$$

Squaring and summing over the photon spin $\underline{e}$ using relations (1) and (2) we have

$$\Gamma_{\pi^+\pi^-\gamma} \sim \sum_{e} |M|^2 = |f(k,q)|^2 |\underline{q} \times \underline{k}|^2$$

$$= |f(k,q)|^2 q^2 k^2 \sin^2 \theta$$

where θ is the angle between the π^+ and the γ in the $\pi\pi$ rest frame.

<u>Case 3.</u> $\eta^o \to \pi^o \gamma\gamma$

Let $\underline{\pi}$ = momentum of π^o in the η^o rest frame and $\underline{k}_1$, $\underline{k}_2$ = the momenta of γ_1 and γ_2 respectively in the same frame. With $\underline{e}_1$, $\underline{e}_2$ as the photon spins the matrix element blocks are

$$\left.\begin{matrix} k_1\underline{e}_1 \\ \\ k_2\underline{e}_2 \end{matrix}\right\} \text{electric moments}$$

$$\left.\begin{matrix} \underline{k}_1 \times \underline{e}_1 \\ \\ \underline{k}_2 \times \underline{e}_2 \end{matrix}\right\} \text{magnetic moments}$$

$\underline{\pi} = -(\underline{k}_1 + \underline{k}_2)$ is not an independent variable and need not be included in M. The matrix element must have $J^P = 0^+$ because the intrinsic parity is $P = P(\pi^o)P(\gamma)^2 = -1$. It must also be symmetric in γ_1 and γ_2. Thus we have

$$M = f_1(k_1\underline{e}_1) \cdot (k_2\underline{e}_2) + f_2(\underline{k}_1 \times \underline{e}_1) \cdot (\underline{k}_2 \times \underline{e}_2) .$$

The model dependent form factors f_1 and f_2 are symmetric functions of k_1 and k_2. The simplest possibility is $f_1 = a$ and $f_2 = b$ where a and b are constants. Then the matrix element is

$$M = a\, k_1k_2(\underline{e}_1 \cdot \underline{e}_2) + b\Big[(\underline{k}_1 \cdot \underline{k}_2)(\underline{e}_1 \cdot \underline{e}_2) - (\underline{k}_1 \cdot \underline{e}_2)(\underline{k}_2 \cdot \underline{e}_1)\Big]$$

$$= k_1k_2 \left[(a + b \cos \theta)(\underline{e}_1 \cdot \underline{e}_2) - b(\hat{k}_1 \cdot \underline{e}_2)(\hat{k}_2 \cdot \underline{e}_1)\right]$$

and

$$|M|^2 = k_1^2k_2^2 \Big[(a + b \cos \theta)^2(\underline{e}_1 \cdot \underline{e}_2)^2$$

$$- 2b(a + b \cos \theta)(\underline{e}_1 \cdot \underline{e}_2)(\hat{k}_1 \cdot \underline{e}_2)(\hat{k}_2 \cdot \underline{e}_1)$$

$$+ b^2(\hat{k}_1 \cdot \underline{e}_2)^2(\hat{k}_2 \cdot \underline{e}_1)^2\Big]$$

where θ is the angle between $\underline{k}_1$ and $\underline{k}_2$. When summed over the photon spins we have

$$\sum_{e_1, e_2} |M|^2 = k_1^2k_2^2 \Big[(a + b \cos \theta)^2(1 + \cos^2 \theta) + b^2 \sin^4 \theta$$

$$+ 2b(a + b \cos \theta) \cos \theta \sin^2 \theta\Big]$$

$$= k_1^2k_2^2 \Big[(a + b \cos \theta)^2(1 + \cos^2 \theta)$$

$$+ b^2(1 + \frac{2a}{b} \cos \theta + \cos^2 \theta) \sin^2 \theta\Big]$$

$$= k_1^2k_2^2\, f(\theta) .$$

In the special case where $b = - a$ (or, indeed, more generally where $f_2 = - f_1$) we have $f(\theta) = 2(1 - \cos \theta)^2$. If $m_{\gamma\gamma}$ is the invariant mass of the two gamma rays, then

$$m_{\gamma\gamma}^4 = 4k_1^2k_2^2\, (1 - \cos \theta)^2.$$

The statement has been made in the literature[44,47,53] that

$$\sum_{e} |\langle \pi^{o}\gamma\gamma|M|\eta\rangle|^{2} \propto m_{\gamma\gamma}{}^{4} .$$

As we can see from the above analysis this is only true if the form factors are such that $f_2 = - f_1$. There is no a priori reason to suppose that this is in fact the case.

B. Phase Space and Momentum Barriers

1. Phase Space

Two-body phase space is the dimensionless quantity $\rho_2 = \frac{\pi p}{m}$; in the case of $\eta^o \to \gamma\gamma$ it is simply $\pi/2$.

Three-body phase space is taken to be

$$\rho_3 = \left[\frac{r_o^{\ 2}}{(2\pi)^3}\right] \int d^4k_1 d^4k_2 d^4k_3\ \delta(k_1^{\ 2} - m_1^{\ 2})\delta(k_2^{\ 2} - m_2^{\ 2})\delta(k_3^{\ 2} - m_3^{\ 2})$$

$$\times\, \delta(k_1 + k_2 + k_3 - K_0)$$

$$= \left[\frac{r_o^{\ 2}}{(2\pi)^3}\right] \pi^2 \int dE_1 dE_2$$

$$= \left[\frac{r_o^{\ 2}}{(2\pi)^3}\right] \pi^2 \int dT_1 dT_2$$

$$= \left[\frac{r_o^{\ 2}}{(2\pi)^3}\right] \frac{\sqrt{3}\ \pi^2}{2} \int dxdy\ .$$

where the integral $\int dxdy$ is taken over the allowed region of a triangular Dalitz plot with co-ordinates $x = \frac{T_3 - T_2}{\sqrt{3}}$, $y = (T_1 - Q/3)$.

The factor $\frac{r_o^{\ 2}}{(2\pi)^3}$ is a normalization necessary in comparing 2 and 3-body phase space. The $(2\pi)^{-3}$ is a normalization which actually belongs in the matrix element as $(2\pi)^{-3/2}$. It is more convenient to include in the phase space all relative normalizations which depend on the number of particles. To give three body phase space the same dimensions as ρ_2, one must introduce $r_o^{\ 2} \sim \frac{1}{(\text{energy})^2}$. Customarily, in strong interaction calculations, one uses $r_o = \lambda\!\!\!^{-} = 1/m_\pi$. Then $\rho_2/\rho_3 \sim 100$. Table B-1 shows the relative phase spaces for $r_o = \lambda\!\!\!^{-}$ and $r_o = 3\lambda\!\!\!^{-}$.

Table B-1. Phase space, ρ, for $r_o = \lambda\!\!\!^{-}, 3\lambda\!\!\!^{-}$.

Mode	Area of triangular Dalitz plot	$\rho(r_o = \lambda\!\!\!^{-})$	$\rho(r_o = 3\lambda\!\!\!^{-})$	Relative Phase Space $\rho(\lambda\!\!\!^{-})$	$\rho(3\lambda\!\!\!^{-})$
$\eta^o \to \gamma\gamma$	-	1.6	1.6	132	14.6
$\eta^o \to \pi^o\gamma\gamma$	25,200 MeV^2	.051	.46	4.2	4.2
$\eta^o \to \pi^+\pi^-\gamma$	14,000 MeV^2	.023	.26	2.4	2.4
$\eta^o \to \pi^+\pi^-\pi^o$	5,900 MeV^2	.01	.11	1	1

2. Angular momentum barriers.

There is no general rule for the treatment of angular momentum barriers. One prescription which is often used can be found in Blatt and Weisskopf,[61] page 361. A p-wave barrier, for example, where $|M|^2 \sim k^2$, would be treated as

$$|M|^2 \sim \frac{k^2 r_o^{\,2}}{1 + k^2 r_o^{\,2}} = \frac{k^2}{k^2 + \mu^2}$$

where $\mu = 1/r_o$ and k is the momentum. This is, however, only valid if $kr_o \ll 1$ or $k \ll \mu$. If $r_o = \lambda\!\!\!^{-}_\pi$, we must have $k \ll M_\pi$. The momenta involved in η^o decay clearly do not satisfy this criterion.

Another approach is to simply render the matrix element dimensionless by dividing each power of k by some characteristic energy in the problem. One could, for example, use the Q value for the decay or M_η. The values of the momentum barriers in Table I, Sec. I. B. 1, were obtained using $|M|^2 \sim (k/M_\eta)^n$.

C. Neutron Counting System

1. Counter Design

Figure 26 shows one of the 20 neutron counters, N_i, contained in a 1/8-in. aluminum canister. The counter itself is an 8-in. cylindrical scintillator, glued to a conical Lucite light guide. An Amperex XP1040 photomultiplier tube rests, without attachment, against the smaller face of the light guide.

To maximize the usefulness of the time of flight information, it is necessary to place the counters at the greatest distance from the hydrogen target consistent with an acceptable counting rate. The counters must be large if they are to be far from the target and still subtend a substantial solid angle. The ultimate choice of size (and, therefore, distance from target to counter) was made on the basis of availability of materials. The cylindrical geometry was chosen because of the relative ease of machining and polishing the counters on a lathe.

The neutron detection efficiency of the counters used in this experiment is calculated by the method of Kurz.[62] This efficiency calculation has been experimentally validated for counters of similar size and geometry to within the claimed accuracy ($\pm$ 10%) of the calculation.[63]

2. Fast timing.

The counters detect neutrons indirectly; scintillation light is produced only when the neutron interacts with a nucleus in the scintillating medium and produces a charged recoil. Such recoils vary widely in energy and the presence of a neutron is manifested by a broad spectrum of photomultiplier pulse amplitudes. The largest pulse will be produced by a recoil proton equal in energy to the incident neutron, or by a proton with a range equal to the maximum dimension of the scintillator, whichever

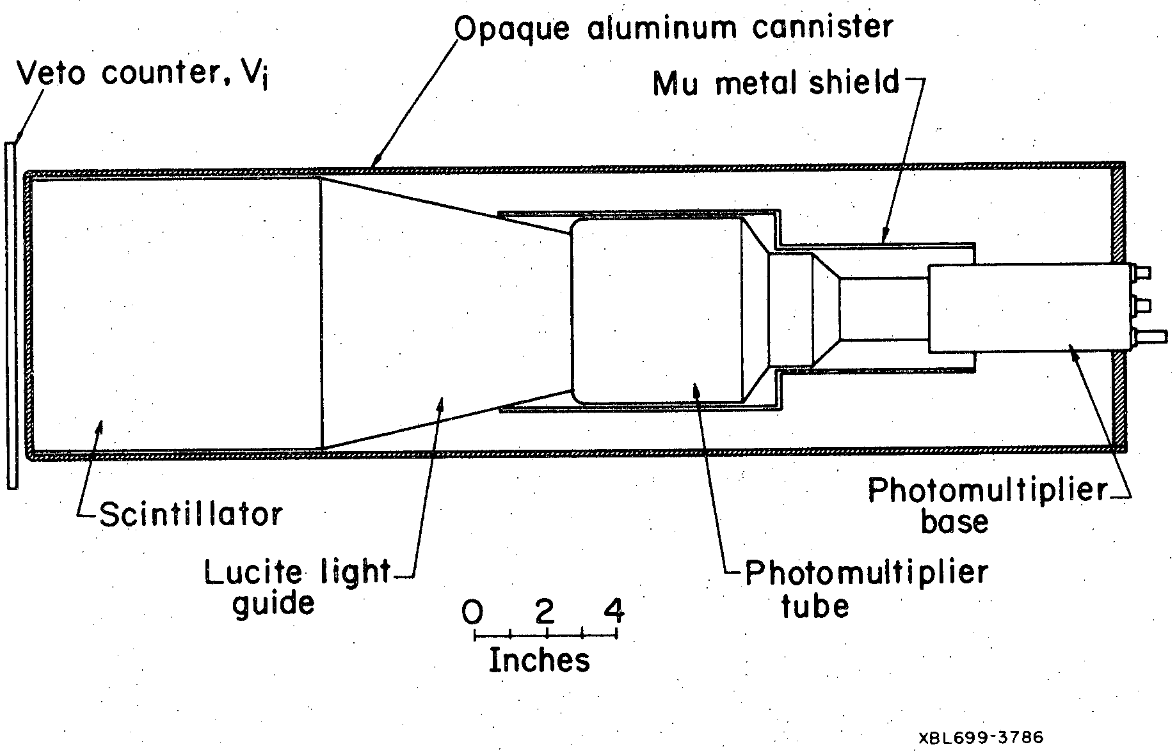

Fig. 26. A neutron counter N_i.

of these two protons has the lesser energy. In this experiment the largest expected proton energy is 122 MeV; the smallest is the minimum threshold energy of 6.0 MeV. The data of Batchelor et al.[64] suggests that protons over this energy range will produce pulses varying in amplitude from 2.37 to 72.0, a dynamic range of 30.

It is difficult to ~~difficult to~~ achieve good timing accuracy when the photomultiplier pulses vary widely in size. Any successful timing technique requires that the timing of some characteristic point on the pulse be independent of pulse amplitude over the expected dynamic range. To achieve pulse shape stability, the photomultiplier tube must be provided with a tapered voltage divider for the following reason: if the dynode-to-dynode voltages increase with the growing electron cloud, space charge shielding of the dynode potentials is avoided and there is no distortion of the pulse. The Amperex XP1040 tube, together with the voltage divider shown in Fig. 27, provides pulses from 100 mV to 4 V without any change in pulse shape.

A standard threshold discriminator will respond to pulses of widely varying amplitude with a timing inaccuracy roughly equal to the rise-time of the pulse (≥ 3 nsec). Simply feeding raw photomultiplier pulses into a standard discriminator is therefore not an adequate technique since we need accuracy of at least $\pm$ 1 nsec.

If the pulse shape is independent of amplitude, a simple and elegant method for achieving timing accuracy is that of "zero-crossing." The photomultiplier anode signal is clipped before it has risen to full amplitude. The resulting bipolar pulse will cross through zero at a point in time which is independent of the original amplitude. A "zero-crossing discriminator" is a tunnel diode circuit which is triggered at the zero-

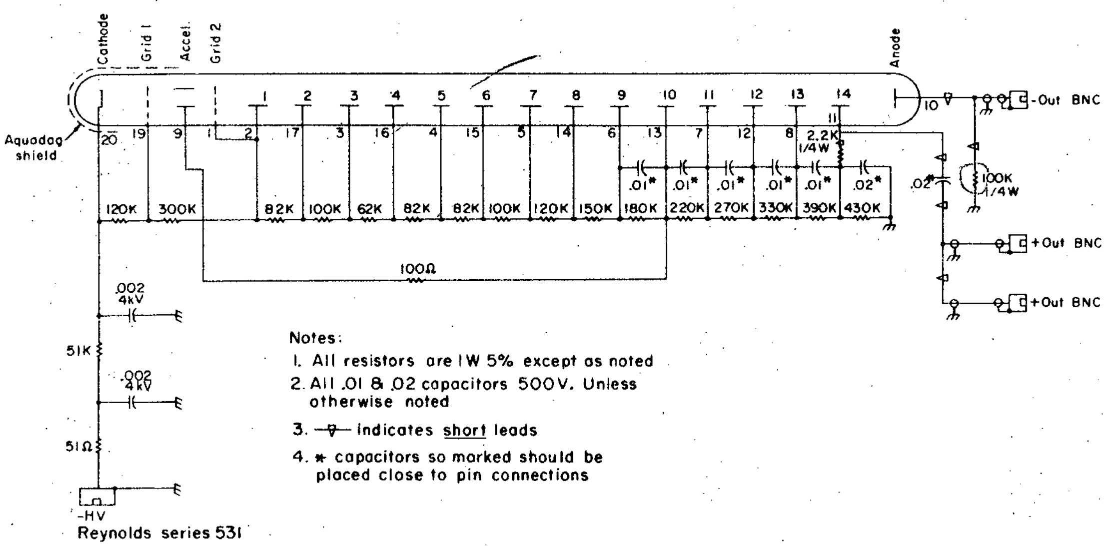

Fig. 27. The XP1040 photomultiplier base wiring diagram.

crossing point. The tunnel diode is biased into a sensitive state by the negative first half of the pulse and fires when the polarity changes.

An EG&G zero-crossing discriminator was investigated for possible use in this experiment. It does indeed respond to pulses over a wide range of amplitudes with excellent timing accuracy. However, the circuit requires that the negative part of the bipolar pulse exceed -250 mV in order that the tunnel diode bias be established. With an expected dynamic range of 30, and with a minimum pulse amplitude of 250 mV, the largest pulses will be -7.5 volts. The photomultiplier tube will not provide pulses of such a large amplitude without distortion.

In this experiment two standard threshold discriminators are used together to simulate a single zero-crossing discriminator. The first, or THRESHOLD discriminator, is used to bias the threshold of the other. The second, or TIMING discriminator, shown in Fig. 28, has a threshold of -120 mV. A wide pulse of -100 mV amplitude is generated by the THRESHOLD discriminator and appears at the TIMING unit simultaneously with a bipolar pulse from the photomultiplier tube. This bipolar pulse crosses zero from positive to negative amplitude. When it arrives at the TIMING unit, the threshold of that discriminator is effectively -20 mV. Thus triggering occurs near but not at the point of zero-crossing.

Rather than clipping the photomultiplier anode signal, an equivalent procedure is used to produce the bipolar pulse. The anode signal is delayed by 6 nsec and is added to an attenuated (6 db) signal from the 14th dynode. The addition is accomplished by a passive mixer composed of 24 ohm resistors and HP2303 hot carrier diodes (Fig. 28). The diodes are present to limit the positive and negative excursions of the pulse without affecting the slope near zero. At the point of anode-dynode mixing there is also added

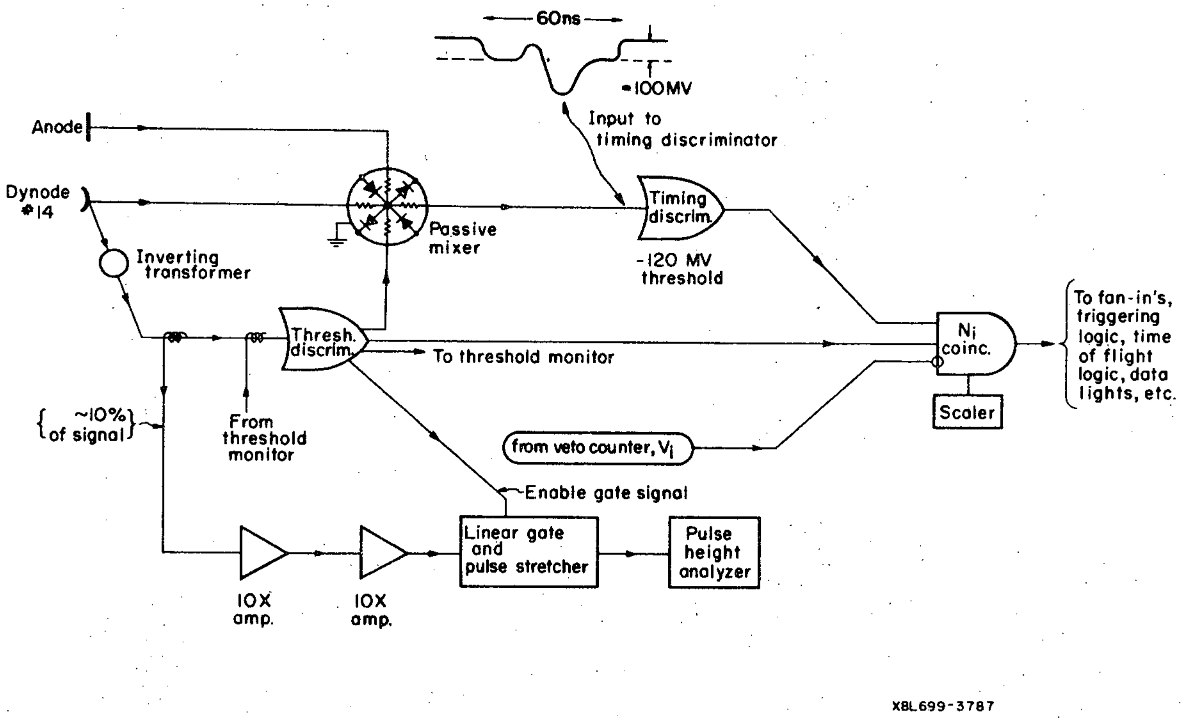

Fig. 28. The neutron counter timing and calibration electronics.

the -100 mV bias pulse from the THRESHOLD discriminator. Various combinations of delay, attenuation, and mixing were examined in order to find that combination which would produce a bipolar pulse crossing from positive to negative with the steepest possible slope. The delay is a function of the cable transit distortion of the pulse as well as being a function of the pulse rise-time. The net pulse emerging from the passive mixer is shown in Fig. 28. This pulse will trigger the TIMING discriminator 20 mV below the point of "zero-crossing."

A second dynode signal generates the bias pulse in the THRESHOLD discriminator. This pulse must be present to achieve good timing accuracy and it is later required in coincidence with the output of the TIMING discriminator. A valid neutron count therefore occurs whenever the THRESHOLD discriminator is triggered. The threshold of this discriminator is carefully set and monitored.

From the data, it appears that the timing accuracy achieved by this technique is $\pm$ 0.65 nsec. This could possibly be improved by making the bias pulse amplitude closer to the threshold of the TIMING discriminator.

3. Neutron Detection Efficiency

The Fortran program TOTEFF computes the neutron detection efficiency as a function of incident neutron energy. This program and the calculations it performs are completely described elsewhere.[62] The input parameters required are: the counter dimensions, the mean threshold, and the fractional resolution at threshold.

The threshold is described in units of "equivalent electron energy" deposited in the scintillator. In the present case this means 7.11 MeV, three times the energy of the maximum recoil electron (2.37 MeV) from the Compton scattering of 2.62 MeV gamma ray. This is equivalent to the energy deposit of a 12.6 MeV proton.[65] The threshold is set using the Compton edge of this 2.62 MeV gamma ray. Then, 10 db attenuation is inserted at the input to the THRESHOLD discriminator to raise the threshold a factor of three from 2.37 MeV ($T_{e^-}^{max}$) to 7.11 MeV.

The fractional resolution is defined as $\tau = \sigma/T_0$, where T_0 is the mean threshold and σ is the standard deviation from that threshold. σ is a composite of σ_D and σ_C, where σ_D refers to the discriminator and σ_C refers to the behavior of the counter. As the discriminator is a far more perfect device than the counter, it suffices to take $\sigma_D \simeq 0$ and $\tau = \sigma_C/T_0$. σ_C is the standard deviation from the mean pulse size produced by a certain energy deposit in the scintillator. It is calculated as a byproduct of the fit to the Compton spectrum of a 2.62 MeV gamma ray. This calculation is described below. The result is $\sigma_C = .55$ and $\tau \simeq .10$. The efficiency is not terribly sensitive to τ.

The results of the efficiency calculations are shown in Fig. 29. The detected neutrons in this experiment at the central momentum ($p_{\pi^-} = 716$ MeV/c) have energies between 50 and 170 MeV.

4. Calibration and Maintenance of Threshold

The threshold of the counter-discriminator system is set using the energy spectrum of the recoil electrons from the Compton scattering of 2.62 MeV gamma rays (Fig. 30). These gamma rays come from an excited state of Pb^{208}, the end product of a sequence of α and β decays beginning with the parent nucleus Th^{228}. The sharp cutoff in the spectrum at $T_{e^-}^{max}$ = 2.37 MeV is known as the "Compton Edge."

The counter is flooded with the 2.62 MeV gamma rays which scatter at random throughout the scintillator. For a perfect counter, the pulse height distribution from the photomultiplier should reproduce the

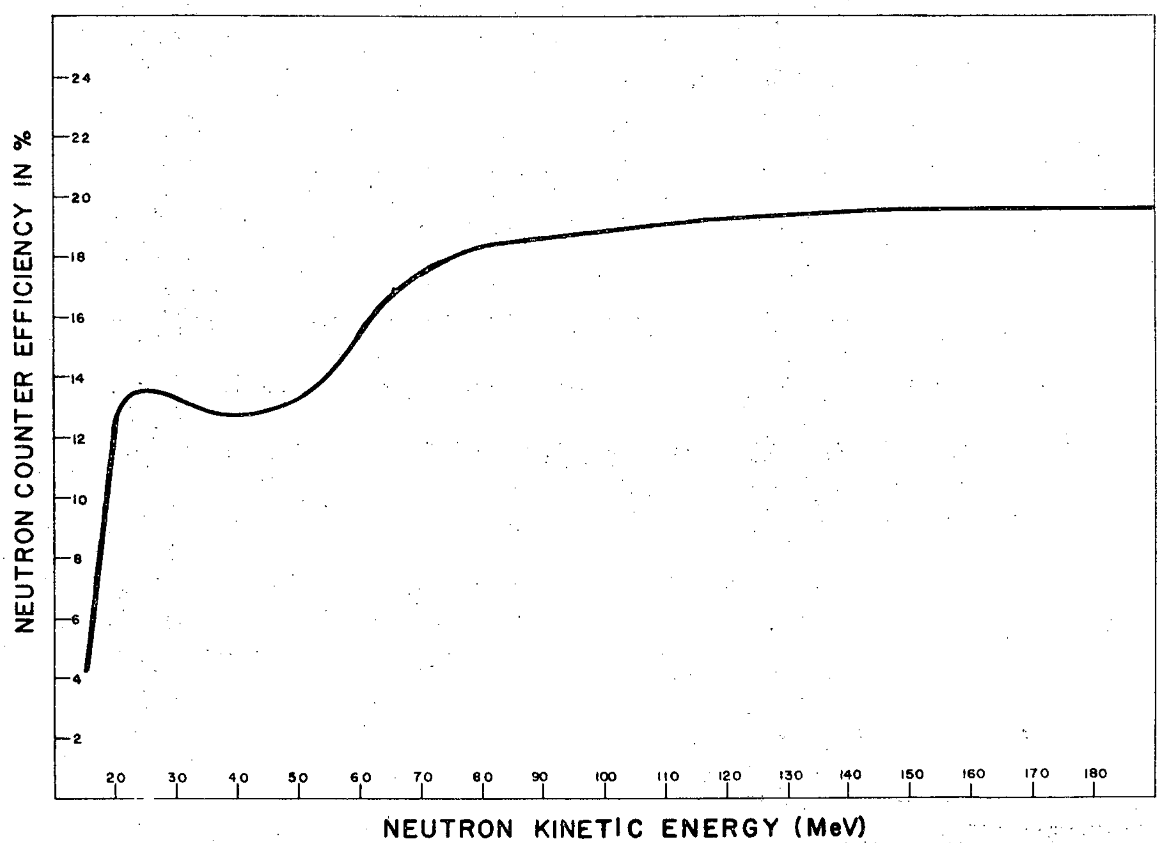

XBL 6910-5736

Fig. 29. Neutron counter efficiency for mean threshold of 7.11 MeV and fractional resolution of 0.10. Detected neutrons in this experiment for the central momentum (716 MeV/c) have energies between 50 and 170 MeV.

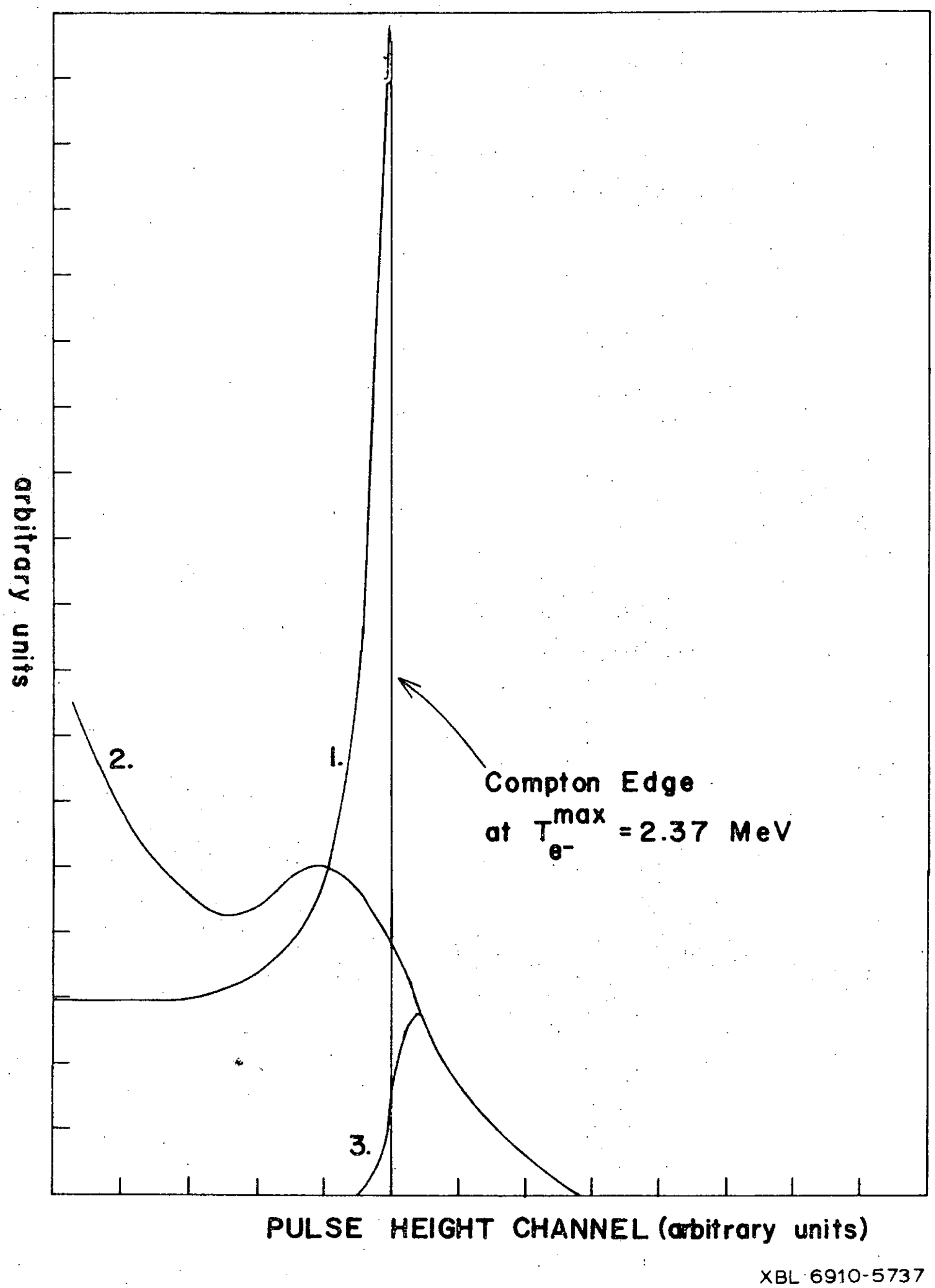

Fig. 30. Compton spectra: (1) Theoretical spectrum. (2) Experimental spectrum. (3) Experimental spectrum cut off by discriminator set at the Compton edge.

theoretical Compton spectrum (Fig. 30, Curve 1). However, light collection from throughout the scintillator is not uniform and the photomultiplication process is statistical. Consequently the distribution is smeared out and must be obtained by folding σ_C with the theoretical spectrum (Fig. 30, Curve 2). An exponential distribution of noise pulses must also be added.[66] The experimental distribution is fitted using σ_C as a free parameter; the value which yields the best fit is the σ_C which is used in the TOTEFF calculation. The location of the true Compton edge is also determined by the fit. This is the intersection of curves 1 and 2 in Fig. 30.

Once the Compton edge has been located, the discriminator output is used to gate a pulse height analyzer and the threshold is changed until the spectrum is cut off at the proper place, namely, at the Compton edge. The Compton spectrum, cut off at the Compton edge by a discriminator with a properly set threshold, is shown as Curve 3 in Fig. 30.

The signal sent to the PHA is approximately 10% of that dynode signal which is input at the THRESHOLD discriminator (Fig. 28). This 10% is taken from the main pulse through a ferrite core. Those pulses which pass this discriminator enable the PHA. The threshold is manipulated until the spectrum is cut off at the pulse height corresponding to the Compton edge. Figure 28 shows the threshold calibration electronics.

At the moment when the threshold is accurately set, a standard Th^{228} source is exposed and pulses above threshold are counted for a specified time interval. The threshold of each counter is set separately and the counting rate with the standard source recorded. The standard Th^{228} source can be exposed between Bevatron pulses and a continuous monitor of the threshold of each counter is available. When attentuation is used to set the threshold higher than 2.37 MeV (equivalent electron energy), the calibration with the standard source can not be continuously monitored. To recalibrate the counters one must remove the attenuation.

Daily observation and recalibration of the thresholds is necessary due to fluctuations in the amplification (gain) of the photomultipliers. These fluctuations are of both short and longer term and vary from tube to tube. The short term fluctuations are oscillatory and have periods varying from minutes to hours. The long term changes in gain are larger, representing steady drifts with time constants of days to weeks. In this experiment the XP1040 tubes were carefully selected. Daily recalibration appears to keep the threshold within $\pm$ 2%. Then the efficiency is constant to within a few percent of its value.

In adjusting the thresholds, two courses of action are open: one is to change the gain of the tube by changing the high voltage; the other is to change the discriminator threshold to match any changes in gain. In this experiment it was considered preferable to do the latter. Changes in photomultiplier high voltage substantially increase the gain fluctuations for several days.

The THRESHOLD discriminators are monitored by an automated digital system.[67] This device sends input pulses to all 20 discriminators simultaneously. These input pulses are applied via ferrite cores to the signal cables from the phototubes. The cores are permanently in place and do not disturb the photomultiplier signals. A fast output from one discriminator at a time is sampled by the system. The input pulses are rapidly increased in size until the discriminator threshold is reached and an output pulse is returned to the monitoring system. The threshold is then displayed digitally. The monitoring system is used to set, change, and observe the 20 discriminator thresholds.

D. Scanning Efficiency Correction Matrix

The scanning correction matrix P_{ij} discussed in the text is easily obtained from the triple-scanned roll. The "true" number of gamma rays (the sum of the reported showers and the number of triggered gamma counters) is taken to be the number found on the fourth scan. In the event that the scanners agreed on the first three scans, the mutually agreed upon number is taken to be the "truth." Table D-I shows the results of the triple-scan for all events with a neutron time of flight greater than 30 nsec. The results are averaged over all three scans. For example, averaged over all three scans the scanners correctly identified 837 out of 883 2γ events.

Table D-I. Triple-scan results for neutron time of flight > 30 nsec.

Observed number of γ rays	True number of gamma rays 0	1	2	3	4	5	6	7
0	35	2						
1	2	144	7	1				
2	1	14	837	22	1			
3	-	1	36	187	15	2		
4	-	-	3	24	294	21	2	
5	-	-	-	2	26	173	20	
6	-	-	-	-	3	26	198	4
7	-	-	-	1	1	3	13	15
8	-	-	-	-	-	-	-	2

The array in Table D-I, when properly normalized, becomes the matrix P_{ij}. The normalization is such that $\sum_i P_{ij} = 1$ where the jth index refers to the true number of gammas. Then we have that

$$\sum_i S_i = \sum_{i,j} P_{ij} T_j$$

$$= \sum_j \left(\sum_i P_{ij} \right) T_j$$

$$= \sum_j T_j \ .$$

That is, the total number of observed events is equal to the total number of true events without regard to the number of gamma rays. In this experiment every event is scanned; there is no possibility of missing an event, only of misreporting one. Table D-II shows the matrix P and Table D-III shows the inverse matrix P^{-1}.

Table D-II. The matrix P.

Observed number of γ rays	True number of gamma rays							
	0	1	2	3	4	5	6	7
0	.921	.014						
1	.061	.892	.008	.004				
2	.018	.089	.947	.093	.004			
3		.004	.040	.790	.043	.009		
4			.004	.100	.866	.092	.010	
5				.008	.077	.770	.084	.016
6				.001	.008	.116	.848	.175
7				.003	.002	.013	.057	.730

The triple-scanned events listed in Table D-I were restricted to those with neutron time of flight greater than 30 nsec. This is done to avoid correcting the scanned events in the η^o time of flight region with a matrix which reflects the peculiar scanning topology of the charge exchange events

Table D-III. The inverse matrix P^{-1}.

Total number of γ rays	Observed number of gamma rays 0	1	2	3	4	5	6	7
0	1.087	-.018						
1	-.075	1.123	-.009	-.005				
2	-.013	-.105	1.062	-.124	.001	.001		
3	.001	-.001	-.054	1.280	-.063	-.007	.001	
4		.001	.002	-.147	1.175	-.138		.003
5			[illegible]	-.001	-.118	1.332	-.131	.002
6			-.001		.006	-.178	1.217	-.287
7			-.003	-.005	-.001	-.010	-.093	1.392

($t_n \sim 25$ nsec). At 716 MeV/c the charge exchange kinematics are such that most of the gamma rays go backward in the laboratory; so much so, in fact, that ~ 60% of the observed two gamma charge exchange events involve a triggered gamma counter (compared with ~ 10% of two gamma η^o events). Any systematic difficulties that the scanners have with events involving triggered gamma counters will be much more important for the charge exchange events. Consequently the two regions of time of flight (above and below 30 nsec) are treated separately. The scanning correction matrix for $t_n < 30$ nsec is not shown here.

Examination of Table D-II or D-III will show that the scanners have a larger efficiency for the detection of 2, 4, and 6γ events. This reflects the fact that they have known since the beginning of the experiment that only even numbers of showers occur naturally. If they find an odd number of showers they have a tendency to rescan the frame to see if they missed one.

The inverse scanning matrix P_{ij}^{-1} is applied to the scanned data to obtain the true data. There are errors associated with each matrix element which reflect the statistically limited sample of data from which the matrix was obtained. These errors are propagated through the branching ratio calculations.

E. Neutron Scattering in the Spark Chambers

Neutrons emerging from the hydrogen target must pass through the lead-plate spark chambers before they reach the neutron counters. Calculations done prior to the experiment indicated that approximately 30% of the neutrons would scatter in the lead before reaching the neutron counters. About 50% of the scattering was expected to be elastic scattering; here ~~the~~ neutron is scattered through very small angles ($\lesssim 3$ deg) with little change in velocity. We did not expect to see much effect from the elastic scattering because of the resolution of our counters. The inelastic scattering, on the other hand, involves large angles and considerable loss of velocity. Even this scattering was expected to be of relatively little importance for $\pi^- p \rightarrow \eta^o n$ or $\pi^- p \rightarrow \pi^o \pi^o n$ processes. However, it should be a very significant effect for the charge exchange events. The data bears this prediction out.

At 716 MeV/c the neutron counters straddle the Jacobian peak for $\pi^- p \rightarrow \eta^o n$. (They also tend to select $\pi^- p \rightarrow \pi^o \pi^o n$ events where the di-pion mass approximates that of the η^o.) The number of neutrons from $\pi^- p \rightarrow \eta^o n$ which should strike the neutron counters (without scattering in the lead plates) is very large compared to the number which should pass near the counters without hitting them. Calculations show that the likelihood of a neutron from $\pi^- p \rightarrow \eta^o n$ scattering <u>in</u> to the neutron counter is very small. The effect of neutron scattering here is to lose $\pi^- p \rightarrow \eta^o n$ events because the neutron scatters <u>out</u> of the counter. The same thing is true of $\pi^- p \rightarrow \pi^o \pi^o n$ events to a lesser degree.

Charge exchange neutrons are produced at all different angles near the angle of the neutron counters. There is no special selectivity here. The likelihood of a neutron scattering <u>in</u> to the counters from larger or smaller angles is quite high. Only about two-thirds of the detected charge exchange events are expected to involve unscattered neutrons; the other one-third will appear to have a longer time of flight. That approximately one-third of the charge exchange events will involve a scattered neutron is exactly what the data shows. The 1 and 2γ distributions for the data at 654 MeV/c (Fig. 14) show what the charge exchange time of flight spectrum looks like. The sharp peak contains mostly events where the neutron did not scatter. The long tail after the peak contains events with scattered neutrons. A similar tail on the charge exchange peak is the background we must account for under the η peak in the 0, 1, and 2γ distributions at 716 MeV/c.

The SIOUX fitting for the "two-shower" events provides ample evidence that this picture of neutron scattering effects is accurate.

One of the kinematical quantities which we may examine for both the passing and failing events is the angle between the two decay gamma rays, the so-called "opening angle." If the two gamma rays come from the two gamma decay of an η or π, they will have a characteristic distribution in the center of mass system for the production of the meson (where the meson has a unique velocity). This distribution is described in Rossi, <u>High Energy Particles</u>,[68] page 199. One of the most distinctive features of the distribution is that there is a minimum opening angle which depends only on the velocity of the particle. In the present case this angle is 157 deg for the η decay and 34 deg for the pion. With the experimental resolution we have, the effective minimum opening angle for the η is approximately 130 deg. Figure 31 shows the opening angle distribution for the "two-shower" events where SIOUX found a fit (these are the same events shown in histogram (2), Fig. 16). Figure 32 shows the same distribution

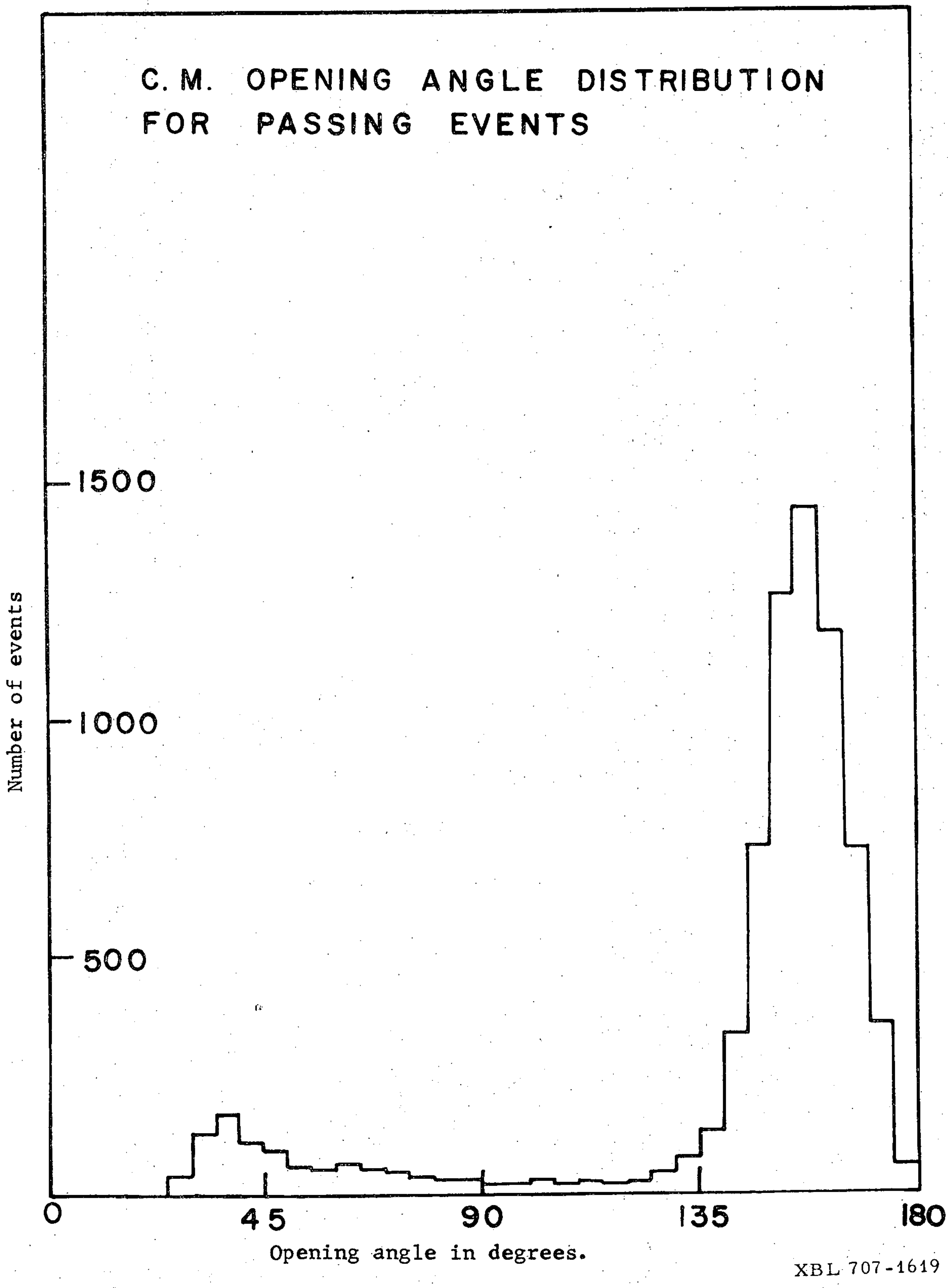

Fig. 31. Gamma ray opening angle distribution for passing events in the $\pi^- p \rightarrow x^0 n$ center-of-mass system.

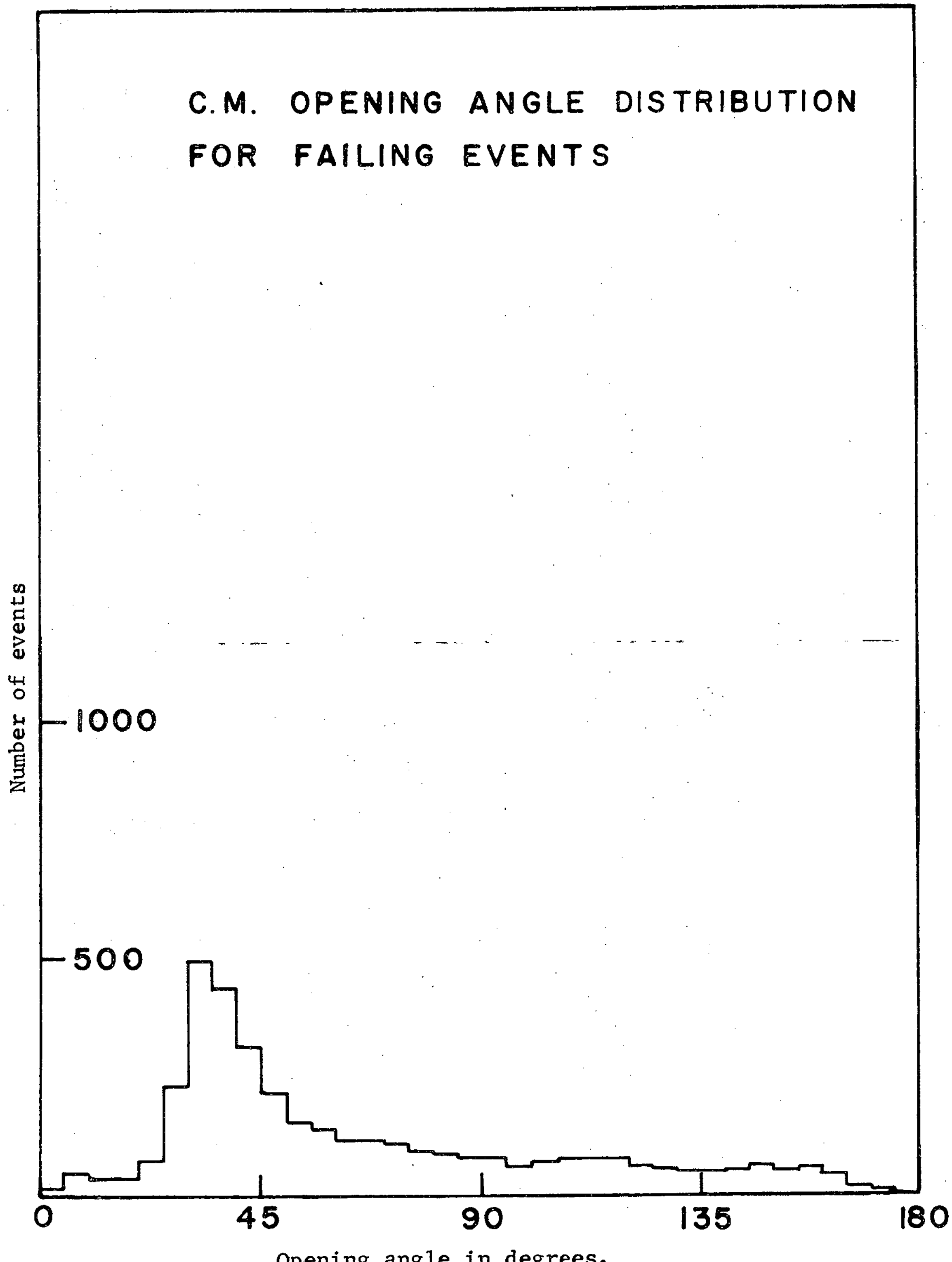

XBL 707-1479

Fig. 32. Gamma ray opening angle distribution for failing events in the $\pi^- p \rightarrow x^o n$ center-of-mass system.

for the failing events (compare with Fig. 16, histogram (3)). Any event with an opening angle less than ~ 130 deg is not an η. The peak near 160 deg in Fig. 31 is the η distribution. (An excellent place to see what the theoretical and experimental opening angle distribution looks like is Ref. 10.) It is clear from Fig. 31 that most of the passing events are η events. Figure 32 indicates that most, if not all, of the failing events are consistent with being charge exchange events. Comparison of histogram (3), Fig. 16, and Fig. 32 shows that most of the failing events have the wrong time of flight (but the right opening angle distribution) to be charge exchange events. The explanation is that the time of flight information is erroneous because the neutron has scattered in the lead plates.

Comparison of Figs. 31 and 32 indicates that approximately two-thirds of the charge exchange events seem to fail due to a scattered neutron and erroneous time of flight information. This appears to contradict thte statement above that one-third of the charge exchange events should involve a scattered neutron. If one were to count the number of charge exchange events in the tail of the charge exchange peak and the number in the peak itself for <u>all</u> the 0, 1, and 2γ events, one would find two-thirds in the peak. There are very few true "two-shower" events involving unscattered neutrons because the kinematics for charge exchange at 716 MeV/c are unfavorable. The "two-shower" events analyzed by SIOUX represent a special class of events, a disproportionally large number of which involve neutrons which have scattered <u>in</u> to the counters.

REFERENCES

1. A. Pevsner, R. Kraemer, M. Nussbaum, C. Richardson, P. Schlein, R. Strand, and T. Toohig, Phys. Rev. Letters 7, 421 (Dec. 1, 1961).
2. D. Duane Carmony, Arthur H. Rosenfeld, and Remy T. Van de Walle, Phys. Rev. Letters 8, 117 (Feb. 1, 1962).
3. Pierre L. Bastien, J. Peter Berge, Orin I. Dahl, Massimiliano Ferro-Luzzi, Donald H. Miller, Joseph J. Murray, Arthur H. Rosenfeld, and Mason B. Watson, Phys. Rev. Letters 8, 114 (Feb. 1, 1962).
4. Charles Zemach, Phys. Rev. 133, B1201-1220 (9 March 1964).
5. Laurie M. Brown and Paul Singer, Phys. Rev. Letters 8, 155 (Feb. 1, 1962); Phys. Rev. Letters 8, 353 (April 15, 1962).
6. M. Gell-Mann, D. Sharp, and W. G. Wagner, Phys. Rev. Letters 8, 261 (March 15, 1962).
7. Arthur H. Rosenfeld, D. Duane Carmony, and Remy T. Van de Walle, Phys. Rev. Letters 8, 293 (April 1, 1962).
8. G. Feinberg, Phys. Rev. Letters 8, 151 (February 1, 1962).
9. G. Puppi, Proc. Inter. Conf. on High Energy Physics, CERN (1962) p. 713.
10. M. Chretien, F. Bulos, H. R. Crouch, Jr., R. E. Lanou, Jr., J. T. Massimo, A. M. Shapiro, J. A. Averell, C. A. Bordner, Jr., A. E. Brenner, D. R. Firth, M. E. Law, E. E. Ronat, K. Strauch, J. C. Street, J. J. Szymanski, A. Weinberg, B. Nelson, I. A. Pless. L. Rosenson, G. A. Salandin, R. K. Yamamoto, L. Geurriero and F. Waldner, Phys. Rev. Letters 9, 127 (August 1, 1962).
11. C. Alff, D. Berley, D. Colley, N. Gelfand, U. Nauenberg, D. Miller, J. Schultz, J. Steinberger, T. H. Tan, H. Brugger, P. Kramer and R. Plano, Phys. Rev. Letters 9, 325 (Oct. 1, 1962).

12. Earle C. Fowler, Frank S. Crawford, Jr., L. J. Loyd, Ronald A. Grossman, and LeRoy Price, Phys. Rev. Letters 10, 110 (1 February 1963).

13. Frank S. Crawford, Jr., L. J. Loyd, and Earle C. Fowler, Phys. Rev. Letters 10, 546 (June 15, 1963).

14. Angela Barbaro-Galtieri, Stephen E. Derenzo, LeRoy R. Price, Alan Rittenberg, Arthur H. Rosenfeld, Naomi Barash-Schmidt, Claude Bricman, Matts Roos, Paul Söding, Charles G. Wohl, Rev. Mod. Phys. 42, 87 (January 1970).

15. G. DiGiugno, R. Querzoli, G. Troise, F. Vanoli, M. Giorgi, P. Schiavon, and V. Silvestrini, Phys. Rev. Letters 16, 767 (25 April 1966).

16. K. C. Wali, Phys. Rev. Letters 9, 120 (August 1, 1962).

17. C. Bacci, G. Penso, G. Salvini, A. Wattenberg, C. Mencuccini, R. Querzoli, and V. Silvestrini, Phys. Rev. Letters 11, 37 (1 July 1963).

18. Laurie M. Brown and Paul Singer, Phys. Rev. Letters 8, 460 (June 1, 1962); Phys. Rev. Letters 16, 424 (7 March 1966).

19. J. B. Bronzan and F. E. Low, Phys. Rev. Letters 12, 522 (4 May 1964).

20. M. Ferro-Luzzi, D. H. Miller, J. J. Murray, A. H. Rosenfeld and R. D. Tripp, Nuovo Cimento 22, 1087 (1961).

21. G. Barton and S. P. Rosen, Phys. Rev. Letters 8, 414 (May 15, 1962).

22. Mirza A. Baqui Beg, Phys. Rev. Letters 9, 67 (July 15, 1962).

23. D. Berley, D. Colley, and J. Schultz, Phys. Rev. Letters 10, 114 (1 February 1963).

24. Frank S. Crawford, Jr., Ronald A. Grossman, L. J. Lloyd, LeRoy R. Price, and Earle C. Fowler, Phys. Rev. Letters 11, 564 (15 Dec. 1963).

25. Frank S. Crawford, Jr., Ronald A. Grossman, L. J. Lloyd, LeRoy R. Price, and Earle C. Fowler, Phys. Rev. Letters 13, 421 (28 Sept. 1964).

26. M. Foster, M. Peters, R. Hartung, R. Matsen, D. Reeder, M. Good, M. Meer, F. Leffler, and R. McIlwain, Phys. Rev. 138, B652, (May 10, 1965).

27. Laurie M. Brown and Paul Singer, Phys. Rev. 133, B812 (10 Feb. 1964).

28. Laurie M. Brown and Harry Faier, Second Coral Gables Conference on Symmetry Principles at high Energy, January 1965 (Freeman Press, San Francisco) p. 219.

29. V. Bisi, G. Borreani, R. Cester, A. De Marco-Trabucco, M. I. Ferrero, C. M. Garelli, A. Marzari Chiesa, B. Quassiati, G. Rinaudo, M. Vigone, and A. Werbrouck, Nuovo Cimento, XXXV, 768 (Feb. 1, 1965).

30. T. Huetter, S. Taylor, E. L. Koller, P. Stamer, and J. Grauman, Phys. Rev. 140, B655 (8 Nov. 1965).

31. S. Taylor, T. Huetter, E. L. Koller and P. Stamer, Nuclear Physics 83, 690 (1966).

32. M. A. Wahlig, E. Shibata, and I. Mannelli, Phys. Rev. Letters 17, 221 (25 July 1966).

33. M. Veltman and Joel Yellin, Phys. Rev. 154, 1469 (25 Feb. 1967).

34. G. Feinberg and A. Pais, Phys. Rev. Letters 9, 45 (July 1, 1962).

35. Ching-Hung Woo, Phys. Rev. 156, 1719 (25 April 1967).

36. Stephen L. Adler, Phys. Rev. Letters 18, 519 (27 March 1967); Phys. Rev. Letters 18, 1036 (5 June 1967).

37. LeRoy R. Price and Frank S. Crawford, Jr., Phys. Rev. 167, 1339 (25 March 1968).

38. Columbia-Berkeley-Purdue-Wisconsin-Yale Collaboration, Phys. Rev. 149, 1044 (30 September 1966).

39. A. Larribe, A. Leveque, A. Muller, E. Pauli, D. Revel, T. Tallini, P. J. Litchfield, L. K. Rangan, A. M. Segar, J. R. Smith, P. J. Finney,

C. M. Fisher and E. Pickup, Phys. Letters 23, 600 (5 Dec. 1966).

40. A. M. Cnops, G. Finocchiaro, P. Mittner, J. P. Dufey, B. Gobbi, M. A. Pouchon and A. Muller, Phys. Letters 27B, 113 (10 June 1968).

41. Z. S. Strugalski, I. V. Chuvilo, I. A. Ivanorskaja, L. S. Okhrimenko, B. Niczyporuk, T. Kanarek, Z. Jabłonski, B. Słowinski, JINR-E1-3100 (1967).

42. Jacob Grunhaus (Ph. D. Thesis) Columbia University (December 1966).

43. M. Feldman, W. Frati, R. Gleeson, J. Halpern, M. Nussbaum and S. Richert, Phys. Rev. Letters 18, 868 (15 May 1967).

44. P. Bonamy and P. Sonderegger, Proc. Inter. Conf. on Elementary Particles, Heidelberg, Sept. 20-27, 1967.

45. F. Jacquet, U. Nguyen-Chac, C. Baglin, A. Bezaguet, B. DeGrange, R. J. Kurz, P. Musset, A. Haatuft, A. Halsteinslid, J. M. Olsen, Phys. Letters 25B, 574 (13 November 1967).

46. S. Buniatov, E. Zavattini, W. Deinet, H. Muller, D. Schmitt and H. Staudenmaier, Phys. Letters 25B, 560 (13 November 1967).

47. C. Baltay, P. Franzini, J. Kim, R. Newman, N. Yeh and L. Kirsch, Phys. Rev. Letters 19, 1495 (25 December 1967).

48. F. W. Bullock, M. J. Esten, E. Fleming-Tompa, M. Govan, C. Henderson, A. A. Owen and F. R. Stannard, Phys. Letters 27B, 402 (19 August 1968).

49. Jewan Kim (Ph. D. Thesis) Columbia University (April, 1969).

50. Stephen Shapiro (Ph. D. Thesis) Columbia University (May, 1969).

51. C. Baglin, A. Bezaguet, B. DeGrange, P. Musset, H. H. Bingham, G. Irwin, W. Michael, A. Ferrando, A. Lloret, J. A. Rubio, M. Tomas, S. DeUnamuno, M. Paty, J. L. Riester, R. Arnold, Phys. Letters 29B, 445 (23 June 1969).

52. B. Cox, L. Fortney and J. Golson, Phys. Rev. Letters 24, 534 (9 March 1970).

53. S. Devons, J. Grunhaus, T. Kozlowski, P. Nemethy, S. Shapiro, N. Horwitz, T. Kalogeropoulos, J. Skelly, R. Smith and H. Uto, Neutral Decay Modes of the η^{o} Meson (to be published in The Physical Review).

54. Thomas J. Devlin, OPTIK: An IBM 709 Computer Program for the Optics of High-Energy Particle Beams, Lawrence Radiation Laboratory Report UCRL-9727 (September 1961).

55. Bruce Cork, Denis Keefe, and William A. Wenzel, Proc. of International Conf. on Instrumentation for High-Energy Physics (Interscience Publishers, New York, September 1960) p. 84.

56. R. J. Cence, B. D. Jones, V. Z. Peterson, V. J. Stenger, J. Wilson, D. Cheng, R. D. Eandi, R. W. Kenney, I. Linscott, W. P. Oliver, S. Parker, and C. Rey, Phys. Rev. Letters 22, 1210 (2 June 1969); William P. Oliver, A Measurement of the Branching Ratio $K_L^{o} \to 2\pi^{o}/K_L^{o} \to 3\pi^{o}$ (Ph. D. Thesis), Lawrence Radiation Laboratory Report UCRL-19397 (November 1969).

57. C. A. Rey and S. I. Parker, Nucl. Instr. Meth. 54, 314 (1967); S. I. Parker and C. A. Rey, Nucl. Instr. Meth. 43, 361 (1966).

58. A. R. Clark, L. T. Kerth, Proc. of the 1966 Inter. Conf. on Instrumentation for High Energy Physics, Stanford, Calif. (September, 1966) p. 355.

59. Janos Kirz, Joseph Schwartz, and Robert D. Tripp, Phys. Rev. 130, 2481 (15 June 1963).

60. Barry C. Barish, Richard J. Kurz, Victor Perez-Mendez, and Julius Solomon, Phys. Rev. 135B, 416 (27 July 1964).

61. J. M. Blatt and V. F. Weisskopf, Theoretical Nuclear Physics (John Wiley and Sons, New York, 1952) p. 361.

62. Richard J. Kurz, A 709/7090 Fortran II Program to Compute the Neutron-Detection Efficiency of Plastic Scintillator for Neutron Energies from 1 to 300 MeV, Lawrence Radiation Laboratory Report UCRL-11339 (March 18, 1964).

63. D. G. Crabb, J. G. McEwen, E. G. Auld and A. Langsford, Nucl. Instr. and Meth. 48, 87 (1967).

64. R. Batchelor, W. B. Gilboy, J. B. Parker and J. H. Towle, Nucl. Instr. Meth. 13, 70 (1961).

65. H. C. Evans and E.H. Bellamy, Proc. Phys. Soc. 74, 212 (1959).

66. Ernst Breitenberger, Progress in Nuclear Physics, Vol. 4 (Pergamon Press, 1955) p. 56.

67. Cordon R. Kerns, IEEE Trans. Nuc. Sci., NS-16, 381 (Feb. 1969).

68. Bruno Rossi, High Energy Physics (Prentice-Hall, N. Y., 1952) p. 199.

TECHNICAL INFORMATION DIVISION
LAWRENCE RADIATION LABORATORY
UNIVERSITY OF CALIFORNIA
BERKELEY, CALIFORNIA 94720